A COMPREHENSIVE INVESTIGATION OF THERMAL AND FLOW-RESISTANCE BEHAVIOUR OF METAL BASED POROUS MEDIA

Thesis

Submitted in partial fulfillment of the requirement for the degree of

DOCTOR OF PHILOSOPHY

by

TRILOK G

DEPARTMENT OF MECHANICAL ENGINEERING

NATIONAL INSTITUTE OF TECHNOLOGY

KARNATAKA, SURATHKAL, MANGALORE – 575025, INDIA

OCTOBER – 2024

A COMPREHENSIVE INVESTIGATION OF THERMAL AND FLOW-RESISTANCE BEHAVIOUR OF METAL BASED POROUS MEDIA

Thesis

Submitted in partial fulfilment of the requirements for the degree of

DOCTOR OF PHILOSOPHY

by

TRILOK G

Under the guidance of

Dr. N Gnanasekaran

Associate Professor

DEPARTMENT OF MECHANICAL ENGINEERING

NATIONAL INSTITUTE OF TECHNOLOGY

KARNATAKA, SURATHKAL, MANGALORE - 575025

INDIA

OCTOBER – 2024

DECLARATION

I hereby *declare* that the Research Thesis entitled **"A COMPREHENSIVE INVESTIGATION OF THERMAL AND FLOW-RESISTANCE BEHAVIOUR OF METAL BASED POROUS MEDIA"**, which is being submitted to the ***National Institute of Technology Karnataka, Surathkal*** in partial fulfillment of the requirements for the award of the Degree of ***Doctor of Philosophy*** is a ***bonafide report of the research work carried out by me.*** The material contained in this thesis has not been submitted to any University or Institution for the award of any degree.

Register Number: **197511ME028**

Name of the Research Scholar: **TRILOK G**

Signature of the Research Scholar: Trilok. G

Department of Mechanical Engineering

Place: NITK, Surathkal

Date: 29/10/24

CERTIFICATE

This is to *certify* that the Research Thesis entitled **"A COMPREHENSIVE INVESTIGATION OF THERMAL AND FLOW-RESISTANCE BEHAVIOUR OF METAL BASED POROUS MEDIA"**, submitted by **TRILOK G** (Register Number: 197511ME028) as the record of the research work carried out by him, is *accepted* as the *Research Thesis submission* in partial fulfilment of the requirements for the award of the degree of **Doctor of Philosophy.**

Research Guide

Dr. N Gnanasekaran
Associate Professor
Department of Mechanical Engineering

Chairman-DRPC
Department of Mechanical Engineering
National Institute of Technology Karnataka
Surathkal, Mangalore - 575025

ACKNOWLEDGEMENT

I extend my honest gratitude to my research guide, Dr. N. Gnanasekaran, for his continuous support, guidance, and motivation throughout my research journey. His dedication, expertise, and encouragement have been invaluable in shaping my research, academic and personality development. All the insightful feedback, constructive criticism, freedom of thought and patience from my guide have been instrumental in helping me face the challenges and refine my ideas. I am truly thankful for his mentorship, which has not only enhanced my research skills but also inspired me to strive for excellence. This accomplishment would not have been possible without my guide's belief in my abilities.

I express my sincere thanks to Dr. SM Murigendrappa, the Head of the Department, and the former Heads of the Department of Mechanical Engineering, for their continuous support and encouragement throughout the completion of my research work. Their leadership and guidance have been very much helpful through my research journey.

I am deeply grateful to the members of my Doctoral committee, Dr. Kumar G N, Professor, Department of Mechanical Engineering, and Dr. Saumen Mandal, Associate Professor in the Department of Metallurgy and Material Science, for their consistent assessment and invaluable suggestions throughout the progress of my research work. My sincere appreciations to all the faculty members of the Department of Mechanical Engineering for their insight and motivation in many ways.

I would like to express my gratitude to the Science and Engineering Research Board, DST for funding the research work.

I would like to express my sincere gratitude to Dr. Moghtada Mobedi for his knowledge and insights that helped shape my research work during the collaboration.

I would like to thank Dr. Prem Kumar, for his directions and motivations towards my research as well as personal growth.

I thank my senior Dr. Ashok Kumar K for being a true well-wisher and a friend who not only motivated me in every aspect including both research and personal journey,

but also, for consistently engaging with discussions on philosophical perspective of the world around and things beyond. I thank my research mate Venkatapathy for his true and genuine friendship that was not just limited to a healthy research environment but also elevated my personal growth. I wish to thank my seniors Dr. Surya, Dr. Radhe, Dr. Rathnesh, Dr. Vinayak, Dr. Ram Babu, Dr. Husein, Ram prasad for inspiring my research journey. I wish to thank all my fellow research mates Phani Kumar, Ganesh, Kishore Babu, Sanjay, Sai kumar for their company that kept this research journey healthy and with discussions that were fruitful. I also thank undergraduate students Sai Srinivas, Devika, Kiran and Dilshad for their engagement during the research work. I am thankful to everyone who helped me and encouraged me in any way possible during this research work.

I thank my friends Sujay, Siddu, Navya, Aishwarya and Dhanu for encouraging my research journey and for being my true well-wishers.

I would like to thank my younger brother Tridev G for not only sharing my responsibility of being an eldest son to the family, but also for inspiring me in many ways, that motivated and supported my research journey. I also thank my other younger brother Trimurthy G, for his moral support which I always received through his genuine expressions towards my wellbeing that has many times uplifted my spirit throughout my research journey and in personal situations.

I thank my fiancé Chandana, a longtime friend, a true accomplice of all my endeavors since our journey together. She has been alongside me in all my ups and downs providing me consistent emotional support whenever it felt short, her presence in my life made my research journey more comfortable.

I finally thank my mother and father; without whose wish and prayers this wouldn't have been possible. Words surely fall short to acknowledge their credit in my accomplishments.

(TRILOK G)

DEDICATED TO

My Beloved Mother

I, dedicate this thesis to my hard working, selfless and beloved mother whose only wish and purpose was to ensure the wellbeing of her children and family. It was her true desire to see her children pursue higher education, that supported and motivated me to dream of this degree. Amma, your unconditional love, hard work, sacrifices and selfless effort towards the wellbeing of our family will always be remembered. I bow down to this pure soul and thank God for placing me in her protecting and loving arms.

Thank you amma for everything

ABSTRACT

This thesis work presents numerical investigation of metal based porous media such as metal foams and stacked wire mesh porous structures, focusing on addressing the issue of incurred flow resistance that is always accompanied with the enhanced heat transfer associated with such media. Key features of porous medium such as their twin structural properties (porosity and pore density), thickness and method of formation (stacking types in terms wire mesh porous structures) are identified as potential influencing parameters that play a key role in the thermo-hydraulic phenomenon.

In the first part, influence of porosity and pore density of porous media is demonstrated for their combined effect on flow resistance and heat transfer enhancement behavior. Significance of considering both of these twin structural properties in analyzing the characteristics of porous medium particularly in forced convection regime is further emphasized through Nusselt number correlations.

In the second part, thickness of porous medium is considered as another parameter along with the structural properties, and various trade-off scenarios between enhanced heat transfer and incurred flow resistance is comprehensively analyzed. TOPSIS A multi-objective, multi-attribute decision making technique is utilized in this regard, and unique potentials of a porous medium corresponding to its various combination of structural and thickness conditions are evaluated in terms of their ability to minimize flow resistance and maximize heat transfer.

In the last part, potentials of stacked wire mesh porous structures are investigated for their various trade-off scenarios between enhanced heat transfer and incurred flow resistance. Expressions pertaining to key morphological features such as porosity, pore density and specific surface area of wire mesh porous structures of various stacking types are derived and used in the porous media modeling to comprehensively analyze the phenomenon of increased pressure drop with increase in heat transfer corresponding to variations in structural properties (porosity and pore density), stacking types and thickness scenarios.

Keywords: porous media, metal foams, wire mesh, flow resistance, heat transfer

TABLE OF CONTENTS

LIST OF FIGURES

LIST OF TABLES

NOMENCLATURE

A	Surface area of Aluminum plate (m^2)
A_{sm}	Total area of the solid mesh in the whole porous block
a_1	Area of total solid fibers constituting an individual mesh layer
a_s	Area of straight running wire fiber (m^2)
a_w	Area of weaving wire fiber (m^2)
a_{sf}	Specific surface area or interstitial area density (m^{-1})
C_p	Specific heat (J/kgK)
D_h	Hydraulic diameter (m)
d_p	Pore diameter (m)
d_f	Fiber diameter (m)
F	Inertial resistance coefficient (m^{-1})
G	Grashof number
h	Spacing (distance) between individual mesh layers.
h_{min}	Minimum possible distance measured from centre to centre of straight running fibres of consecutive mesh layers for closely packed condition
h_{sf}	Interstitial heat transfer coefficient (W/m^2K)
h_{wall}	Wall heat transfer coefficient (W/m^2K)
K	Permeability (m^2)
Nu	Nusselt number
P	Pressure (N/m^2)
Pi	Performance index
Pr	Prandtl number of fluid

Q Heat input (W)

r Dimensionless ratio (df/dp)

Re Reynolds number

Ri Richardson number

S Euclidean distance

T Temperature (K)

u Velocity vector (m/s)

v Velocity at inlet (m/s)

Greek symbols

β Thermal expansion co-efficient

ε Porosity

ω pore density

λ Thermal conductivity (W/mK)

$\boldsymbol{\mu}$ Dynamic viscosity (N-s/m^2)

ν Kinematic viscosity (m^2/s)

ρ Density (kg/m3)

Subscript

fe Fluid effective

se Solid effective

p_m Fluid saturated porous medium

CHAPTER – 1

INTRODUCTION

Porous media under a broad perspective can be observed to be the form of occurrence in many naturally existing entities that aids several vital natural phenomena comprising both biological and physical processes. A few such examples strengthening the statement can be seen in processes such as water infiltration, water retention, ground water flow, exchange or transportation of gases, minerals in living and non-living entities and in phenomena such as respiration, evaporation etc., Synthesized porous media of definite structural, thermal and flow properties have been recognized as a supplement in solving major problems in many engineering applications. A plethora of possibilities exist in achieving a kind of porous medium with respect to its morphological, thermal, hydraulic and material characteristics. Every such possibility serves the given purpose or provides solution to the problem uniquely. Therefore, understanding the nature of the porous medium as a structure, as a medium allowing fluid flow and its property of assisting heat transfer becomes crucial in arriving at a better solution to many engineering applications specifically where both heat transfer and flow phenomenon are of prime importance. Evolution of the field 'computational fluid dynamics' has enabled to visualize and predict the flow and thermal behavior of these porous media using several numerical techniques employed to solve the equations that govern the phenomena. However, it is crucial to know the stages in which the governing equations are arrived and the approach in which they are used to represent the key behaviors of flow and heat transfer in mediums that are porous in nature. Upon proper understanding of the nature of existence, flow and heat transfer behavior in porous media and their respective governing mathematical equations, it enables the main objective of finding a better solution to engineering problems using computational methods. In this regard the present chapter discusses about the existence and nature of porous media, terminologies involved, applications of porous media, modeling of such media and the governing equations involved.

1.1 POROUS MEDIA IN GENERAL

Porous medium can be broadly defined as the medium that is characterized by void spaces distributed along the stretch of the whole domain. Generally, it is these void spaces that makes the medium to be permeable for any fluid to flow through it, however commonly creating a highly convoluted path ways for the fluid flow due to the intricate internal structure of the medium.

In engineering applications point of view the porous medium can broadly be classified into two major groups namely, non-metal based and metal-based.

1.1.1 Non-metal based porous media

Porous medium formed by non-metallic substances can be seen widely in common naturally occurring substances and biological life promoting various phenomena. Many such instances include beach sand comprised of various minerals and particles forming a porous bed that helps in water infiltration, leaves that comprises of minute pores called 'stomata' that helps in exchange of gases and water vapor with the environment, ground water that flows through the subsurface medium which is porous in nature, wood can also be perceived as a porous medium which can allow air or water to pass through it, decomposed organic material 'peat' seen in wetlands is also an example of heigh porosity medium that helps in retaining water. Many biological features like walls of a cell, surface of skin, walls of blood vessels, nature of alveoli of lungs etc., may also be perceived as porous medium that allows exchange of vital gases, minerals, nutrients and even waste products between the outer medium.

1.1.2 Metal-based porous media

Metal-based porous media that are naturally occurring like, some volcanic rocks with metal inclusions, geological sediments infiltered with metals and some meteorites with metal inclusions are however rare compared to the availability and possibility of engineered pure metallic porous structures such as, metal foams, wire meshes, perforated sheets, lattice structures etc., as shown in Figure 1.1. Metal based porous media are quite well known and have been found useful in many engineering applications typically involving heat transfer processes.

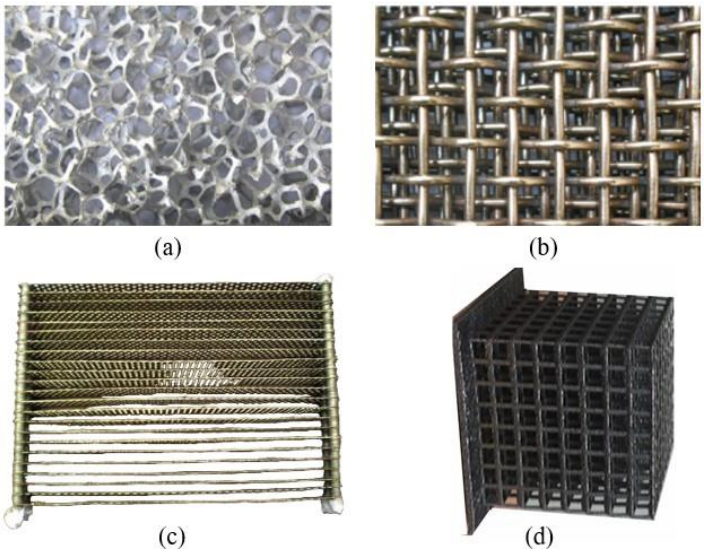

Figure 1.1. Few examples of metal based porous media including, a) Metal foams (Kamath et al. 2011), b) Wire mesh (Kurian et al. 2016a; b), c) Perforated sheets (Venugopal et al. 2010a), d) Lattice structure (Caket et al. 2022; Qian et al. 2023).

1.2 TERMINOLOGIES

Terminologies associated with porous media and their definitions can be seen as followed (Kaviany 1995).

- Porosity

Porosity of a medium is a non-dimensional quantity that signifies the amount of pore or void space compared to the dimensions of the whole medium that is characterized by such pores. It is commonly represented by the symbol 'ε'.

It is mathematically represented as the ratio of volume of the fluid space or pore space to that of the whole medium comprising of both pore spaces and solid structures as specified in Eq. (1.1).

$$\varepsilon = \frac{Volume\ of\ pore\ space}{Volume\ of\ the\ porous\ media\ as\ a\ whole} \tag{1.1}$$

$$\varepsilon = \frac{Volume\ of\ pore\ space}{Volume\ of\ pore\ space + Volume\ of\ solid\ structures}$$

- Pore density

Pore density is yet another important property of the porous media that generally represents one of the geometrical natures of the porous media. It signifies how close the solid structures are to one another throughout the stretch of the pore filled solid porous media. It is generally represented in its abbreviated form as 'PPI' meaning pores per inch.

- Pore diameter

Pore diameter denoted by the term 'd_p' a most commonly used terminology more exclusive to porous media like metal foams, specifies the diametrical dimension of the void space in terms of its average diameter.

- Fiber diameter

Yet another terminology more specific to porous media like metal foams and wire meshes is their fiber diameter specifying the average diameter of the solid structures that forms the porous media. It is generally denoted by term 'd_f'.

- Permeability

Permeability one of the key flow determining properties of the porous media is the measure of the ease with which a fluid is allowed to pass through the medium. It is generally denoted by the letter 'K'.

1.3 APPLICATIONS

The phenomenon of flow and heat transfer through porous media can be seen in variety of applications and can broadly be classified into the fields of heat transfer, energy storage, chemical engineering, biomedical, environmental pollution control, geological sciences and many more. A broad view of these fields of application can be seen in Figure 1.2 and the details of them can briefly be discussed as followed.

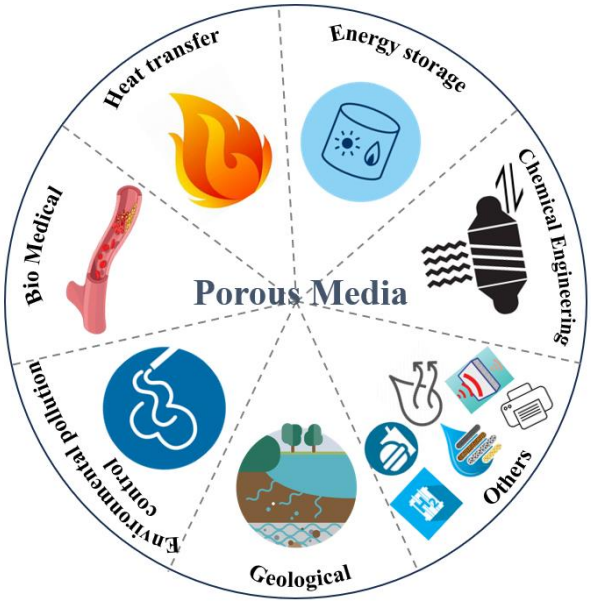

Figure 1.2. A broad view of applications of porous media

1.3.1 Heat transfer

In applications associated with heat and mass transfer, porous media, specifically metallic in nature can be found useful in variety of form, shape and thermo-hydraulic properties. Some of such applications include solar air receivers (Saedodin et al. 2017), microchannel heat sinks (Li et al. 2020), exhaust gas heat recovery, heat exchangers (Sayed et al. 2020), Battery thermal management (Liu et al. 2021), cryocoolers (Garg et al. 2020), regenerators (Boroujerdi and Esmaeili 2015) etc., It is the property of high specific surface area, low density and good thermal conductivity that makes metallic porous structures a highly sought-out candidates for the applications where heat transfer is a major concern.

1.3.2 Energy storage and conversion

Porous media can also be observed in applications involving energy storage (Hoseini et al. 2023) such as latent heat storage supplemented by metal based porous media along with phase change materials, sensible heat storage with the help of porous rocks, porous aquifers used as seasonal underground energy storage to utilize the excess thermal energy during one season (summer) and supply it back during the season when required (winter), concrete thermal energy storage in buildings is also one such example where thermal energy is stored and utilized based on availability and requirement.

1.3.3 Chemical engineering

High surface area, promoting the chemical reactions and controllable mass transfer being the features of porous media, these properties are highly harnessed in the field of chemical engineering (Detmann 2021). Such examples include, catalysts which are porous in nature like mesoporous silica, zeolites etc., are used to enhance selectivity and reaction rates. For processes such as purification of gas porous media like activated carbon are used as adsorbents. Separation of mixtures using distillation process are found to be achieved with high efficiency with the usage of porous media. In electrochemical systems such as batteries and fuel cells porous media are used as electrodes that can not only facilitates required chemical reaction but also promote efficient transport of both reactants and the products within the system. Chemical reactors such as fluidized bed reactors are commonly used with the porous bed as a major component of the system that promotes optimized flow rates and heat transfer suitable for various chemical processes. Other applications include membrane technology where porous membranes are the key components that are harnessed for their property of selective permeability.

1.3.4 Biomedical

Biocompatibility, possibilities of various pore sizes and permeability makes porous medium made up of specific materials a good candidate in biomedical applications (Udenni Gunathilake et al. 2017) that include, implant and prosthetics making which uses porous medium that blends with the surrounding environment and promote transportation of nutrients. During the process of dialysis porous membranes are used to differentiate waste products and excess fluid content from the blood. Artificial organs also make use of porous medium as a building block or supporting system. In order to achieve controlled drug delivery nano porous media are used that helps in encapsulation of therapeutic fluids and targeted delivery. In biomedical field, knowledge of flow through porous media is also used to numerically study blood flow analysis through blood vessels under several conditions such as aneurysms, stenosis etc., transportation of gases like oxygen and carbon dioxide are also investigated under various conditions using the knowledge of porous media.

1.3.5 Environmental pollution control

Porous media are found useful in controlling environment pollution majorly comprising air (Mishra et al. 2018) and water pollution (Shu et al. 2023). Activated carbon in porous form is used in air pollution control devices such as catalytic converters and carbon absorption system. They are also known to capture pollutants that are volatile, and can absorb odors and hazardous gases emitted from industries. Porous materials are also used to clean up oil spill over water bodies. Porous media are found extremely useful in promoting green infrastructure by treating runoff water from pollutants before they reach ground water or its natural water body. Knowledge of porous media is also being implemented in capture and storage of carbon dioxide for longer duration. Hence water pollution from variety of ways and air pollution are found to be efficiently treatable with porous media.

1.3.6 Geological sciences

Porous nature of soil and rocks are well known, and it is for this reason the knowledge of porous media plays a crucial role in many geological processes (Ma and Ranjith 2019) involving flow of fluids such as crude oil, gas and water. Water supply, ground water regeneration, transportation of contamination etc., are used to analyze and take required precautions with the help of porous media modelling using numerical techniques. In oil and gas industries, knowledge of flow through porous media plays a vital role in deciding the requirements for a specific production rate and in efficient extraction of the resource. The efficiency of geothermal systems is dependent on knowledge of porous media for efficient extraction of geothermal energy. Porous media modelling is also found to be useful in predicting landslides based on water flow and pressure conditions. Many more such applications can be seen in geological sciences where porous media and its knowledge being highly advantageous.

1.3.7 Other miscellaneous applications

Porous media can be seen in many other applications including, inkjet printers, food storage, dehumidification, sound absorbent, combustion, water filters, air conditioning, drying etc.

1.4 MODELING POROUS MEDIA

1.4.1 Representative Elementary Volume (REV) Approach

Porous media exhibit intricate and irregular geometries at the microscopic level, characterized by a network of interrelated pores and solid matrix. The irregularities in the porous structure can lead to local variations in velocity, pressure and temperature. Flow through porous media is also characterized by nonlinear phenomena due to the occurrence of additional inertial effects (form drag) along with the viscous effects that arises due to the complex interactions between the fluid and the solid matrix in porous media. The conventional Navier-Stokes equations assume a linear relationship between fluid velocity and pressure, neglecting the nonlinear effects. In order to accurately model porous media, it is necessary to incorporate the effects of the microscale details and their interactions with the macroscale behaviour (Das et al. n.d.; Nield and Bejan 2017). The REV approach provides a framework for bridging these length scales by considering a representative volume that captures the essential features of the porous medium. The pictorial representation of such REV is shown in Figure 1.3.

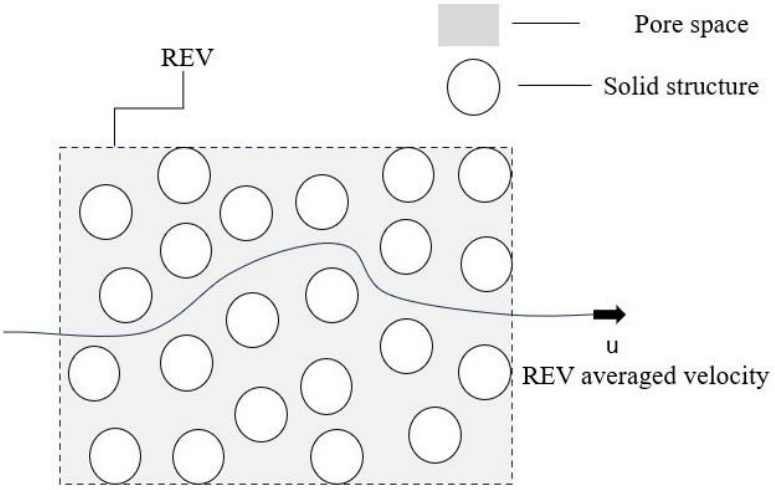

Figure 1.3. Sketch describing representative elementary volume (REV)

The representative elementary volume (REV) approach is a methodology used to model porous media by considering a representative volume that accounts for the average properties and behaviour of the porous media. The REV aids in capturing the relevant flow and heat transfer characteristics of the porous system accurately. Within the REV, the complex microscale processes can be approximated using simplified models or

numerical techniques using computational fluid dynamics (CFD) methodology. The REV approach nonlinearities in pressure-velocity relation can be appropriately considered and temperature fields corresponding to, either effective thermal conductivity of the fluid saturated porous media or distinct fluid and solid properties can be formulated.

1.4.2 Pore Scale Modelling

In contrast to REV modelling approach that simplifies the analysis by considering a representative volume that captures the average behaviour of the porous material at a larger scale, the pore-scale modelling focuses on capturing the detailed fluid flow and transport processes occurring at the microscopic level within individual pores (Chen et al. 2022). It requires high computational resources whereas, REV modelling, on the other hand, simplifies the system by averaging properties over a representative volume.

While focusing on the implementations, pore-scale modelling is found to be useful in studying phenomena such as capillary effects, dispersion, and reaction kinetics. It is employed in various fields, including petroleum engineering, geosciences, and materials science, to analyse and optimize transport processes in porous media. REV modelling, on the other hand, is commonly used in macroscopic flow and transport studies where the focus is on large-scale behaviour. It is often employed in reservoir engineering (Okoroafor et al. 2022), groundwater flow modelling (Cattaneo et al. 2016), porous media incorporated thermal exchange devices modelling (Qi et al. n.d.) and porous media characterizations. Both approaches have their respective advantages and are used in different contexts based on the specific purposes. In the present work REV scale modelling technique is used to analyse the thermo-hydraulic characteristics of metal based porous media.

1.5 GOVERNING EQUATIONS

1.5.1 Darcy's Law

Darcy's law is regarded as the founding stone of all REV based porous media models that for the first time demonstrated pressure drop and velocity relationship in a porous media and provided respective empirical formulation. The background of its formulation, its advantages and limitations are detailed as followed.

1.5.1.1 Darcy Formulation

Darcy illustrated that the flow rate of the fluid passing through the porous medium was proportional to the gradient in pressure across the test section and the cross-sectional area of the test section filled with porous medium, and it was found to be inversely proportional to the viscosity of the considered fluid (Nield and Bejan 2017) as depicted in Eq. (1.2).

$$\dot{Q}\ \alpha\ A\left(\frac{1}{\mu}\right)\left(-\frac{\Delta P}{L}\right) \tag{1.2}$$

Permeability of the porous medium was resulted as the suitable proportionality constant to the above equation that eventually arrived at the expression for the average velocity through the porous medium as given in Eq. (1.3).

$$u = -\left(\frac{K}{\mu}\right)\left(\frac{\Delta P}{L}\right) \tag{1.3}$$

Where, 'u' is the averaged REV velocity, 'P' is the pressure at the pore scale, 'μ' is the dynamic viscosity of the fluid and 'K' is the permeability of the considered porous medium. The REV for treating Darcian flow through porous medium can now be established by incorporating the REV with additional terms owing to the properties of the porous medium considered as shown in Figure 1.4.

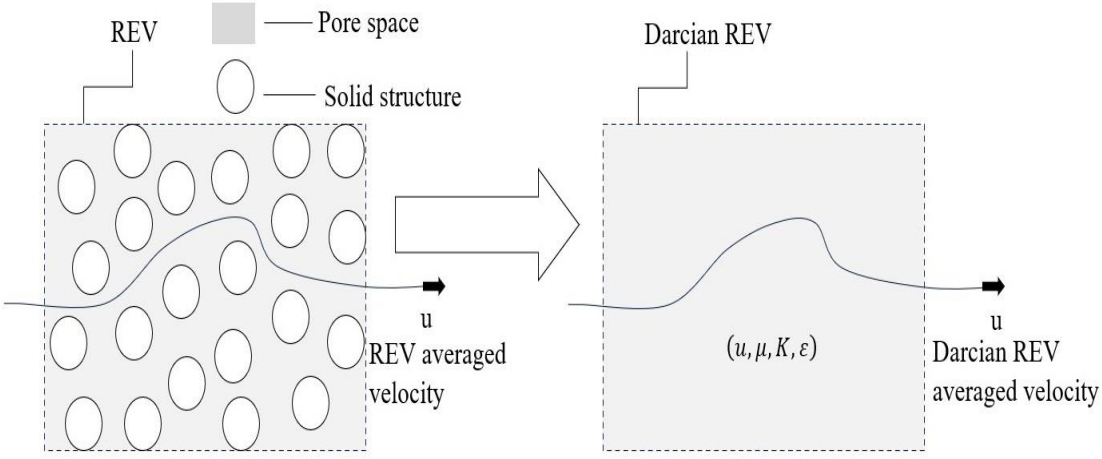

Figure 1.4. Description of Darcian REV with porous media properties.

The local pore-scale velocity 'u*' can be approximated using the porosity value of the considered porous medium as given in Eq. (1.4).

$$u^* = \frac{u}{\varepsilon} \tag{1.4}$$

1.5.1.2 Limitations of Darcy Law

The major limitation of the Darcy Law is associated in the very nature of its formulating scenario which is the creepy flow condition. This makes the Darcy law invalid under flow conditions where inertial effects are much significant in influencing the flow behavior. In various practical applications the flow conditions through the porous media can be witnessed falling in the regime of non-creepy flow conditions, especially while dealing with gaseous fluids that are relatively less viscous in nature and may require special considerations to the original Darcy Law to accurately predict the flow behavior.

1.5.2 Darcy-Extended Forchheimer Law

Significant formulations that later arrived, following the Darcy's work addressed its limitations and gave models that were more generic and applicable to various types of porous media under various flow conditions. Well known model with respect to the above-mentioned aspects is one formulated by Ernst Forchheimer.

Forchheimer in his extended model rightly addressed the situations where, the inertial effects significantly exist which could be a result of complicated geometrical structure in the considered porous medium and higher velocity of the fluid flowing through it, unlike the nature of conditions involved in arriving at the famous Darcy's law where the inertial effects are neglected over the viscous forces. To the existing Darcy's law, additionally a quadratic term is introduced so that the effect of induced form drag or inertial resistance is appropriately treated in the existing Darcy's Law to model flow through porous media (Nield and Bejan 2017). Thereby allowing the more accurate depiction of nature of flow through variety of porous media.

1.5.2.1 Darcy-Extended Forchheimer model formulation

The Forchheimer equation as expressed in the Eq. (1.5) can be seen with the additional term on the right-hand side modifying the existing Darcy's law. The supplementary quadratic term in the Eq. (1.5) accounts for the form drag or the inertial resistance experienced during the fluid flow through intricate porous media.

$$\frac{\Delta P}{L} = -\frac{\mu}{K}u - \frac{F\rho|u|\mathrm{u}}{\sqrt{K}} \tag{1.5}$$

Similar to the usual notations observed in the Darcy's law, here in Forchheimer's permeability of the porous medium is denoted by 'K', 'μ' as the fluid viscosity, ($\Delta P/L$) denoting the observed pressure gradient, fluid density by 'ρ', and 'u' for the average fluid velocity. Second term on the right-hand side of the equation can be seen with the expression 'F' representing the Forchheimer coefficient / inertial coefficient / form drag coefficient as a product of squared average velocity emphasizing quadratically varying relationship between pressure and velocity. The pressure gradient in the porous medium is obtained as a result of the contribution from the momentum sink terms that comprises of Darcy's viscous resistance term (first term on the right-hand side of Eq. (1.5)) as well as Forchheimer's extended inertial resistance term (second expression on the right-hand side of Eq. (1.5)). In other words, the pressure gradient required for the flow through the porous media for given velocity is now contributed by the Forchheimer's inertial resistance term along with the Darcy's viscous resistance term. It can be noted that in inertial resistance term the notation to one of the velocity vector terms is written in modulus to counter the effect on the sign due to negative velocity that may arise from change in the flow direction (due to adverse pressure gradient), which will thereby accordingly address the effect of inertial resistance either as source or sink for the flow. In the Forchheimer's equation for relating velocity and pressure as shown in Eq. (1.5) we may observe the non-linear pressure-velocity relationship which is the general scenario while dealing with porous media of complex geometries and relatively high flow velocities.

The representation of REV that considers Forchheimer's modification for flow through porous medium can now be established by incorporating the Darcian REV with the additional inertial resistance factor 'C' or Forchheimer's coefficient 'F' corresponding to the properties of the porous medium considered as shown in Figure 1.5.

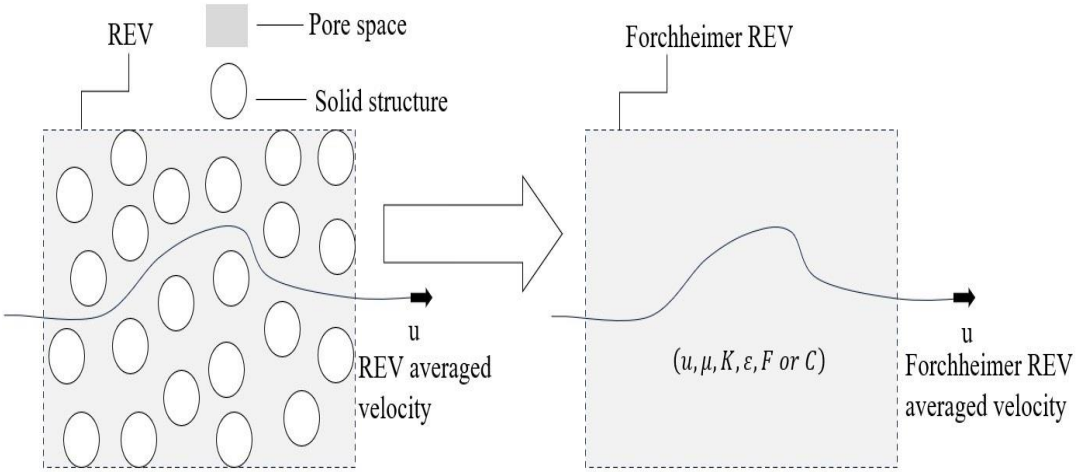

Figure 1.5. Representation of REV incorporated with Forchheimer's modifications.

1.5.2.2 Generalized Darcy-Extended Forchheimer Model for Numerical Solutions

Though Darcy's law and Forcheimer's extension relate pressure drop with velocity based on empirical and theoretical analysis, it mainly emphasizes on viscous and inertial resistances experienced by a fluid during the flow through porous media. In order to numerically model flow through porous media various other factors needs to be addressed in the phenomenon. Which mainly includes acceleration components for the cases of flow through porous media in a domain of non-uniform area which could be the general case in the applications and diffusion of momentum due to viscosity of the fluid.

Acceleration of the fluid can be written as provided in Eq. (1.6) using the Lagrangian reference frame which can be expanded to Eularian frame of reference as given in Eq. (1.7) (Nield and Bejan 2017). Where, 'a' is acceleration of the fluid, and 'u' is the average velocity (REV scaled average velocity) and 'ε' is the porosity of the medium.

$$a = \frac{1}{\varepsilon}\frac{du}{dt} \tag{1.6}$$

$$a = \left(\frac{du}{dt} + \frac{1}{\varepsilon}u.\nabla u\right)\frac{1}{\varepsilon} \tag{1.7}$$

It can be noted that, the fluid that accelerates through the pores of the medium (local velocity) is considered in the acceleration term (Eq. (1.4) can be referred for relation between REV averaged and local velocity).

The viscous diffusion term can similarly be expressed as given in Eq. (1.8). This viscous force is due to the confined walls of the flow domain unlike the viscous forces in the Darcy's resistance term where it signifies the effect of viscous force experienced due to fluid and porous structure interaction.

$$\frac{\mu}{\varepsilon}\nabla^2 u \tag{1.8}$$

The comprehensive mathematical formulation for modelling flow through porous media can be arrived by equating the product of mass and acceleration to all the balancing forces experienced by the fluid as shown in Eq. (1.9).

It can be observed that, this generalised comprehensive mathematical equation can be used to solve flow through any porous media where it computationally be discretised into REV scaled volumes that comprises of new porous parameters such as porosity, viscous resistance, inertial resistance arising from local averaging along with fluid property such as viscosity.

The fluid that passes through the porous medium is well known to trace a tortuous path due to which it may experience local adverse pressure gradients (reversed flow behaviour that resists the desired flow) and flow separation. Though this phenomenon can be well treated as acceleration or deceleration, this phenomenon is blended within the equation during the REV averaging stage in terms of correction given by Forchheimer using inertial resistance term. However, the explicitly written acceleration terms in the generalised form (Eq. (1.9)) comes into effect while addressing the flow which is unsteady in nature and/or while the flow domain is of non-uniform cross-sectional area.

$$\rho\left(\frac{du}{dt}+\frac{1}{\varepsilon}u.\nabla u\right)\frac{1}{\varepsilon} = -\frac{\Delta P}{L}-\frac{\mu}{K}u-\frac{F\rho|u|u}{\sqrt{K}}+\frac{\mu}{\varepsilon}\nabla^2 u \tag{1.9}$$

Observing Eq. (1.9) one can realise that when porosity of the medium reaches unity and the permeability reaches to infinity (meaning no restriction for the flow by the structures of the medium) the generalised equation of Darcy-extended Forchheimer model takes the form of the classical Navier-Stokes equations. Thus, sharing common features to that of Navier-Stokes equations such as, nonlinear nature of partial differential equations that are first order in time and second order in space.

Therefore, one can employ CFD numerical techniques suitable for solving Navier-Stokes equations to solve generalised Darcy-extended Forchheimer equation and obtain the solution for the flow field predicting the nature of fluid flow through the considered porous media.

1.5.3 Energy equations for modeling heat transfer through porous media

Energy equations for modeling heat transfer through porous media have been known to be formulated in two ways. In one way the whole fluid saturated porous medium is perceived as a whole new kind of medium with effective properties defining the medium taking properties of both fluid and solid structures into account. The other way of approach is to treat the properties of fluid and solid structures separately acknowledging their actual contribution for the heat transfer between themselves (fluid in the pore space and the surrounding solid structure). The model obtained from the former consideration is known as thermal equilibrium model and the later as thermal non-equilibrium model. Both having their own advantages and suitability of implementation under specific scenarios are detailed as followed.

1.5.3.1 Thermal Equilibrium Model: A Single Equation Energy Model

Thermal equilibrium model as the name suggests assumes equilibrium between the temperatures of the fluid and solid fractions of the whole fluid saturated porous medium. The resulting energy equation is straight forward and similar to the conventional energy equation (Nield and Bejan 2017). For a homogenous fluid domain which is incompressible in nature having no heat generation, negligible viscous dissipation with constant properties and negligible radiation effects, conventional energy equation takes the form as given in Eq. (1.10).

$$\rho_f C_{pf} \left(\frac{\partial T}{\partial t} + u.\nabla \mathrm{T} \right) = \lambda_f \nabla^2 T \tag{1.10}$$

Where, 'λ_f' represents fluid's thermal conductivity, subscript 'f' denoting the properties specific to the fluid and all other notations representing usual parameters such as density, temperature, time and average velocity.

A similar equation can be used for modeling heat transfer through porous medium if the parameters required to solve the equation and the interested variable that is

temperature, all being scaled down to the REV averaged quantities using a new set of effective properties unique to the given fluid saturated porous media. This approach ultimately solves for the average temperature in the REV as though the fluid and the solid structures are in thermal equilibrium and the respective properties required to solve the equation are new set of effective properties and not individual properties of the fluid and the solid structures of the porous medium. The resulting equation for solving heat transfer through porous media is provided in Eq. (1.11). However, it can be noted that, as the expression representing derivative of time corresponds to the rate of change of energy (sensible energy) of the whole porous medium averaged over the REV, it is multiplied with effective value of 'ρC_p' for the whole fluid saturated porous medium represented by the subscript 'p_m'. Contrarily as the advection term represents the transport of energy exclusively by the fluid medium, 'ρC_p' term here refers to that of the fluid medium denoted by its respective subscript 'f'. Thermal conductivity described in this equation is for the whole fluid saturated porous medium denoted by the symbol 'λ_{p_m}'.

$$\left(\rho C_p\right)_{p\_m} \frac{\partial T}{\partial t} + \left(\rho C_p\right)_f u.\nabla \mathrm{T} = \lambda_{p\_m} \nabla^2 T \tag{1.11}$$

It can be noted that the effective properties for a fluid saturated porous medium can be modelled in variety of forms and simplest approach being the 'series model' or the mixture model that yields the upper limit and followed by the 'parallel model' that yields the lower limit.

Thermal equilibrium model is simple in nature and can be implemented comfortably under the situations where the fluid and the solid structures of the porous medium are more likely to achieve thermal equilibrium. This a likely situation where fluid and the solid structures have similar thermal conductivity or when the fluid flow is very slow enough to be in thermal equilibrium with the solid structures. However, this model fails to predict accurate heat transfer through porous media when thermal equilibrium between the fluid and solid structures is not the scenarios. This situation can be observed in scenarios where the thermal conductivities of the fluid and the solid medium are highly dissimilar and/or the fluid velocity is high enough to always have a

significant temperature gradient between the solid and fluid medium of the fluid saturated porous medium.

1.5.3.2 Thermal Non-Equilibrium Model: A Dual Equation Energy Model

Following the limitations of the thermal equilibrium model, consideration of significant heat transfer between fluid and the solid medium of the fluid saturated porous medium and modeling the same is achieved with the help of two equations representing thermal non-equilibrium between the fluid and solid phases.

In order to quantify heat transfer between fluid and solid phases, two separate energy equations each for fluid and solid phases are considered with a common heat transfer phenomenon as a link to the equations coupling the nature of heat transfer between the fluid and solid structures of the fluid saturated porous medium (Nield and Bejan 2017). This is achieved by treating the energy equations of solid and fluid phases with a heat source term and a heat sink term respectively (if fluid's temperature is more than that of the solid) or vice versa (if fluid's temperature is less than that of the solid). It is this term through which both of the equations are coupled to signify a common heat transfer phenomenon. Following these physical conditions, the expressions of energy transfer for fluid and solid medium can be obtained as shown in Eqs. (1.12) and (1.13) respectively for the case when fluid temperature is lesser than that of solid which is a general case in thermal management.

$$\varepsilon\left(\left(\rho C_p\right)_f \frac{\partial T_f}{\partial t} + \left(\rho C_p\right)_f \frac{u}{\varepsilon}.\nabla T_f\right) = \lambda_f \nabla^2 T_f + Q_{f\leftarrow s} \tag{1.12}$$

$$(1-\varepsilon)\left(\rho C_p\right)_s \left(\frac{\partial T_s}{\partial t}\right) = \lambda_s \nabla^2 T_s + Q_{s\leftarrow f} \quad \text{or} \tag{1.13}$$

$$(1-\varepsilon)\left(\rho C_p\right)_s \left(\frac{\partial T_s}{\partial t}\right) = \lambda_s \nabla^2 T_s - Q_{f\leftarrow s}$$

It can be seen that fraction of solid $(1-\varepsilon)$ and fluid (ε) phases are appropriately treated in the heat capacity term such that the combined equation solves for the overall energy balance between the solid and fluid fraction that forms the whole REV of a fluid saturated porous medium. Unlike in thermal equilibrium model the thermo-physical properties here employed are not effective properties of the whole fluid saturated porous medium but the individual properties of fluid and solid phases. It is quite comprehensible that, the energy source terms here used are equal in magnitude but

apposite in sign due to continuous energy transfer between solid and fluid phases specific to the direction of the gradient (based on which of the two phases are considered to be cold or hot). For the situation where fluid phase is cold and solid phase is hot the respective source terms expressed in Eq. (1.12) and (1.13) can be explicitly written as shown in Eqs. (1.14) and (1.15).

$$Q_{f \leftarrow s} = h_{sf} a_{sf} \left(T_s - T_f\right) \tag{1.14}$$

$$Q_{s \leftarrow f} = (-Q_{f \leftarrow s}) = h_{sf} a_{sf} \left(T_f - T_s\right) \tag{1.15}$$

Terms 'h_{sf}' and 'a_{sf}' appearing in Eqs. (1.14) and (1.15) are respectively known as 'interfacial heat transfer coefficient' defined for the heat transfer between fluid and solid phases and 'specific area' or 'area density' defined as the surface area per unit volume (m^2/m^3).

Thermal non equilibrium model can be observed to be more generic in nature and will even yield for the equation of thermal equilibrium upon several treatments involving the assumption of thermal equilibrium condition which can be done by nullifying the source terms in the Eqs. (1.12) and (1.13) meaning no heat transfer between the solid and fluid phases which is physically feasible when interfacial heat transfer coefficient (h_{sf}) approaches infinity, indicating a quick transfer of energy between the phases such that the difference between the temperatures of the phases becomes zero ($T_s - T_f = 0$). Thus, thermal non-equilibrium model for predicting heat transfer is not only suitable for conditions where heat transfer between solid and fluid phases are evident such as in cases of high difference in thermal conductivities of the phases and/or high velocity conditions that promotes the temperature gradient, but also for the otherwise scenario as a generic equation.

1.6 ORGANIZATION OF THESIS

The thesis is aimed at addressing the issue of pressure drop that always accompanies the benefit of heat transfer enhancement commonly associated with metal based porous media. In this regard structural aspects of metal foam type porous media, namely porosity and pore density are extensively analyzed in order to emphasize the effect of combinations of these structural properties that could exhibit various flow resistance

and heat transfer characteristics. Further, thickness of porous medium being another flow and heat transfer influencing parameter, is considered along with the variations of the earlier mentioned structural properties, and various heat transfer enhancement and flow resistance minimization potentials of metal foam type porous medium are analyzed under a broad perspective using a suitable multi objective optimization tool. Then, the required expressions for describing the flow and heat transfer influencing morphological properties of wire mesh porous structures are obtained that helps in numerical modeling of such media. Their thermohydraulic potentials and advantages are analyzed with various structural and thickness combinations under various stacking types.

The whole thesis is aligned into eight chapters, and the contents of each chapter are summarized as follows:

Chapter-1: In this chapter an elaborated introduction to porous media is provided including various aspects such as types of porous media, terminologies involved, applications of such media in various applications. Further numerical modeling aspects of such medium is elaborated, by providing information on the types of modelling techniques and governing laws associated with their flow and heat transfer phenomenon.

Chapter-2: In this chapter, a detailed review of previous works reported in literature is made highlighting on the issues associated with conventional way of analyzing metal foam like porous media for their thermo-hydraulic behavior. Works pertaining to stacked wire mesh porous media focusing on the expressions required for their numerical modeling are discussed. Further, works that report thickness as pressure drop reduction parameter are discussed and out of the insights from literature review, motivation and scope for the research work is presented followed by the defined objectives of the present thesis.

Chapter-3: This chapter provides a detailed insight into the methodology followed in the present work in order to achieve the considered objectives. Experimental domain and the numerical domain, boundary conditions, numerical details, grid independent

study, essential correlations, validation studies are presented along with a detailed description on the TOPSIS techniques that is utilized in the present work.

Chapter-4: This chapter emphasizes on the effect of the various combinations of the twin structural property of a metal foam porous medium namely porosity and pore density on flow and heat transfer characteristics. Starting with how interfacial properties affect flow and heat transfer phenomenon, connection of these properties with changes in the combinations of the mentioned structural property, correlations of wall Nusselt number are provided for various convection regimes that signifies the consideration of effect of these properties in their various combinations, predominantly associated with forced convection phenomenon compared to that in natural and mixed convection regimes.

Chapter-5: In this chapter, along with the variations in porosity and pore density of the metal foam porous medium, thickness of such medium is simultaneously studied in order to comprehend their potential to minimize pressure drop and maximize heat transfer. Various trade-off scenarios exhibited by these porous media of various structural and thickness configurations are analyzed arriving at the suitability of a given structural and thickness conditions to fulfill various affordable cost (pressure drop) and desired benefit (heat transfer) scenarios using TOPSIS a multi-objective multi-attribute decision making technique.

Chapter-6: In this chapter, essential expressions that describe the key flow and heat transfer influencing morphological properties such as porosity, pore density, interfacial specific surface area, relating to fiber diameter, pore width of stacked woven wire mesh porous structures of various stacking types are derived that are required to numerically model such type of porous medium. Interpretations of the arrived expressions are made emphasizing on their appropriateness. This enables the analysis of potentials of such type of porous media through numerical simulations that are elaborately discussed in chapter 7.

Chapter-7: In this chapter potentials of stacked woven wire mesh porous structures are analyzed under varied structural and thickness combinations under different stacking conditions. Various trade-off scenarios between the ability of stacked wire mesh

structures to enhance heat transfer and their ability to curtail flow resistance are comprehensively analyzed.

Chapter-8: In this chapter all the work presented in the thesis is summarized and key conclusions out of the studies are drawn. Further, the aspects of future scope arising out of the present work is provided.

CHAPTER – 2

LITERATURE REVIEW

2.1 INTRODUCTION

Thermo- hydrodynamic characteristics of porous media may not be a single parameter dependent phenomenon, instead it is likely to be dependent on various aspects like thermal conductivity of fluid–foam sample, type of porous media, its structural configuration (porosity and pore density), filling ratio (fully filled or partially) and so on. Among the structural variations, looking at only one variable aspect i.e., either porosity or pore density and analyzing on thermo-hydrodynamic characteristics of a porous medium would be incomplete. It is very much important to study the effect of ordered variation in structural properties of the porous samples, because every possible combination of porosity and pore density of a porous sample has the potential to exhibit altered thermo-hydrodynamic characteristics. Similarly, the changes in the thermo-hydraulic characteristics that can be observed with the introduction of other parameters such as thickness, type of porous media along with the structural variations seems promising to provide improved optimal choices of metal based porous media for many engineering applications demanding specific thermo-hydraulic criteria.

In this regard the present chapter discusses about the features of metal foams, wire mesh porous media based on the observations made in previous studies reported in the literature and thereby noting the research gap and the scope of research in the area, leading to the objectives of the present work.

2.2 METAL FOAMS AND THEIR THERMO-HYDRAULIC CHARACTERISTICS

Calmidi and Mahajan (2000a) performed experimental as well as numerical investigation of metal foams of porosity ranging from 0.89 to 0.97 each with various pore densities (5, 10, 20 and 40 PPI). Using air they examined these foams under forced convection and obtained Nusselt number for each of the cases. In numerical approach, local thermal non-equilibrium model was assumed to model heat transfer. This study

formulated interstitial heat transfer coefficient with the help of physical influences. Through this study the authors found that the thermal dispersion effect is very less for air-metal-foam combinations and could be ignored in numerical modeling. Also, existence of thermal non equilibrium between metal foam and air was emphasized in this study.

Kamath et al. (2013) conducted a vertical channel forced convection experimental study, where aluminum and copper foams were investigated for thermo-hydrodynamic performances. The study mainly highlighted the effects of thermal conductivity, thickness and porosity of the foam samples. Increased heat transfer was witnessed with increase in thickness of the foam. Interestingly, pressure drop was found to be not much significantly varying with thickness. It can be noted that the authors used foam samples that had different porosity and pore density combinations in random. They provided Nusselt number correlation which was found to be a strong function of thickness and Reynolds number. In terms of heat transfer only 4 percent increase was observed for copper foams in comparison with its aluminum counterparts. Hence aluminum foams were preferred over copper ones for a better cost and benefit trade-off.

Albanakis et al. (2009) made an experimental investigation giving comparative performances of metal foams of distinct materials on heat transfer and pressure drop in volumetric concentrated solar receivers. The study highlighted on pressure drop correlations associated with several metal foams and found to be in accordance with Darcy-Forchheimer law. In terms of heat transfer the study concluded that foams of Nickle material was more than that of Inconel material. The effects of varying structural parameters of any considered foams were not emphasized in these studies.

In an experimental study by Mancin et al. (2010) evaluated heat transfer co-efficient of seven different aluminum foam samples subjected to airflow and their thermo-hydraulic performance was studied that was restricted to foam samples of limited structural variations.

Sener and Yataganbaba (2016) performed experiments to evaluate the performance of aluminum foams of two pore density (10PPI and 20PPI) in terms of thermal enhancement factor (TEF) in a channel where 20PPI foam samples showed greater TEF

than 10PPI for both laminar and turbulent conditions. Contradictory to the results of this study, an experimental study by Arbak et al. (2017) revealed that 10PPI foam sample performed better than 20PPI foam whereas 40PPI foam dominated both 10PPI and 20PPI foam samples in terms of heat transfer enhancement ability.

Another such study that strengthens the ambiguity in understanding the performance of foams either based on the porosity or the pore density is evidenced in a study by (Nithyanandam and Mahajan 2018) on the performance of metal foam heat exchanger in thermo electric generators (TEG), where 5 PPI foams performed better than 20PPI foams.

Xia et al. (2017) showed the effect of pore density and porosity of foam samples on heat transfer behavior in a tube filled with metal foams. The study considered Nickel foams of two distinct structural properties, copper foams of five distinct structural properties and SiC foams of two distinct structural properties. However, the selection of foam samples of different structural properties was on a random basis.

Metal foams as an application in miniaturized condensers was studied by (Ribeiro and Barbosa 2013), in which comparative results were discussed between foams of pore density 10PPI and 20PPI with corresponding porosity of 0.893 and 0.947 respectively. A similar study was reported by Lin et al. (2013) proposing a graphite foam filled heat exchanger for vehicle cooling application. Different configurations were investigated for low flow resistance using numerical approach. Results showed that the wavy corrugated foam presents high heat transfer and low flow resistance. The study lacked predetermined idea on performance contribution of the considered foam sample owing to its structural configuration.

Baragh et al. (2018) experimentally represented the effect of different arrangements of porous media under forced conditions in a channel. Results showed that a fully filled channel gave the best heat transfer augmentation for both turbu- lent and laminar flow regimes, whereas the annulus shaped porous zone gave the best thermal performance in turbulent flow conditions. The same study would have given better results if the selection of samples in the study were based on predetermined knowledge on performances of the samples corresponding to their structural properties.

Calmidi and Mahajan (2000b) studied forced convection in high porosity metal foams. Various aluminum metal foams of different porosity and pore density were considered for experimental as well as numerical study. However, like the other studies, it failed to represent the performance of metal foams based on the combination of its structural properties.

Mancin et al.(2013a) in their study considered 21 aluminum and copper foams falling under various structural property combinations in a random fashion whose pore density ranged from 5PPI to 40PPI and porosity from 0.896 to 0.956. Existence of foams of various combinations of structural properties can be witnessed from this study and inadequate collective analysis on variation of heat transfer and flow resistance with ordered variation in structural properties of the foam samples can be witnessed.

Kim and Kim (2019a)examined thermo-hydrodynamic behaviors of nickel and copper foams for heat exchangers. New correlations to find heat transfer co-efficient was given taking foam geometry and material into consideration. This study reported that foams of higher porosity and higher thermal conductivity perform better in single phase flow. However, performances of foams in this study were categorized based on only one structural property i.e., porosity along with thermal conductivity of the foam material.

Lai et al. (2019) studied the effect of pore density of coated hydrophilic foams on heat transfer and pressure drop when subjected to wet air flow. They considered foams of five different pore densities all of them having same porosity condition, limiting the study to restricted structural variables. In this experimental study, coated metal foams of 5, 10, 15, 20 and 40 PPI pore density each with porosity of 0.95 were considered and examined under hydrophilic coating and non-coating conditions subjected to flow of air with different humidity. At lower humidity the heat transfer was found to increase with increase in pore density due to increased surface area for heat transfer. Increase in pressure drop was found for increase in pore density at all humidity conditions.

Sun et al. (2020) in their study emphasized on heat transfer enhancement with increase in porosity as well as with increase in pore density conditions, with the help of pore scale simulation. The study considered 0.9, 0.87 and 0.82 porosity foam samples of 40, 20 and 10 PPI pore density respectively. Pressure drop was observed to increase with

increase in pore density and decrease with increase in porosity. Interestingly, pressure drop was observed to be more sensitive to porosity than pore density. In terms of heat transfer they found it to be increasing with increase in pore density while they observed it to be decrease with porosity. It can be noted that these observations were made by metal foams that exhibit random porosity and pore density combinations whereas the same behaviors may be exhibited differently when observed for metal foams of orderly varied structural combinations.

As far as numerical modeling of heat transfer through porous media is concerned, selection of thermal transport model plays a determining role in predicting temperature fields. According to the assumption of the classical theory of porous media, local thermal equilibrium exists between the fluid phase and the solid phase. However, the heat transfer rate between solid and fluid may not be quick enough to achieve a local thermal equilibrium due to the drastic change in the thermal conductivity of two-phase Gandomkar and Gray (2018).

Lin et al. (2016) compared LTE and LTNE heat transport models. The study showed that LTNE and LTE models resulted in the near same Nusselt number inside aluminum foam when air velocity was higher meaning aluminum is in a thermal equilibrium state with air. Besides a higher interfacial heat transfer coefficient is required for the aluminum foam to reach a thermal equilibrium state as the height of the foam is reduced. This study showed that LTE model can be applied to predict the thermal performance at a higher fluid velocity or for the case with a large height. Whereas for lower fluid velocity thermal equilibrium assumption will not be valid.

A numerical study by Torabi et al. (2015) analyzed heat transfer and entropy generation in a channel partially filled with porous media. The study found that LTNE approach yields more accurate results on temperature fields producing realistic Nusselt number and Entropy generation rates.

Kumar et al. (2019) numerically studied re-generators for a sterling cryocooler using LTE and LTNE models. It was identified from the study that both the models predict the overall temperature variations closely but accurate predictions were given on adopting LTNE model. A similar numerical study was done by (Xu and Gong 2018)

investigating the effects of graded copper foams on Nusselt number and friction factor under LTNE conditions where, suitability of the model can be observed.

2.3 ESSENTIAL THERMO-HYDRAULIC FEATURES OF WOVEN WIRE MESH POROUS MEDIA

Stacked woven wire-mesh has been known to be aiding the thermo-hydraulic performance in many prominent engineering applications and has been used as the conventional heat transfer medium in applications like regenerators of Sterling engine Xiao et al. (2017) and other heat exchanging devices.

Jiafei et al. (2021) recently reviewed forced convection in porous structures emphasizing the expressions describing morphological characters such as porosity, fiber diameter, pore diameter and surface area density and correlations depicting thermo-hydraulic behaviors of porous media of various types like metal foam, lattice frame, packed bed and woven wire-mesh. Scarcity of comprehensive expressions (cross relations) for describing the morphological characteristics of woven wire-mesh type of porous media can be witnessed compared to the widely discussed and established cross relations for other kind of porous media (especially open-celled type porous media).

Kang (2015), provided an elaborated review on metallic woven wire structures emphasizing on mechanical, topological and thermal properties of various types of woven-wire porous structures. Single-layered and multi-layered woven wire meshes have been collectively summarized in this work, where the authors emphasized on various aspects like fabrication techniques involving pre-forming, assembling, post-forming, fixing, post treatment and machining. The study also summarized the characteristics of woven-wire metal structures based on relative density and equivalent strengths. In terms of thermal and hydraulic behavior, the study showcased several studies that acknowledge the benefit of wire mesh in aiding the heat transfer and minimizing the pressure drop compared to metal foams.

Sypeck (2001), proposed a textile-core, a multi-layered woven wire mesh where the porous block of woven wire-mesh is formed by node to node (inline) stacking of the weaved wire mesh screens which has received good attention among the plethora of existing and possible metallic woven wire-mesh structures, as variations in cell size and

porosity can easily be achieved. Obtaining such potentially less expensive porous structures were demonstrated using textile-based technique which resulted in topology that can allow fluid flow with less flow obstruction while aiding the heat transfer.

Tian et al. (2007) experimentally investigated heat transfer and flow resistance in textile-core woven wire-mesh porous structure. The study demonstrated the effect of porosity and cell-topology on flow resistance. Heat transfer was attributed to surface area density, porosity and solid conductivity. The study highlighted that, at a given flow rate, surface area density that depends on pore density and porosity that in turn depends on fiber diameter and cell size plays a major role in heat transfer augmentation. Textile based woven wire porous structures made of copper were compared with conventional metal foam of same material and found that the heat transfer of porous structure obtained from woven wire mesh was on par with that of the copper foams that had similar specific surface areas. However, the benefit of reduced pressure drop was demonstrated in this study with the use of wire mesh structures compared to conventional open-celled foam.

Costa et al. (2013) investigated pressure drop in stacked woven wire structures as an application in stirling engine regenerator. Exact three-dimensional geometries were modeled that considered aligned and misaligned stacking. Flow through the wire-mesh porous block was accomplished numerically and respective correlations for friction factor was obtained in terms of hydraulic-diameter based Reynolds number and wire diameter. Since the study involved exact geometry simulations, discussion related to parameters that are essential for flow models of such porous medium was not emphasized without which numerical modeling of such zones cannot be accomplished.

Costa et al. (2014) in their another work, discussed heat transfer aspects of woven wire mesh porous structures as an application in stirling engine regenerator by giving Nusselt number correlations. They observed that, wire diameter and porosity combinations highly affected wire mesh porous structure's geometrical aspects, and heat transfer area. They reported decrease in volumetric porosity for same wire mesh increases the specific heat transfer area. However, detailed illustration or deeper insight towards such changes in porous parameters was not dealt in the study. Also, the study emphasized on the

requirement of in-depth study to individually distinguish the influence of wire mesh geometrical parameters, specific surface area and volumetric porosity.

Bussière et al. (2017) made an experimental analysis on flow resistance in stacked woven wire-mesh used in electrical safety. This study emphasized on assessing drag coefficient and pressure drop of such woven wire-mesh screens and their stacked arrangement in order to increase the efficiency of circuit breakers. They considered eight different wire mesh stacks of almost same porosity ranging between 0.61 to 0.68, however with different specific surface area as a result of varied wire diameters. Specific surface area of these stacked wire mesh porous structures ranged from 1272 to 9167 (in m^3/m^2). This paper also hints at possibility of various combination of porosity and pore density (due to varied fiber diameter) that can potentially alter the flow resistance by significant margin.

Armour (1968) elaborately studied flow through woven wire-mesh layers of five various weave patterns. In each of the considered weave patterns, various diameters of wire fibers can be seen resulting in porosities of close magnitudes, implying the existence of various combinations of porosity and pore densities resulting in different specific surface area. Also, expressions for screen thickness, specific area, porosity and pore diameter is provided for the considered woven wire-mesh screen layers in this study. However, it can be noted that these expressions are exclusive to single mesh screen layer and not for porous media formed from the stacks of wire-mesh screen which is the conventional way of incorporating them for any heat exchange applications.

Garg et al. (2019) in a recent study, performed numerical study of regenerator for stirling cryocooler using porous media modeling technique to simulate flow and heat transfer through stack of stainless-steel wire-mesh screens. The part containing the stack of wire-mesh screens was modelled as porous medium. They used both the energy models namely, equilibrium and non-equilibrium model and illustrated the higher accuracy level of non-equilibrium model over its counterpart. While modeling wire mesh porous zones in the domain, parameters like porosity and interstitial area density (specific area) were determined based on expressions that are formulated for single wire

mesh screens. However, these parameters are more likely to be varied by great margins due to stacking and the manner of stacking which requires appropriate considerations.

Recently Iwaniszyn et al. (2021) made numerical analysis on thermo-hydraulic behavior in woven wire mesh screens. They used expressions provided by (Armour 1968) to describe specific surface area and porosity of the mesh screens. Correlations for heat transfer and pressure drop were provided in this study, however restricted to single mesh screen layers of various porosity and specific surface area.

Wang et al. (2021) recently obtained analytical model for friction factor as an exclusive function of pore structure and quantified pressure drop using morphological parameters of wire-mesh. This study also defined properties of wire-mesh screens such as porosity and specific surface area using expressions provided by (Armour 1968).

Xu et al. (2007) made an effort to provide expressions for porosity and specific surface area for textile-core type stacked wire mesh porous media for heat exchange application. However, this study simplified the expression by assuming the curved wires woven over the shute wires to be straight. Though with this assumption the authors were able to arrive at a simple expression to calculate the mentioned parameters, possibility of incurring with large errors with increased number of screens in the stack or with increased fiber diameter of the screen wires, is inevitable.

Zhao et al. (2013) gave new expressions to calculate these parameters by considering stacking manner, fiber diameter, compactness factor etc., however, the complexity of the expressions and difficulty in appropriately obtaining compactness factor defined in this study is high. It can be observed in this study that, need of simple and comprehensive expressions that can describe/classify such type of porous medium with the help of information on only few easily available parameters such as mesh-size/pore-density and fiber (wire) diameter that distinguish a given stacked woven wire-mesh type of porous medium corresponding to various stacking scenarios should be of high priority.

Kurian et al. (2016c) made an experimental study on thermo-dynamic performance of brass woven wire-mesh of textile-core fashion which can be observed to be misaligned in stacking in a vertical channel. This study showed that, the overall performance factor

could be achieved at wire-mesh porous samples of higher porosity, though the analysis was made for wire-mesh porous samples of three different porosity, no discussion relevant to pore density that affects the interstitial area density was considered in the study. Similar such analysis could be seen in another study by the same authors (Kurian et al. 2017) (Kurian et al. 2017), but for stainless steel wire-mesh porous block.

Kotresha and Gnanasekaran (2019) made a numerical analysis by considering porous media modeling technique to investigate fluid flow and heat transfer through stacked wire-mesh porous media. However, for modeling, expressions provided by (Xu et al. 2007) and (Tian et al. 2007) were used to obtain specific surface area (one of the parameters that highly affects heat transfer) of the wire-mesh stack of same characteristics as that of (Kurian et al. 2016c). Though the study successfully demonstrated modeling technique of stacked wire-mesh type of porous media, emphasizing the suitability of the used expressions was not the prime focus of the study.

As a result of well-established and debated correlations pertaining to metal foams that provide expressions for describing/categorizing their thermo-hydraulic and morphological parameters, enormous numerical investigations have been performed considering porous media of metal foam type in the field of research to evaluate and/or obtain optimum performance of metal foams involving thermal exchange phenomenon. However, expressions for evaluating thermo-hydraulic and morphological parameters of wire-mesh type porous media can noticed to be not well established/debated in the open literature, without whose knowledge it becomes difficult to perform a comprehensive numerical study using porous media modeling methodology considering such type of porous structures subjected to variation in their morphological properties and stacking manner.

2.4 FEATURES OF POROUS MEDIA UNDER PARTIAL FILLING OR VARIED THICKNESS SCENARIOS

The benefit of augmented heat transfer with the use of metal foams in heat exchanging applications is always compromised with increased pressure drop due to high flow obstruction offered by such materials. It is interesting to note that different combinations of flow and heat transfer influencing aspects of porous media, result in

varied pressure drop and heat transfer, thus allowing the possibility of a better trade-off between enhanced heat transfer with the accompanied pressure drop.

Zuo et al. (2021) numerically investigated optimal design of partially filled metal foams on improved performance of latent heat storage unit. Five various thickness ratios and six filling angles were considered. They demonstrated the reduction of melting time as a result of increased heat transfer due to increase in thickness of the copper foams. However, to decrease the cost involved with foams, optimum thickness conditions were illustrated for optimum melting time that provides relatively higher cost performance along with increased thermal performance. The authors also proposed filling shape-based design criteria suitable for partially filled copper foams in thermal storage system. This study considered various thickness, filling angle and filling shape of copper foams of just one structural combination i.e., 0.94 porosity with 45 PPI pore density.

Li et al. (2018) experimentally investigated on enhancement of heat transfer using partially filled gas tube with metal foams. Copper foams of 0.98 porosity with different pore densities of 10, 20 and 40 PPI at 50 and 75 percent filling rate was considered in this study. In terms of filling rate, they observed increase in heat transfer with increase in filling rate. In terms of pore density, the authors revealed that for a given thickness and porosity condition, increase in pore density increased heat transfer.

Bianco et al. (2021) made an attempt to understand the trade-off between pressure drop and heat transfer in a heat sink with metal foam and metal foam fins. They provided optimization procedures using genetic algorithm to enhance heat transfer at a given pumping power with the help of Pareto plots. Finned metal foam heat sinks showed better optimum performance compared to that of non-finned case. In terms of dimensionless thickness, increase in heat transfer is observed. The study provided one metal foam of structural configuration 0.85 porosity and 40 PPI to be performing at optimum level considering trade-off between pressure drop and heat transfer. However, it can be observed from this study that, justification to such behavior and obtaining performance levels of other foams of different structural combination is difficult using techniques like genetic algorithm.

Siavashi et al. (2018) considered gradient and multilayered metal foams to understand flow and heat transfer behavior with nanofluid as the working fluid. Optimized properties of metal foams and various types of arrangements to enhance heat transfer with reduced pumping power is analyzed in this study. Variation of thermo-hydraulic behaviors with variation in porosity and pore density is emphasized in this study under scenarios where they are varying either continuously or in step wise fashion from center to wall (making the porous filling as gradient and multi layered).

Shikh Anuar et al. (2018) investigated effects of pore density and height of metal foam on pressure drop characteristics experimentally. The study reported enhancement of pressure drop with increase in blockage ratio and pore density. Metal foams of 5, 10 and 30 PPI were considered in the study each having average porosities of 0.92, 0.87 and 0.91 respectively. They demonstrated increased pressure drop with increase in pore density and blockage ratio. However, at higher blockage ratio increased pressure drop was noticed for 30 PPI foam sample compared to 10 PPI. However, the pressure drop at lower velocity was quite insignificant at lower blockage ratio irrespective of pore density. Information on pressure drop with metal foams of other structural (porosity and pore density) combinations would add more insight to this study.

Mancin et al. (2012b) investigated pressure drop and heat transfer through metal foams of 20 PPI and 0.93 porosity with various heights. The study revealed that though pressure drop was same for both the height conditions (20 and 40 mm) and significant change was observed in terms of heat transfer. As a result of same structural condition (20 PPI and 0.93 porosity), the foam-finned surface area efficiency of 20 mm high sample was demonstrated to be better than that of 40 mm height that could significantly increase the global heat transfer co-efficient (product of foam finned efficiency and heat transfer coefficient) for 20 mm height case. This was reasoned because of unchanged specific surface area of foam samples of both heights due to constant structural combination (porosity and pore density).

Jadhav et al. (2021) investigated the performance of metal foams under partially filled scenario of various configurations. Partially filling was achieved by varying the diameter both externally (from core of pipe) and internally (from outer wall). Metal foams of different combinations of pore density and porosity were considered for the

analysis. The study reported the variation in heat transfer corresponding to the metal foam sample and type of partial filling configuration. Though the study did not consider any relation between the porosity and pore density of foam samples, significant variation in terms performance factor could be observed for considered metal foams and filling scenarios.

Singh et al. (2020) investigated the influence of thickness on heat transfer through jet array impingement in foams to arrive at scenario with high heat transfer and reduced pressure drop conditions. 5, 10 and 20 PPI pore density foam samples of 19, 12.7 and 6.35mm thickness was considered for the analysis. Optimum thermo-hydraulic performance for a considered pore density foam sample was reported to be observed at intermediate foam thickness.

2.5 MOTIVATION AND SCOPE OF RESEARCH WORK

A thorough literature survey, has enabled to identify crucial gaps in understanding the thermo-hydrodynamic performance of metal based porous media such as metal foams and woven wire-mesh porous media.

- **Metal foams structural properties (porosity and pore density) in handling the incurred flow resistance:** It can be observed that, the current literature lacks a comprehensive consideration of both the structural properties, namely porosity and pore density, when evaluating the thermo-hydrodynamic behaviour of metal foams. The performance of these foams cannot be solely attributed to individual structural properties; as it can be predicted to be a synergistic effect that requires further exploration. By categorizing metal foams based on their combined structural characteristics, it is possible to arrive at the optimum performance suitable to variety of engineering applications. Exploring this will not only provide enormous choices for the selection of foam samples for a given problem, but will also provide a deeper understanding of the nuanced interactions between twin structural properties (porosity and pore density), paving the way for efficient utilization of these materials particularly in handling the penalty of increased flow resistance associated with application of such media along with the benefit of enhanced heat transfer.

- **Wire mesh porous media, its potential and numerical modelling:** Wire mesh porous medium has several advantageous towards controlling the flow and heat transfer behaviour, as it provides easy means of variations in its porous conditions. The ease with which it can be formed in many varieties, just with modification of its easily variable fibre diameter is the highlight of this type of porous media. The literature review highlights a significant gap concerning expressions required for modelling stacked woven wire-mesh porous media. This gap limits the diversity of numerical studies exploring the flow and heat transfer characteristics of such media. Addressing this by providing expressions that detail the morphological features of stacked wire-mesh porous media will enable the categorization of various samples, considering parameters like porosity, specific surface area, fibre diameter, pore density/mesh-size, and stacking type. This research is not only a step towards assisting the numerical modelling of wire mesh porous media but also opens the door for investigating the performance of different wire-mesh porous samples, thus contributing valuable insights to the field.

- **Thickness as a variable parameter in metal based porous media, capable of exhibiting varied trade-offs in heat transfer and flow resistance behaviour:** The previous studies on metal foams often focuses on individual variable conditions or sets of constant variable conditions when assessing flow resistance and heat transfer characteristics. However, a critical gap in considering the simultaneous variation of thickness along with structural aspects (pore density and porosity) in metal based porous media studies can be witnessed the literature survey. The various trade-off scenarios between the enhanced heat transfer and incurred penalty of pressure drop can be greatly altered with change in thickness of the porous medium. Introduction of thickness as an additional variable parameter, with the structural variations, offer several trade-off scenarios suitable to variety of applications demanding specific thermo-hydraulic criteria. This holistic approach enables a deeper understanding of the trade-off scenarios between pressure drop minimization and heat transfer enhancement potentials associated with metal based porous media.

Addressing these research gaps, is believed not only to advance the theoretical understanding of metal based porous media such as metal foams and woven wire-mesh porous media but also have practical implications for optimizing their performance satisfying specific thermo-hydraulic demands in variety of engineering applications.

2.6 OBJECTIVES

1. Numerical modelling of metal foam porous medium in a vertical channel, to identify and emphasize on the effect of ordered variation of structural properties (porosity and pore density) on thermo-hydraulic performance.
2. To evaluate the trade-off between the potential of metal foams to enhance heat transfer and minimize flow resistance subjected to changes in porosity, pore density and thickness combinations.
3. Obtaining expressions of morphological parameters of wire mesh porous media of various possible stacking types, benefiting the numerical modeling procedure to analyze their thermo-hydraulic performances.
4. Performance analysis of wire mesh porous structures and analyzing the trade-off between their potential to enhance heat transfer and minimize flow resistance subjected to variations in porosity, pore density and thickness conditions.

2.7 CLOSURE

This chapter provided a comprehensive overview of the literature review conducted for the current research. The literature review encompasses a thorough analysis of the existing research works in the field to establish the research gap, and research objectives. Moreover, the chapter also discusses the motivation behind the research work, which highlights the significance, relevance and scope of the study.

CHAPTER – 3

METHODOLOGY

3.1 INTRODUCTION

A vertical channel experimental set up used by (Kamath et al. 2011) to study convection phenomenon in porous media is adopted as the present numerical domain. Pictorial representation of the experimental and numerical domain is shown in Figure 3.1 (a) and (b). It mainly consists of a vertical channel of dimensions 27 × 250 × 390 (mm), a heater plate supplying constant heat input of 20W is sandwiched between two aluminum vertical flat plates of dimensions 3 × 250 ×150 (mm) each at the middle of the channel flow passage. A part of the channel is filled with porous samples of 10 × 250× 150 (mm). It is well known that if the entrance of physical model is not long enough, the heat transfer improvement may be partly caused by the entrance effect. However, in the experimental set up by (Kamath et al. 2011) considered 140 (mm) of entrance length which is 7.28 times the hydraulic diameter (7.28D). The present study incorporated the same experimental vertical channel set up as that of work carried out in literature and numerical results were validated against experimental data of the same work. Therefore, same dimensions of the vertical channel experimental setup as shown in Figure 3.1(a) is retained in the present numerical model. Since, it is not an empty channel and because of the presence of porous assembly, where heat transfer is greatly enhanced, entrance length of 7.28D is considered to be sufficient to ignore the heat transfer enhancement due to entrance effect compared to the rich heat transfer enhancement at the porous media assembly. Airflow in the laminar regime is forced into the channel passage with porous samples to study their thermo-hydrodynamic performances. Flow and heat transfer phenomenon through the porous-filled vertical channel are numerically modeled using the Darcy–Forchheimer flow model and LTNE thermal model respectively (aptness and description of these models are elaborated in section 1.5 (introduction). Porous samples of various structural (porosity and pore density), configurational (thickness) and stacking (in terms of wire mesh) types are considered for the thermo-hydrodynamic performance study. At steady-state condition,

porous samples of above-mentioned combinations are evaluated by the numerically obtained pressure drop across the foam samples as well as wall heat transfer co-efficient with the help of numerically obtained information on average wall temperature fields along the vertical plate. Since, heat flux is numerically employed, heat loss to the surroundings is neglected in the present study.

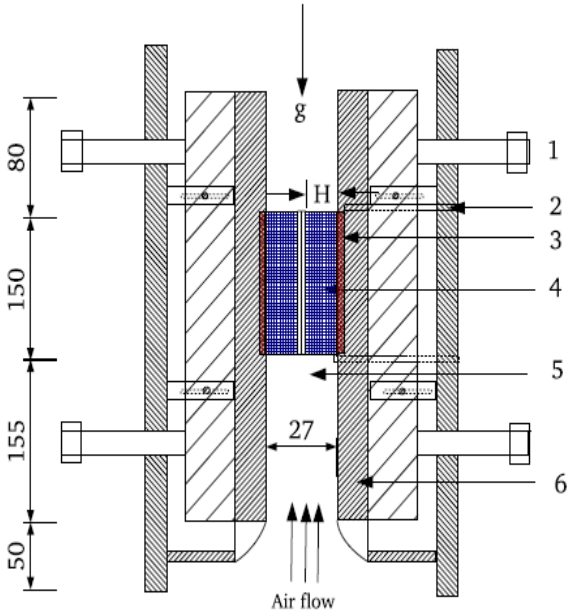

1-Tightiening screws, 2-pressure tap, 3-teflon plate, 4- Porous assembly, 5- vertical duct, 6-non-rubberized cork (Kamath et al. 2011).

(a)

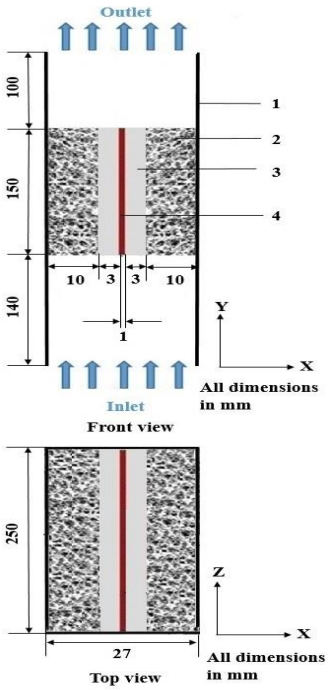

1-walls of the channel, 2-porous medium, 3-aluminum plate, 4-heater.

(b)

Figure 3.1 a) Pictorial representation of experimental domain and b) Numerical domain.

3.2 NUMERICAL DOMAIN WITH BOUNDARY CONDITIONS

Computations are carried out in a two dimensional numerical using commercially available ANSYS FLUENT software. The two-dimensional computational domain along with boundary conditions considered for the numerical investigation is shown in Figure 3.2. Appropriate interfaces have been established between solid–solid, solid–fluid, fluid–fluid, porous-solid and porous-fluid zones to obtain continuity in momentum and energy between contact regions. Due to the symmetrical configuration

of the actual experimental set-up about its vertical axis, only one half of the symmetrical portion is considered as the numerical domain which in turn reduces the computational cost. It consists of a heater attached to aluminum plate that is connected to channel passage that houses porous samples to be studied. The bottom of the channel passage is given with a uniform velocity boundary condition whereas the top opening of the channel is given with zero-gauge pressure boundary condition as it opens up to the ambient pressure conditions. Constant heat flux boundary condition is assigned to the heater plate. Axis that distinguishes symmetrical portions of the vertical channel is given with symmetry boundary conditions while the side walls enclosing the channel passage are defined to be adiabatic boundary condition. The working fluid is air and the properties are estimated at an initial temperature of 30 ^{o}C.

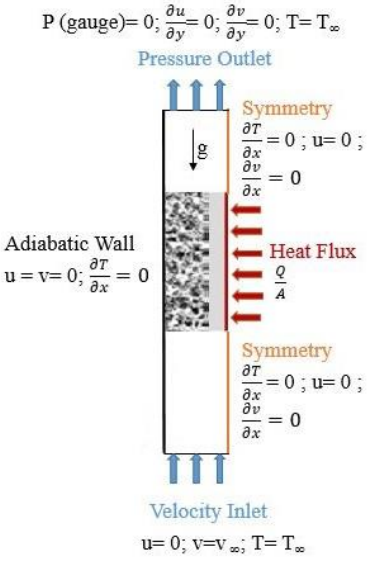

(a)

Figure 3.2 Illustration of the computational domain with boundary conditions.

3.3 DETAILS OF NUMERICAL SIMULATION

- Commercially available software ANSYS FLUENT
- Working fluid considered as air with constant heat flux scenario.
- LTNE thermal model is employed.
- The pressure-based coupled algorithm is used that enables full pressure-velocity coupling.

- Second-order upwind scheme is used to obtain higher-order accuracy at the cell faces.
- Convergence criteria for continuity and momentum equations are set as $10^{-5}$and convergence for energy equation is set as 10^{-10}.
- Further for accounting natural and mixed convection phenomenon Boussinesq approximation is invoked in the momentum equation.

Correlations given by (Calmidi and Mahajan 2002) and (Zukauskas 1987a) to find the interfacial specific surface area and interfacial heat transfer co-efficient are considered for the present numerical simulations which are shown in Eqs. (3.10), (3.11). It can be observed that in Eq. (3.11), correlations from (Zukauskas 1987a) with characteristic length taken from (Calmidi and Mahajan 2002) is used to describe interfacial heat transfer coefficient. Despite many correlations proposed for interfacial heat transfer coefficient pertaining to metal foams, with some of these obtained from empirical corrections of cross-flow tube banks correlations (Calmidi and Mahajan 2002), (Wu et al. 2011), (Iasiello et al. 2017), (Vijay et al. 2015), (Iasiello et al. 2020), the correlation employed here is more appropriate since fiber diameter is used as characteristic length with a correction (1-exp(-(1-porosity)/0.04)) to take into account fiber-section variations (Calmidi and Mahajan 2002).

Interfacial specific surface area,

$$a_{sf} = \frac{3\pi d_f \left(1 - exp^{-\left(\frac{1-\varepsilon}{0.04}\right)}\right)}{\left(0.59 d_p\right)^2} \tag{3.10}$$

Interfacial heat transfer coefficient,

$$\frac{h_{sf} d_f \left(1 - exp^{-\left(\frac{1-\varepsilon}{0.04}\right)}\right)}{\lambda_f} \tag{3.11}$$

$$= \begin{cases} 0.76\, {Re_{d_f}}^{0.4}\, Pr^{0.37}, \left(1 \le Re_{d_f} \le 40\right) \\ 0.52\, {Re_{d_f}}^{0.5}\, Pr^{0.37}, \left(40 \le Re_{d_f} \le 10^3\right) \\ 0.26\, {Re_{d_f}}^{0.6}\, Pr^{0.37}, \left(10^3 \le Re_{d_f} \le 2\,\text{x}10^5\right) \end{cases}$$

Where λ_f is the thermal conductivity of operative fluid, Pr represents Prandtl number, Re_{d_f} represents Reynolds number which is evaluated based on the fiber diameter by the Eq. (3.12).

$$Re_{d_f} = \left\{ u d_f \left(\frac{1 - exp^{-\left(\frac{(1-\varepsilon)}{0.04}\right)}}{\varepsilon \nu} \right) \right\} \tag{3.12}$$

Where d_f represents the fibre diameter and d_p represents the pore diameter.

The properties of metallic foams such as pore size, fibre diameter, permeability and inertial coefficient are calculated using Eqs. (3.13), (3.14), (3.15) and (3.16) (Lu et al. 2016).

Pore size (d_p),

$$d_p = \frac{0.0254}{PPI} \tag{3.13}$$

Fibre diameter (d_f),

$$\frac{d_f}{d_p} = 1.18 \sqrt{\frac{(1-\varepsilon)}{3\pi}} \left(\frac{1}{1 - e^{\left(\frac{(1-\varepsilon)}{0.04}\right)}} \right) \tag{3.14}$$

Permeability (K),

$$K = 0.00073\, (1-\varepsilon)^{-0.224} \left(\frac{d_f}{d_p}\right)^{-1.11} d_p^2 \tag{3.15}$$

Inertial / form drag coefficient (F),

$$F = 0.00212 (1-\varepsilon)^{-0.132} \left(\frac{d_f}{d_p}\right)^{-1.63} \tag{3.16}$$

3.4 MESH INDEPENDENT STUDY

A grid independence study was carried out for the numerical domain in the present study comparing the domain with 26,130; 56,700 and 88,400 cells as shown in Table 3.1. Having the highest cell domain as the base line, it was observed that the percentage deviation of pressure drop and wall temperature are found to be at least 0.07% and 0.42%, respectively, for the meshed domain of 56,700 cells. However, with a lower mesh size of 26,130 cells, the respective percentage deviations of pressure drop and wall temperature were found to be 0.22% and 0.94%, and any further decrease in the number of cells in the meshed domain would increase the deviation of the mentioned heat transfer and flow parameters. Therefore, in the current study for optimum computational effort, a mesh domain with 56,700 elements is chosen, and subsequent simulations were carried out in the same meshed domain throughout the present work.

Table 3.1 Grid independence study

Mesh Type	**No. of Elements**	**Pressure Drop** ΔP, **N/m^2**	**Temperature Difference** ΔT **°C**	**Deviations** ΔP, **%**	**Deviations** ΔT, **%**
1	26,130	27.60	7.74	0.22	0.94
2	56,700	27.56	7.70	0.07	0.42
3	88,400	27.54	7.66	Base line	

3.5 VALIDATION STUDIES

Considering metal foams, the numerical procedure involved in the present study is validated against the experimental work of (Kamath et al. 2011). Variations of numerically predicted thermal parameters, such as wall temperature and wall heat transfer coefficient, with those of experimental data (Kamath et al. 2011) are shown in Figure 3.3 for 20 PPI and 0.9 porosity porous foam. Similarly, the variation of the numerically simulated and experimentally obtained flow parameter is shown in Figure 3.4 in terms of variation in pressure drop for a foam sample of 0.9 porosity and 20 PPI.

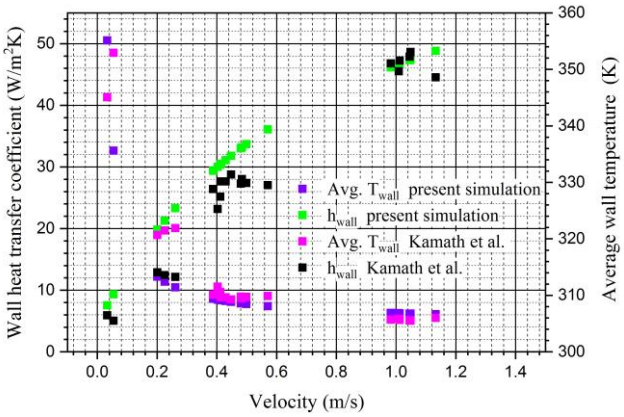

Figure 3.3 Assessment of closeness of numerically predicted thermal parameters (wall heat transfer coefficient and wall temperature) for metal foam of 0.9 porosity and 20 PPI with that of experimental data.

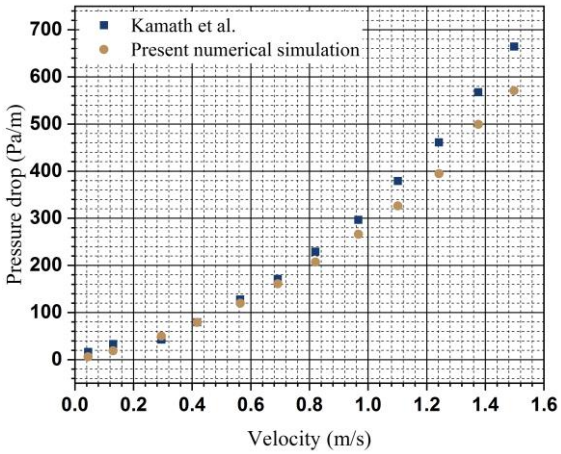

Figure 3.4 Assessment of closeness of numerically predicted flow parameters (pressure drop) for metal foam of 0.9 porosity and 20 PPI with that of experimental data.

Numerically predicted data of thermal and flow parameters are observed to be in good agreement with that of the experimental work. Maximum percentage deviation of numerically predicted temperature data was found to be only 2.75% from that of experimental value and a 0.048% of minimum deviation was observed between the numerically predicted and experimentally obtained data. Similarly, with good agreement in trend of pressure drop variation, numerically predicted data showed an average percentage deviation of 12%. This confirms the aptness of the current numerical procedure and adopted models to predict flow and temperature field in the domain consisting of metal based porous media.

3.6 EVALUATION OF THERMO-HYDRAULIC PARAMETERS

Numerically obtained temperature data is used to compute important parameters such as wall heat transfer coefficient calculated using Eq. (3.17) and wall Nusselt number calculated using Eq. (3.19) with the help of numerically obtained information on average wall temperature fields along the vertical plate calculated using Eq. (3.18). Characteristic length to find Nusselt number is considered to be the hydraulic diameter of the channel similar to that of the work flow carried by (Kamath et al. 2011) for comparison and reference.

$$h_{wall} = \frac{Q}{A\Delta T_w} \tag{3.17}$$

Where, (3.18)

$$\Delta T_w = \overline{[T - T_\infty]}$$

Nusselt number, (3.19)

$$Nu_{wall} = \frac{h_{wall} D_h}{\lambda_{effective}}$$

Where,

$$\lambda_{effective} = (\lambda^{\varepsilon}{}_f)(\lambda^{1-\varepsilon}{}_s) \tag{3.20}$$

3.7 TOPSIS TECHNIQUE

For adequately analysing an inevitable cost and benefit scenario, Technique for order preference by similarity to ideal solution (TOPSIS) a multi-objective multi criteria decision making tool presents itself as a right candidate serving the purpose (Hendiani and Walther 2023). Provided a given phenomenon involving conflicting outcomes while achieving the primary goal, the trade-off in which the outcomes participate with each other can be comprehended with the help of this multi-attribute technique. In the present work this method is utilised to analyse the thermo-hydraulic scenarios in the field of thermal management where heat transfer enhancement is always achieved at the cost of pressure drop or pumping power.

TOPSIS is a highly reliable and suitable tool that can be employed in various fields of applications where there exist multiple objectives with contrary interests like maximizing one parameter and minimizing the other. This method works on the principle of sorting / selecting / arranging the cases that arises contrarily desired parameters. This is accomplished by measuring the closeness of a problem's proximity to an ideal or optimized solution corresponding to the weights placed on parameters to be minimized and maximized. Through this methodology one can get the output (select single output / segregate the range of outputs / arrange the outputs based on the order of preference) subjected to user's desire. As the current study involves dependent parameters like pressure drop and heat transfer, where contrary magnitudes of out puts are desired, i.e., for instance in the current study, minimizing pressure drop and maximizing heat transfer (one objective is to minimize and the other is its contrary). To solve such multi objective problems TOPSIS gives well desired results by placing the outputs in the order of preference chosen by the user. Another advantage of this methodology is that the user can place various magnitude of importance on the objectives that one is wishing to employ that depends on application and interest, this is done by placing different weights on the objective functions. Here in the present work, 5 distinct preferences are achieved namely, criteria I, II, III, IV and V based on the varied thermo-hydrodynamic characteristics that are primarily obtained by numerical simulations of the present study.

The steps included in this methodology can be briefly mentioned as follows:

- Distinguish the existing outcomes in terms of the one to be maximized (desired outcome which is the heat transfer in the present study) and the one to be minimized (unsought outcome, which is the flow resistance in the present study).
- Normalize the considered outcomes whose trade-off is subjected to analysis, which are in the present study pressure drop and wall heat transfer coefficient arising out of all the considered scenarios (porosity, pore density and thickness of porous media).
- Assign suitable weights on the normalized values of the conflicting outcomes so that eventually all the various scenarios considered could be ranked based on

their potential to meet the assigned trade-off with which the maximization of the benefit outcome and minimization of the cost outcome is involved.

- Analyse under various weight criteria, focusing on the ability of wire mesh porous structures in maximizing the desired outcome and their ability of minimizing the undesired outcome. Maximum weight of '1' and a minimum of '0' implies highest and lowest importance that could be placed on the potential of maximizing the benefit outcome and the potential of minimizing the cost outcome or even the weight distribution of other way around.
- Consider such various criteria (5 in the present study) where the performances corresponding to every considered scenario can be analysed subjected to various weightage of importance given on their potential of maximizing the benefit and minimizing the cost outcome.
- Obtain performance score for every scenario specific to a considered / required trade-off situation by examining the proximity of every scenario to an ideal worst and best value corresponding to the specific trade-off criterion.

The mathematical steps involved in implementing the TOPSIS method are:

- Step 1: Obtain matrix of normalized columns.

Produce a matrix of two columns each comprising values of wall heat transfer coefficient (h_{i1}) and values of pressure drop (p_{i2}), respectively. Produce another set of two columns each comprising normalized magnitudes of heat transfer coefficient and pressure drop (h_{i3}) and (p_{i4}), respectively, using Eqs. (3.21) and (3.22).

$$\overline{h_{\iota 3}} = \frac{h_{i1}}{\sqrt{\sum_{i=1}^{m} {h_{i1}}^2}}, \tag{3.21}$$

$$\overline{p_{\iota 4}} = \frac{h_{i2}}{\sqrt{\sum_{i=1}^{m} {p_{i2}}^2}}. \tag{3.22}$$

where 'i' indices (i = 1, 2, …, m) indicate the rows of the matrix, and 'm' represents the total number of metal foam models (pertaining to all variable conditions).

- Step 2: Obtain matrix of weight assigned normalized columns.

Additionally, the matrix is extended with weighted normalized columns, using Eqs. (3.23) and (3.24); the weight of unity is distributed (that varies from 0 to 1) to the formerly computed values of normalized magnitudes of heat transfer coefficient and pressure drop. The allotted weight entirely depends on the particular interest of the design.

$$V_{i5} = \overline{h_{\iota 3}}.W_h, \tag{3.23}$$

$$V_{i6} = \overline{p_{\iota 4}}.W_p. \tag{3.24}$$

where W_h and W_P are 0 and 1, respectively, for criteria I, whereas it is 0.25 and 0.75, 0.5 and 0.5, 0.75 and 0.25 and 1 and 0 for criteria II, III, IV and V, respectively. Various criteria and their significance are elaborated in the later discussion.

- Step 3: Obtain the ideal best *V*+ and ideal worst *V*- values.

The ideal worst and best values are achieved from the formerly computed weighted normalized columns of pressure drop and the heat transfer coefficient values. Ideal best value (*V*+) is the highest value in the set of beneficial parameters and the lowest value in the set of unfavourable parameters. Similarly, ideal worst value (*V*-) is the lowest value in the set of favourable parameters and the highest value in the set of unfavourable parameters. In the present study, since pressure drop is considered as the unfavourable parameter while average heat transfer coefficient is considered as the favourable parameter, the highest value among the weighted normalized columns of pressure drop is regarded as the ideal worst, and the lowest value amongst the weighted normalized column of pressure drop is chosen as the ideal best value. On the other hand, the maximum value among the weighted normalized column of heat transfer coefficient is chosen as the ideal best value, and the lowest value among the weighted normalized column of heat transfer coefficient is considered as the ideal worst value. Identification of the ideal best value *V*+ and the ideal worst value *V*– is expressed using the Eqs. (3.25) to (3.28).

$$V_h{}^{+} = \max\,(V_{i5}) \tag{3.25}$$

$$V_p{}^{+} = \min(V_{i6}) \tag{3.26}$$

$$V_h^- = \min(V_{i5}) \tag{3.27}$$

$$V_p^- = \max(V_{i6}) \tag{3.28}$$

- Step 4: Obtain the Euclidean distance.

Euclidean distance refers to the relative distance of each weighted normalized value from the obtained (best or worst) ideal values. Positive Euclidean distance is the measure of distance of each value in the weighted normalized column from the ideal best value and is evaluated as given in Eq. (3.29). Similarly, negative Euclidean distance is the measure of distance of each value in the weighted normalized column from the ideal worst value and is evaluated as given in Eq. (3.30).

$$S_i^+ = \left[(V_{i5} - V_h^+)^2 + (V_{i6} - V_p^+)^2\right]^{0.5} \tag{3.29}$$

$$S_i^\pm = \left[(V_{i5} - V_h^-)^2 + (V_{i6} - V_p^-)^2\right]^{0.5} \tag{3.30}$$

- Step 5: Evaluate the performance score.

Performance scores of metal foams of all considered variable conditions are evaluated using Eq. (3.31). It ranks the metal foams subjected to variable conditions (pore density, porosity and thickness) based on the values of the heat transfer coefficient and pressure drop exhibited, under the restriction of how close is its performance in meeting the given weighted criteria.

$$P_i = \frac{S_i^-}{S_i^+ + S_i^-} \tag{3.31}$$

3.8 CLOSURE

This chapter provided a detailed description of the methodology involved in the present work, including description of the experimental and numerical domain, numerical details, validation of the numerical results, evaluation of thermo-hydraulic parameters and description of the TOPSIS methodology. In the coming chapters the results out of various considerations are discussed following the provided methodology in order to achieve the considered objectives.

CHAPTER – 4

NUMERICAL STUDY ON EMPHASIZING THE CONSIDERATION OF BOTH THE TWIN STRUCTURAL PARAMETERS (POROSITY AND PORE DENSITY) OF METAL FOAMS

4.1 INTRODUCTION

Thermo-hydrodynamic characteristics of metal foams may not be a single parameter dependent phenomenon, instead a multi variable dependent phenomenon that could vary with different aspects like thermal conductivity of fluid-foam sample, foam filling ratio (fully filled, partially filled with various aspect ratios), type of flow (turbulent or laminar) and so on. Another such vital parameters that could affect the performance of metal foams are their structural properties namely porosity and pore density (PPI). Looking at only one structural aspect i.e., either porosity or pore density and analysing on thermo-hydrodynamic characteristics of a foam sample would be incomplete. In Table 4.1 the possibility of foams with varied combination of these twin structural property of a foam i.e., porosity and pore density can be witnessed. It is very much important to study the effect of ordered variation in these structural properties of the foam samples, because every possible combination of porosity and pore density of a foam sample is likely to exhibit different thermo-hydrodynamic characteristics. Despite the extensive research works carried out by the researchers on the categorization of metal foams based on their performance, ambiguity in understanding the contribution of metal foams in heat transfer and flow resistance phenomenon owing to their various combinations of their structural properties remains unreduced in the available open literature.

Due to the fact, that in the available literature the performance abilities of metal foams exclusively based on their structural characteristics in various applications is neither emphasized nor is the appropriate justification to the selection of the foam sample is made, the present study demonstrates that, without the knowledge on distinguished and

combined effect of structural properties (pore density and porosity) on thermo-hydrodynamic performance, selection / categorization of foam samples for optimum performances characteristics cannot be achieved. Therefore, the present study focuses on analysis of metal foams of variety of structural combinations and their varied impacts on heat transfer and flow resistance.

Table 4.1 Foams of different structural properties used in various studies

S.No.	Foam Material	Porosity	Pore density	Study
1	Copper	0.8596, 0.8683, 0.8769	10	Convection heat transfer study (Kamath et al. 2013)
		0.8567	20	
	Aluminium	0.9417, 0.9449, 0.9481	10	
		0.9043, 0.9294	20	
2	Copper	0.893	18	Study on foams in compact heat exchanger (Kim and Kim 2019b)
		0.876	31	
	Nickel	0.922	24	
		0.88	33	
3	Copper	0.893	10	Study on metal foams in miniaturized condenser (Ribeiro and Barbosa 2013)
		0.947	20	
4	Aluminium	0.921, 0.920	5	Air forced convection study (Mancin et al. 2013b)
		0.956, 0.934, 0.903, 0.954, 0.926, 0.896	10	
		0.932, 0.930	20	
		0.930, 0.926	40	
	Copper	0.933, 0.935	5	
		0.933, 0.905	10	
		0.933, 0.935	20	
		0.934, 0.936	40	

5	Aluminium	0.9726, 0.9118	5	Forced convection
		0.9486	10	study (Calmidi and
		0.9546, 0.9005	20	Mahajan 2000a)
		0.9272, 0.9132	40	
6	Copper	0.933	5	Heat transfer and
		0.933, 0.905	10	pressure drop study
		0.933	20	(Mancin et al. 2012a)
		0.934	40	
7	Aluminium	0.899, 0.93	5	Natural convection
		0.9085, 0.9386	10	study in high porosity
		0.92, 0.9353	20	metal foams
		0.9091, 0.9586	40	(Phanikumar and
				Mahajan 2002)
8	Aluminium	0.92	10	Flow and heat transfer
		0.92, 0.89, 0.94, 0.96	20	study of porous fin in
		0.92	40	plate-fin heat
				exchanger (Kim et al.
				2000)
9	Aluminium	0.95	10	Mixed convection
		0.90	20	study (Kamath et al.
		0.92	30	2011)
		0.90	45	
10	Aluminium	0.914	5	Frictional
		0.918	10	characteristics study
		0.870, 0.909, 0.935	20	(Liu et al. 2006)
		0.935	40	
11	Aluminium	0.918	10	Study on performance
		0.918	20	of aluminium and
		0.918	40	carbon foams for air-
				side heat transfer

				enhancement (Garrity and Klausner 2010)
12	Copper	0.90	10	Convective heat transfer study (Xia et al. 2017)
		0.90	20	
	Nickel	0.9	10	
		0.9	20	
		0.9	40	
		0.97	20	
	Silicon-Carbide	0.88	10	
		0.88	20	

4.2 RESULTS AND DISCUSSION

4.2.1 Effect of interfacial properties of metal foams on heat transfer and flow resistance characteristics and their dependency on porosity and pore density combinations.

Heat transfer and flow phenomenon through porous media are characterized by solid-fluid interfacial parameters namely, interfacial heat transfer coefficient (h_{sf}) and interfacial area density or interfacial specific surface area (a_{sf}) that exists as a result of presence of solid structures of the porous media that interact with the fluid flow offering enhanced heat transfer at the cost of resistance offered to the flow. Empirical relations that are used to evaluate these parameters along with formulations for the evaluation of wall heat transfer co-efficient (h_{wall}), Nusselt number (Nu_{wall}) and friction factor (f) are described in sections 3.3 and 3.6 of chapter 3 (methodology).

Interfacial parameters being the main characteristics of a porous medium, the contribution of these parameters on heat transfer and flow resistance can be observed from Figure 4.1 (a) and (b). This gives an overall impression on how a foam sample's interfacial parameters could potentially influence the thermo-hydraulic performance. The variations in these interfacial parameters with respect to change in porosity and pore density, adds on further emphasise on possible distinct flow and heat transfer behaviour of a given foam sample owing to its twin structural properties.

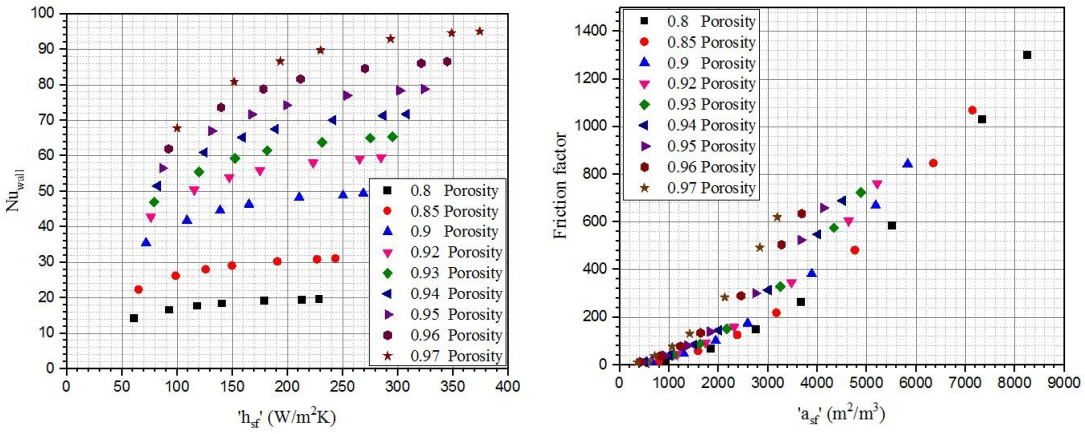

(a) (b)

Figure 4.1 (a) Variation of the wall Nusselt number with respect to the interfacial heat transfer coefficient. (b) Variation of friction factor with respect to the changes in interfacial specific surface area.

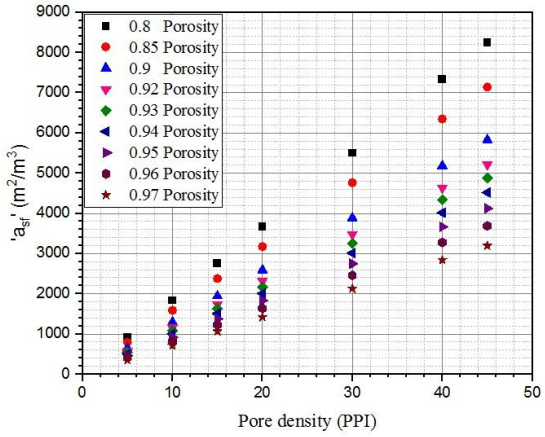

Figure 4.2 Graphical representation of variation of interfacial specific surface area with porosity and pore density.

Variation of 'a_{sf}' with porosity and pore densities of the foams is illustrated in Figure 4.2. It is evident that the interfacial specific surface area decreases with an increase in porosity for any foam sample of given pore density and it increases with pore density for given porosity of foams. On the contrary, the interfacial heat transfer coefficient 'h_{sf}' increases with porosity for any foam of given pore density, and increases as well as with increase in pore densities as shown in Figure 4.3 in similar to the variation of 'a_{sf}'.

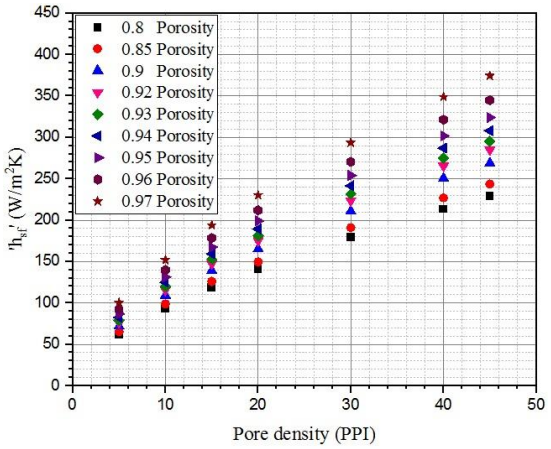

Figure 4.3 Changes in interfacial heat transfer coefficient with porosity and pore density.

4.2.2 Heat transfer characteristics in various convection regimes through Nusselt number correlations: A further emphasis on the need of considerations of both the twin structural properties (porosity and pore density).

The influence of twin structural properties (porosity and pore density) is further explored exclusively in terms of heat transfer characteristics under different convection regimes (natural, mixed and forced convection regimes). For successfully describing heat transfer through metal foams, many authors have depicted Nusselt number as a function of certain heat transfer influencing parameters (pertaining to metal foam and/or working fluid). Table 4.2 show some of the correlations used to evaluate Nusselt number for describing heat transfer associated with foams. It can be observed that, many of the works available in the open literature deals with analysing metal foams of limited variations in their porosity and pore density and thus many studies concluded Nusselt number as a function of only flow characteristics i.e., Reynolds number, and few works included porosity as one of the parameters to describe Nusselt number. However, when analysing foam samples of various possible changes in their porosity and pore density, both these parameters influence heat transfer characteristics of the corresponding foam sample. Therefore, the present study mainly aims at demonstrating the influence of these structural parameters (pore density and porosity) on heat transfer behaviour of metal foam considering various convection regimes. In this regard, the effect of several orderly varied combinations of the dual structural properties is considered. Forced convection over a range of flow velocities and natural convection

phenomenon are studied numerically in the channel housing porous samples as described in the previous chapters. Two limiting solutions for Nusselt number (Nu) i.e., Nu_n (for natural convection) and Nu_f (for forced convection) for $Ri \rightarrow \infty$ and $Ri \rightarrow 0$ respectively, as a function of independent variable Richardson number (Ri) with structural properties pore density and porosity are obtained. Further these asymptotic solutions are blended using technique illustrated in the literature in order to obtain solutions for Nusselt number corresponding to the intermediate mixed convection phenomenon (Nu_m). Correlations for Nusselt number as a function of combination of porosity and pore density are obtained emphasizing on the varied significance of these parameters in different convection regimes. The present study is thus focused on further emphasising on the effect of combination of structural properties of metal foams on heat transfer characteristics.

Table 4.2 Nusselt number correlations provided by various studies

Study regime	**Foam material**	**Pore density and/or porosity**	**Nu-correlation**
Natural (Zhao et al. 2005)	Steel alloy	30, 60, 90 PPI	$Nu_m = C(Ra_m)^n$, Ra is based on saturated medium's thermal conductivity.
Natural (Bhattacharya et al. 2002)	C/A	0.9-5	$Nu = 11.24Ra^{0.25}Da^{0.16}$, Darcy number is incorporated to describe Nu.
Natural (Barbieri et al. 2017)	Al	5 PPI, 0.95 porosity	$Nu = nRa^{0.19}Da^{0.16}$, $n = 8.51 – 0.35(H/L)^{-1.36}$
Forced (Mancin et al. 2013b)	Al and Cu	5-40 PPI, 0.896-0.956 porosity	$Nu = 0.418\ (Re)^{0.53}Pr^{0.33}$, Re is based on fiber thickness.

Forced (Leong and Jin 2005)	Al	40 PPI	$Nu = 12.38(A_o)^{0.95}(Re_w)^{0.31}$, A_o is dimensionless amplitude and Re is based on oscillatory frequency.
Forced (Leong and Jin 2005)	Al	10 PPI	$Nu_H = 0.51(Re_{dp})^{0.38}$
Forced (Tzeng and Jeng 2006)	Al	10-40 PPI, 0.93 porosity	$Nu = 21.1(Re_H)^{0.457}$, Re is based on height of porous sample.
Forced (Hsieh et al. 2004)	Al	20 PPI, 0.91 porosity 40 PPI, 0.94 porosity	$Nu = 0.49(Re_{dp})^{0.44}$ $Nu = 0.63(Re_{dp})^{0.46}$, Re is based on equivalent pore diameter.
Forced (Iasiello et al. 2017)	Al	5-40 PPI, 0.87-0.94 porosity	$Nu = 1.59(Re_c)^{0.438}\varepsilon^{0.164}$, Re is based on cell size to porosity ratio.
Forced (Tzeng 2007)	Al	10 PPI, 0.97 porosity	$Nu = 4.835(Re_H)^{0.52}$, Re is based on height of the foam.
Forced (Noh et al. 2006)	Al	10 PPI, 0.9 porosity	$Nu = 23.1(Re)^{0.4}Pr^{-0.1}Da^{0.09}$, Re is based on permeability.
Forced (Wu et al. 2011)	Ceramic	0.66-0.93 porosity	$Nu = 2.0696(Re)^{0.438}\ \varepsilon^{0.38}$, Re is based on mean pore diameter.
Forced (Calmidi and Mahajan 2000a)	Al	5, 10, 20, 40 PPI, 0.91-0.97 porosity	$Nu = 0.76(Re)^{0.4}Pr^{0.37}$, where Re is based on fiber diameter ($1 \leq Re \leq 40$)

Forced (Ichimiya and Asme 1999)	Ceramic	20 PPI, 0.87 porosity	$Nu = 2.43(Re_{dp})^{0.4}$, ($64 \leq Re \leq 457$), Re is based on pore diameter.
Forced (Hwang et al. 2002)	Al	10 PPI, 0.95 porosity	$Nu = 0.32(Re)^{0.6}$, ($1900 \leq Re \leq 7800$), Re is based on height of flow passage.
Forced (Hwang et al. 1995)	Sintered bronze leads	-	$Nu = 0.081(1 - \varepsilon)\varepsilon^2 Re^{1.35} Pr^{0.33}(D_p/d)^{0.35}$ for $Re \leq 75$. $Nu = 21.65(1 - \varepsilon)\varepsilon^2 Re^{0.59} Pr^{0.33}$ for $Re \leq 75$.
Mixed (Kamath et al. 2011)	Al	10-45 PPI, 0.9-0.95 porosity	$Nu = 0.223(Re)^{0.723}\ \varepsilon^{6.81}(1 + Ri^{0.46} Re^{-0.73})$, Re is based on hydraulic diameter.
Mixed (Kurian et al. 2016b)	Brass wire mesh	0.77-0.85 porosity	$Nu = 0.124(Re)^{0.707}\ \varepsilon^{7.57}(1 + Ri^{0.690} Re^{-0.549})$. Re is based on thickness.
Mixed (Venugopal et al. 2010b)	Brass perforated sheets	0.85-0.92 porosity	$Nu = 1.366(Ri_D/(1+Ri_D))^{-0.034} Pe^{0.563}(0.6734\ \varepsilon^2 + 0.5391\varepsilon - 0.3367)^{0.563}$, Re is based on hydraulic diameter.

For evaluation of heat transfer characteristics, the considered numerical domain and numerical details follow same as described in chapter 3 (methodology). Ordered variation of porosity (0.8, 0.85, 0.9, 0.92, 0.93, 0.94, 0.95, 0.96, 0.97) of foam samples each with various pore density (5, 10, 15, 20, 30, 40, 45PPI) are considered. Air velocity is varied from 0.02 m/s to1.2 m/s that resulted in Richardson number values presenting Nusselt number for extreme limits of convection phenomenon i.e. natural and forced convection regimes. Reynolds, Grashoff number and Richardson number are calculated as given in Eqs. (4.1), (4.2), (4.3) respectively. Among the simulated data

for mentioned velocity range, highest Richardson number of 531 (for 0.02 m/s flow velocity) and lowest Richardson number of 0.0032 (for 1.2 m/s flow velocity) was considered as the extreme limits of natural and forced convection phenomena. Respective correlations to compute wall Nusselt number is obtained as a function of independent parameters including both pore density and porosity. Later, these asymptotically varying solutions are blended using technique provided by (Churchill and Usagi 1972) to obtain solutions that quantify wall Nusselt number of the considered foam samples specified to mixed convection dominant regime. Characteristic length to find Nusselt number is considered to be the hydraulic diameter of the channel similar to that of the work flow carried by (Kamath et al. 2011) for comparison and reference. In a recent study (Nakate et al. 2019), Nusselt number correlations for natural and forced convection regimes are adopted for air flow in an empty vertical channel as given in Eqs. (4.4) and (4.5), values of powers of Gr and Re are considered as 0.25 and 0.5 as provided by (Bejan and Kraus 2003) for laminar flow condition. In the present study same Nusselt number correlation structures for natural and forced convection regimes are considered that provides relation of Gr, Re and Ri with Nu in natural and forced convection regimes, however the effect of porous medium filled in the channel is attributed to porosity and pore density of the metal foam samples as given in Eqs. (4.6) and (4.7), and its respective constants and powers are evaluated based on the numerical simulations carried out in the present study.

Reynold's number, (4.1)

$$Re = \frac{\rho V D_h}{\mu}$$

Grashof number, (4.2)

$$Gr = \frac{g\beta\Delta T_w {D_h}^3}{v^2}$$

Richardson number, (4.3)

$$Ri = \frac{Gr}{Re^2}$$

$$\frac{Nu_n}{Gr^{0.25}} = aRi^b \quad (4.4)$$

$$\frac{Nu_f}{Re^{0.5}} = mRi^n \quad (4.5)$$

Steps involved and structure of Nusselt number correlations used in the present study are as follows.

- STEP I: Obtaining correlation for Nu_n

From simulated results dependent parameter Nu_n as a function of independent parameters Richardson number, Grashoff number, pore density and porosity is obtained as given in Eq. (4.6).

$$Nu_n = aGr^{0.25}Ri^b\omega^c\varepsilon^d \tag{4.6}$$

- STEP II: Obtaining correlation for Nu_f

From simulated results dependent parameter Nu_f as a function of independent parameters Richardson number, Reynold's number, pore density and porosity is obtained as given in Eq. (4.7).

$$Nu_f = mGrRe^{0.5}Ri^n\omega^o\varepsilon^p \tag{4.7}$$

- STEP III: Blending of the obtained asymptotic solutions

The obtained two asymptotically varying solutions are blended as shown in Eq. (4.8) in the form of $Y= [1 + (Z)n]^{1/n}$ as illustrated to finally obtain a suitable correlation that accounts for intermediate mixed convection phenomenon (Nu_m). The blending technique that reduces the computational cost is elaborated in section 4.2.5.

$$Nu_n/Nu_m = \left[1 + (Nu_n/Nu_f)^n\right]^{1/n} \tag{4.8}$$

4.2.3 Heat transfer characteristics

From Figure 4.4 and Figure 4.5, the dependency of the heat transfer characteristics (defined by wall Nusselt number) of foam samples on twin structural properties i.e., pore density and porosity and on Richardson number can be observed. For each foam sample (of unique pore density and porosity combination) Nusselt number values are observed to be increasing with decrease in 'Ri' value as the flow velocity increased from natural-dominant regime to forced-dominant regime. For a foam sample, wall Nusselt number is found to increases with increase in porosity and pore density. From the present study it is observed that, the variation in heat transfer with changes in porosity and pore density for a given metal foam sample examined under natural convection regime is smaller compared to the variation in heat transfer in scenarios where the convection phenomenon is approaching forced regime. That is, the effect of changes in porosity and pore density combinations plays a dominant role in exhibiting

distinct heat transfer characteristics as the convection regime approaches forced scenario and the magnitude of increase in Nusselt number seems to be continuously increasing with increased flow velocity even under forced convection regime. This is due to increased total heat transfer due to interstitial heat transfer and direct heat transfer with increased air flow. Under natural convection scenario, substantial change in the amount of relative heat transfer among the foam samples of different pore density and porosity is found to be less significant. Thus, it can be observed that, pore density and porosity are two vital twin structural properties that play a key role in thermal performance of metal foams particularly working under forced convection regime. Foam sample of given porosity can have a multiple combinations of pore density similar to cases where a foam sample of given pore density can have multiple combinations of porosity, with changes in fiber diameter to compensate the required changes. It can be noted that, with increase in porosity (for any given pore density scenario) heat transfer characterized by Nusselt number increases due to enhancement in convection heat transfer as a result of increased void spaces, resulting in enhanced heat transfer through convection phenomenon compared to that of with conduction phenomenon (as the effective thermal conductivity of the fluid saturated porous medium decreases with increase in porosity) thereby decreasing the heat transfer through conduction while promoting the heat transfer phenomenon due to convection. Similarly, Nusselt number is observed to increase with increase in pore density (for any given porosity scenario), as a result of increased interfacial surface area density, that promotes increased interfacial heat transfer phenomenon through interfacial convection contributing to the overall heat transfer process. In the present work, it can be noted that, heat transfer augmentation due to increase in pore density and porosity of metal foams is more significant in forced convection scenario. Though relative variation of heat transfer corresponding to changes in pore density and porosity is similar in all convection regimes, forced convection scenario resulted in much significant variations in heat transfer due to increased heat exchange process as a result of enhanced mass flow rate of the working fluid, whereas the variation in heat transfer in natural convection dominant regime is observed to be not much significant with variation in pore density and porosity due to lesser flow interaction of the working fluid with the metal foam structures participating in the heat exchange phenomenon.

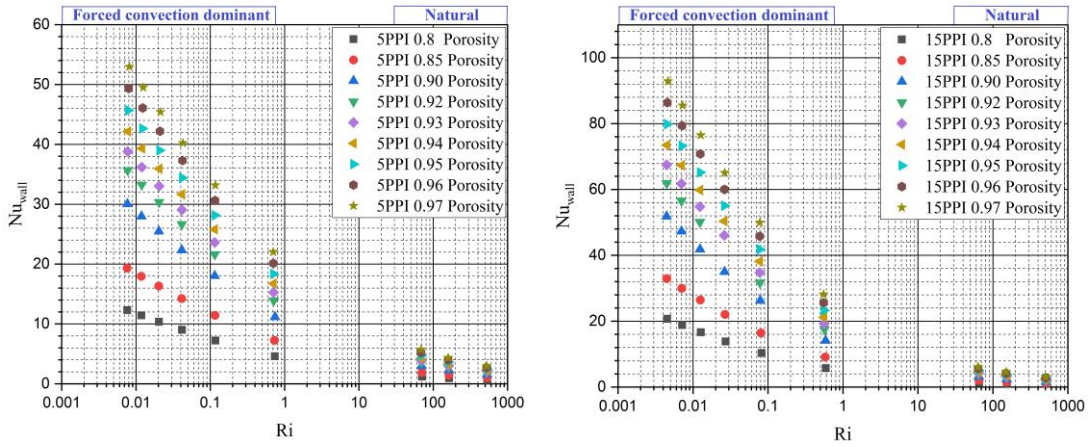

(a) (b)

Figure 4.4 (a) Variation of wall Nusselt number with Richardson number for 5PPI foam samples of various porosity (b) Variation of wall Nusselt number with Richardson number for 15PPI foam samples of various porosity

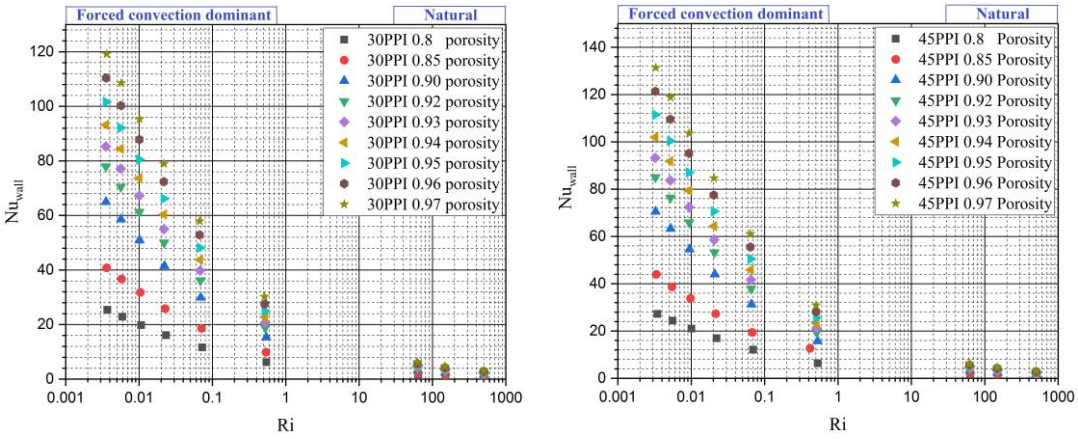

(a) (b)

Figure 4.5 (a) Variation of wall Nusselt number with Richardson number for 30PPI foam samples of various porosity (b) Variation of wall Nusselt number with Richardson number for 45PPI foam samples of various porosity

4.2.4 Obtaining Nu_n and Nu_f correlations (for natural convection dominant and forced convection dominant regimes respectively)

With a total of 252 data points in the limit accounting for natural convection dominant regime, wall Nusselt number description for natural convection dominant regime, involving heat transfer influencing independent-parameters such as porosity, pore density, Grashoff number and Richardson number is assumed as shown in Eq. (4.10). Similarly with a total of 378 data points in the limit accounting for forced convection

dominant regime wall Nusselt number description for forced convection dominant regime, involving heat transfer influencing independent-parameters such as porosity, pore density, Reynolds number and Richardson number is assumed as shown in Eq. (4.9).

$$\frac{Nu}{Re^{0.5}} = aRi^b\omega^c\varepsilon^d \tag{4.9}$$

$$\frac{Nu}{Gr^{0.25}} = aRi^b\omega^c\varepsilon^d \tag{4.10}$$

Further, for multi linear regression Eqs. (4.10) and (4.9) are rewritten in the form of Eq. (4.11).

$$\ln(G) = \ln(a) + b(\ln(Ri)) + c(\ln(\omega) + d(\ln(\varepsilon)) \tag{4.11}$$

which is of the form as given in Eq. (4.12),

$$Y = C + lx + my + nz \tag{4.12}$$

where, Y = ln(G), C is a constant to be regressed implying ln(a) and x, y and z are ln(Ri), ln(pore density) and ln(PPI)respectively with l, 'm' and 'n' co-efficients to be found by multi linear regression referring to their respective constants b, c and d.

That is obtained by taking log on both side of Eq. (4.13).

$$G = aRi^b\omega^c\varepsilon^d \tag{4.13}$$

where, G for correlating natural convection dominant and forced convection dominant regime are given as Eqs. (4.14) and (4.15) respectively:

$$G = Nu/Gr^{0.25} \tag{4.14}$$

$$G = Nu/Re^{0.5} \tag{4.15}$$

After completing the multi linear regression, for natural convection dominant regime with 252 data points Nu_n is obtained as shown in Eq. (4.16) with R^2 value of 0.99 showing good suitability of the obtained correlation to describe wall Nusselt number for natural convection dominant regime.

$$Nu_n = 1.1725Gr^{0.25}Ri^{-0.4112}\omega^{0.03157}\varepsilon^{8.02214} \tag{4.16}$$

Similarly, after completion of the multi linear regression, for forced convection dominant regime with 378 data points Nu_f is obtained as shown in Eq. (4.17) with R^2

value of 0.97 showing good suitability of the obtained correlation to describe wall Nusselt number for forced convection dominant regime.

It has been also noted that, with a straight forward polynomial regression, same expressions for Nusselt numbers are arrived.

$$Nu_f = 0.618Re^{0.5}Ri^{-0.08175}\omega^{0.27808}\varepsilon^{8.08507} \quad (4.17)$$

Parity plot showing comparison of wall Nusselt number data correlated for natural convection and forced convection dominant regime with simulated data is shown in Figure 4.6 (a) and (b) emphasizing on the aptness of the obtained correlations.

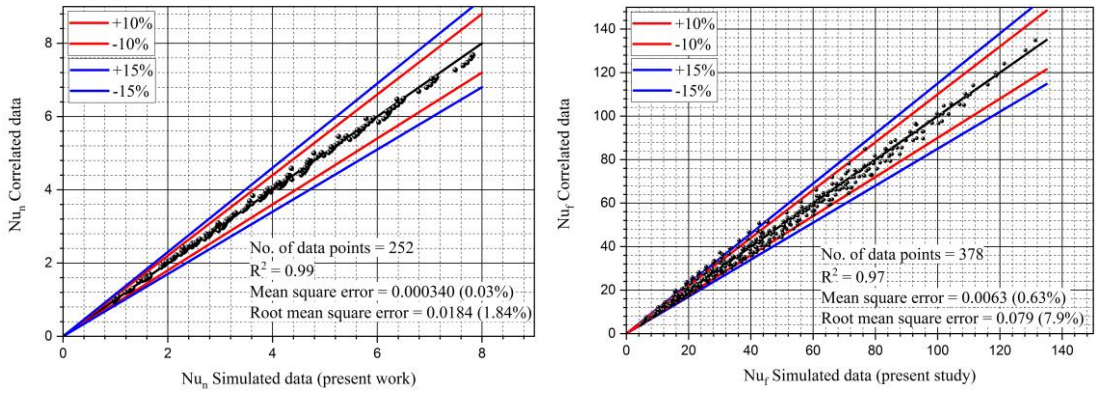

(a) (b)

Figure 4.6 (a) Parity plot depicting comparison of wall Nusselt number data correlated (for natural convection dominant regime) with simulated data (b) Parity plot depicting comparison of wall Nusselt number data correlated (for forced convection dominant regime).

4.2.5 Obtaining Nu_m correlation (for mixed convection dominant regime) using blending technique

The correlation for Nusselt number corresponding to mixed convection regime is obtained using a solution blending technique, that avoids the computational efforts involved with the numerical simulation. As the present study involves well suited asymptotically varying phenomena, this technique is employed to arrive at the correlation for mixed convection regime with the help of the known solutions for its two extreme phenomena (natural and forced convection).

An equation of the form $Y= [1 + (Z)^n]^{1/n}$ could be successfully used to depict the data points where the dependent variable varies uniformly for small and large values of the

independent variable. Y and Z are represented in the form of two limiting solutions (Churchill and Usagi 1972). If P1 and P2 are solutions for required parameter of two limiting phenomena as function of the asymptotically varying independent parameter, the solution for the intermediate phenomenon (P) can be obtained as the n^{th} order sum of the solutions of the extreme limiting phenomena. i.e., $P(i) = P1^n+P2^n$ and the same can be written in the form of $Y= [1 + (Z)^n]^{1/n}$ with following considerations. For phenomenon where 'P' is a function of the independent variable 'i' such that 'P' increases with increase in 'i' then equation of the form $Y= [1 + (Z)^n]^{1/n}$ can be obtained by substituting 'Y' as $P(i) / P2(i\rightarrow0)$ and 'Z' as $P1(i\rightarrow\infty) / P2(i\rightarrow0)$. Which takes the form $P(i) / P2(i\rightarrow0) = [1 + (P1(i\rightarrow\infty)/P2(i\rightarrow0))^n]^{1/n}$. For phenomenon where 'P' is a function of the independent variable 'i' such that 'P' decreases with increase in 'i' then equation of the form $Y= [1 + (Z)^n]^{1/n}$ can be obtained by substituting 'Y' as $P1(i\rightarrow\infty)/P(i)$and 'Z' as $P1(i\rightarrow\infty) / P2(i\rightarrow0)$. Which takes the form $P1(i\rightarrow\infty) / P(i) = [1 + (P1(i\rightarrow\infty) / P2(i\rightarrow0))^n]^{1/n}$. It can be noted that Y and Z are now represented in the form of two limiting solutions P1 and P2. This correlation is equivalent to n^{th} order sum of the asymptotic solutions $P1(i\rightarrow0)$ and $P1(i\rightarrow\infty)$. Flow chart emphasizing on ways of depicting the solutions in canonical form for various phenomenon that vary differently with increase or decrease in the value of independent parameter is shown in Figure 4.7 as illustrated by (Churchill and Usagi 1972). In the present work, as the Nusselt number values vary uniformly from lower and higher limiting value of independent parameter Ri , respective correlations of Nusselt number for natural convection (Nu_n) and forced convection (Nu_f) being asymptotically varying solutions for large and small independent-parameter (Ri), the whole data can be represented in the form of $Y= [1 + (Z)^n]^{1/n}$ as $Nu_n(Ri\rightarrow\infty) / Nu(Ri) = [1 + (Nu_n(Ri\rightarrow\infty) / Nu_f(Ri\rightarrow0))^n]^{1/n}$. Various other forms of representing the asymptotic solutions in the required canonical form for various phenomena (that differently varies with independent parameter) is shown with examples in Figure 4.7. In the present work, parameter 'P' is Nusselt number where $P(i\rightarrow\infty)$ corresponds to solution for Nusselt number in natural convection regime i.e., Nu_n, obtained when $Ri\rightarrow\infty$and $P(i\rightarrow0)$ corresponds to solution for Nusselt number in forced convection regime i.e., Nu_f, obtained when $Ri\rightarrow0$. Nu_n and Nu_f are two asymptotic solutions varying at limits of independent parameter Ri, such that Nu decreases with increase in independent parameter Ri and Nu increases with decrease in

independent parameter Ri. Correlations for Nu_n and Nu_f are obtained from numerical simulations of the present study. Correlation for the intermediate mixed convection phenomenon Nu_m occurring at mid-way between the extreme limits of the independent parameter Ri is found as illustrated by (Churchill and Usagi 1972). In an equation of the form $Y= [1 + (Z)^n]^{1/n}$, exponent 'n' can be found from a single intermediate value of Y(i), provided 'Y' is known at condition Z=1. Then, $n=\ln(2)/\ln[Y(Z= 1)]$. In the present work, the n^{th} order sum of the two numerically obtained limiting solutions can be seen represented as, $Nu_n/Nu_m= [1 + (Nu_n/Nu_f)^n]^{1/n}$, value of 'n' can be evaluated from a single intermediate value of Nu_n/Nu_m, provided at the condition when $Nu_n/Nu_f=1$.

After obtaining suitable correlation for describing wall Nusselt number for natural and forced convection dominant regimes (two asymptotically varying phenomenon) represented by extreme limits of the Richardson number, for obtaining solution for an intermediate phenomenon (i.e., mixed convection) it requires only solutions of the other extreme phenomena (of natural and forced convection regimes) but not any effort, as this technique requires no data from simulation or experimentation to obtain a suitable correlation (Churchill and Usagi 1972).

The obtained correlations for Nu_n and Nu_f are represented in the canonical $Y= [1 + (Z)n]^{1/n}$ form as shown in Eq. (4.8), which is obtained as,

$$\frac{Nu_n}{Nu_m} = [1 + (1.897249Ri^{-0.07937}\omega^{-0.24651}\varepsilon^{-0.063})^n]^{1/n} \quad (4.18)$$

The criteria as explained in (Churchill and Usagi 1972) to find the value of 'n' is that in the canonical form $Y= [1+(Z)^n]^{1/n}$, if 'Y' is known for condition where Z= 1, then, $n = \ln(2)/\ln[Y(Z= 1)]$.

From Eq. (4.18) we know that $Z= 1.897249Ri^{-0.07937}\omega^{-0.24651}\varepsilon^{-0.063}$. Evaluating this for central value of Richardson number where, 'Z' is equal to 1. From set of simulated data, it is identified that, for 5PPI and 0.8 porosity foam sample there exists 25.79484 'Ri' value when subjected to air velocity of 0.0568 m/s. At this central value, the value of 'Z' becomes equal to 0.99975 which is closer to 1.

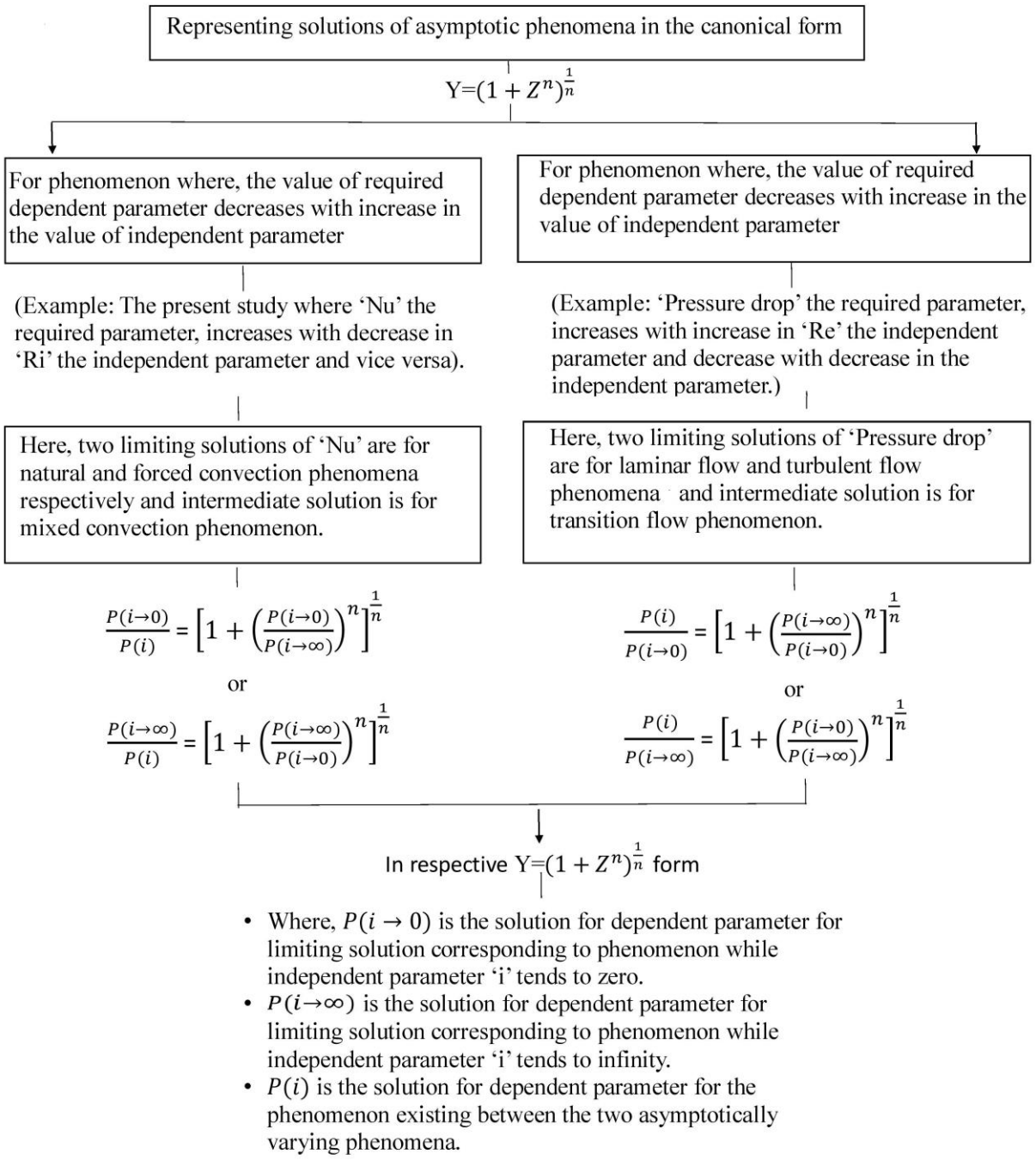

Figure 4.7 Flowchart depicting solutions of required parameter for asymptotically varying phenomena.

Therefore, the value of 'n' obtained is 21.78. By substituting this value in Eq. (4.18) we get Eq. (4.19) as,

$$\frac{Nu_n}{Nu_m} = \left[1+(1.897249Ri^{-0.07937}\omega^{-0.24651}\varepsilon^{-0.063})^{21.78}\right]^{1/21.78} \quad (4.19)$$

Deducing to the required solution for wall Nusselt number of mixed convection, we get Eq. (4.20) and (4.21) respectively as,

$$Nu_m = Nu_n[1 + (1.897249Ri^{-0.07937}\omega^{-0.24651}\varepsilon^{-0.063})^{21.78}]^{-1/21.78} \quad (4.20)$$

$$Nu_m = 1.1725Gr^{0.25}Ri^{-0.4112}\omega^{0.03157}\varepsilon^{8.02214}[1 + (1.897249Ri^{-0.07937}\omega^{-0.24651}\varepsilon^{-0.063})^{21.78}]^{-1/21.78} \quad (4.21)$$

Variation of wall Nusselt number value calculated from simulated data with 'Ri' values is shown in Figure 4.8 (a) and (b). Increase of heat transfer characteristics of each foam sample while approaching to forced convection regime can be observed. Similar to what was observed from both natural and forced convection results, Nusselt number in mixed convection is also observed to increase greatly with porosity compared to increase in the parameter with increase in pore density.

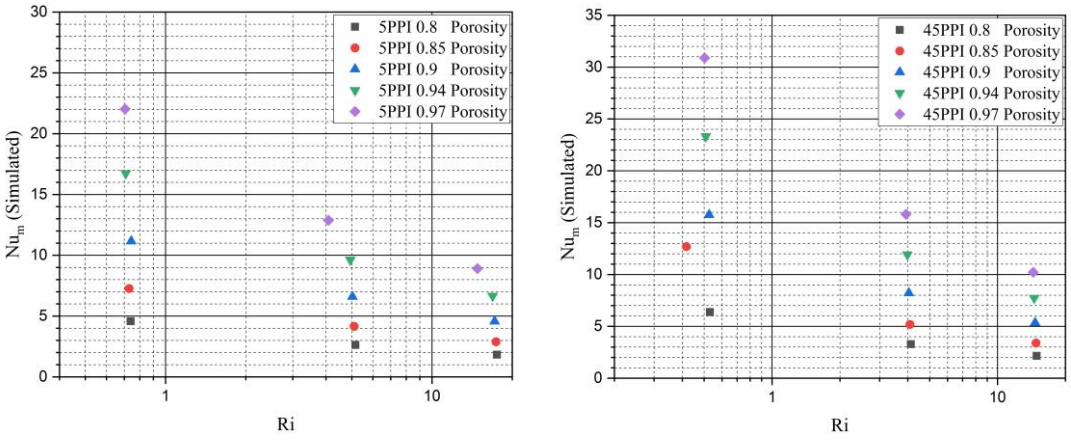

(a) (b)

Figure 4.8 (a) Simulated wall Nusselt number against Richardson number in mixed convection regime for 5PPI foam sample of various porosity (b) variation of simulated wall Nusselt number against Richardson number in mixed convection regime for 45PPI foam sample of varying porosity.

Parity plot depicting the variation of correlated Nusselt number values given in Eq. (4.21) obtained from the solution blending technique with simulated data for wall Nusselt number is depicted in Figure 4.9, the correctness of the correlated data with that of simulated data is well illustrated with the parity plot of less than ±10%.

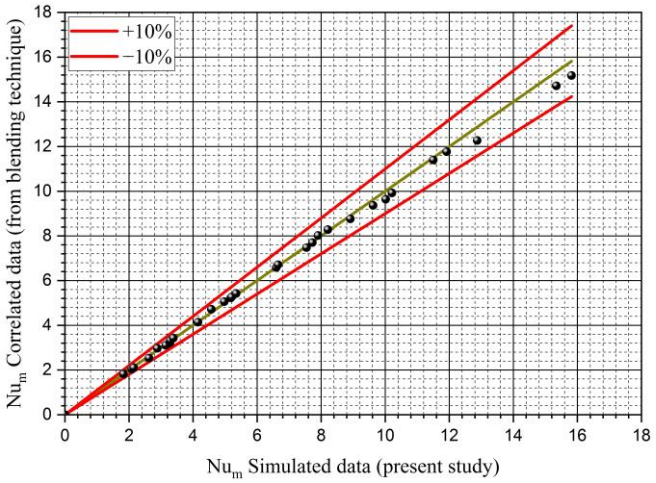

Figure 4.9 Parity plot depicting variation of correlated data for Nu_m obtained by blending technique with that of simulated data for Num under mixed convection regime.

Division of convection regimes based on the slopes of wall Nusselt number, is shown in Figure 4.10 (a) and (b).

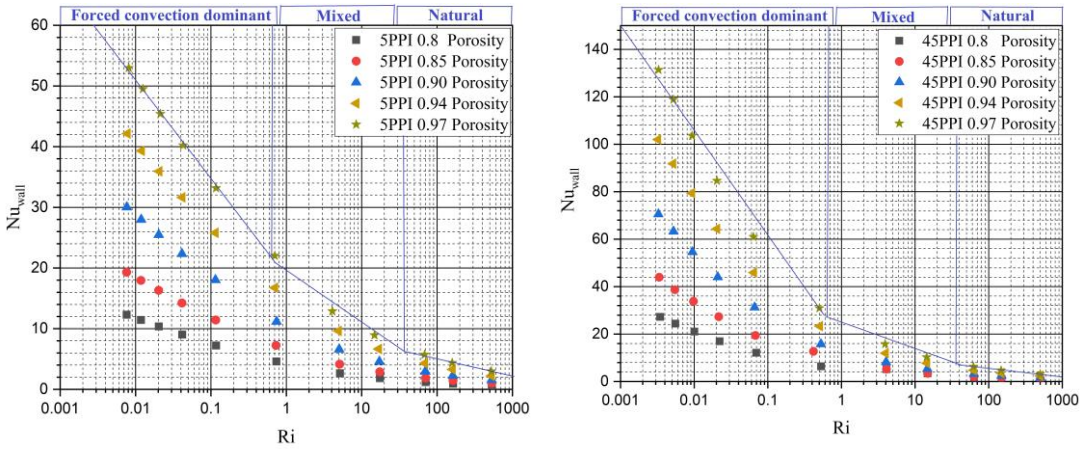

(a) (b)

Figure 4.10 (a) Plot showing division of convection regimes for 5PPI foam samples of varying porosity (b) Plot showing division of convection regimes for 45PPI foam samples of varying porosity based on wall Nusselt number produced for corresponding Richardson number values.

Based on this observation the convection regimes can be classified as follows:

- Natural convection dominant regime $Ri \geq 39$

- Mixed convection dominant regime $0.6 \leq Ri \leq 40$
- Forced convection dominant regime $Ri \leq 0.6$

Comparison of wall Nusselt number obtained from correlations provided in the present study (as shown in Eqs. (4.16), (4.17) and (4.21)) with that of obtained from correlation provided in experimental work of (Kamath et al. 2011) for porous filled vertical channel is shown in Figure 4.11.

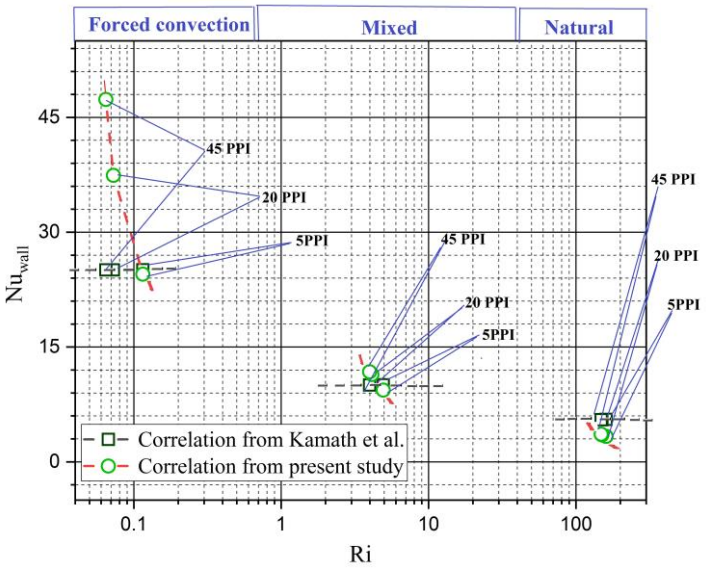

Figure 4.11 Comparison of wall Nusselt number data obtained from correlations presented in the current study with that of experimental work of (Kamath et al. 2011) for 0.94 porosity foam samples of various pore density.

The correlation provided by (Kamath et al. 2011) to evaluate wall Nusselt number to account heat transfer through metal foam filled vertical channel is shown in Eq. (4.22). It describes the wall Nusselt number in terms of flow parameter 'Re', heat transfer parameter 'Ri' and metal foam parameter porosity. However, accounting only porosity as the heat transfer influencing parameter results in inappropriate prediction of the required data, as the heat transfer in porous media is mainly accounted due to combination of both porosity and pore density and not solely on any of the only parameters. In Figure 4.11 it can be observed that, wall Nusselt number predicted using correlation of (Kamath et al. 2011) yields no deviation with changes in pore density for metal foam sample of given porosity. However, the increment in heat transfer due to

increased pore density for a given porosity of foam samples can be seen rightly predicted by the correlation provided in the present work. For better illustration purpose, only foam samples of 0.94 porosity with varying pore densities such as 5, 20 and 45 PPI is shown in the figure, however the variation is similar to other combinations of pore density and porosity.

$$Nu = 0.223\varepsilon^{6.81}Re^{0.723}(1 + Re^{-0.73}Ri^{0.46}) \quad (4.22)$$

for,

$0.005 \leq \mathrm{Ri} \leq 1032$

$24 \leq \mathrm{Re} \leq 3730$

$0.9 \leq \varepsilon \leq 0.95$

4.3 SUMMARY

In this chapter, the necessity of consideration of the effect of both the structural properties i.e., porosity and pore density on thermo-hydraulic behaviour is emphasized. Their prominent potential in influencing the flow and heat transfer phenomenon owing to various combinations of their porosity and pore density is highlighted as a result of the corresponding changes in their interfacial properties. Correlations for wall Nusselt number as a function of the mentioned twin properties is obtained for natural convection and forced convection dominant regimes with the help of numerically simulated data. Further these two asymptotically varying solutions were blended using the technique to arrive at a suitable correlation that predicts heat transfer characteristics under mixed convection the intermediate phenomenon existing between the formerly mentioned two phenomena. A comprehensive heat transfer analysis is made for all three convection regimes involving metal foams of orderly varied structural properties, with an aim to further demonstrate the possible variations of heat transfer characteristics with altered combinations of pore density and porosity. Inaccuracies involved if ignoring the effect of combination of these twin structural properties is demonstrated with the example of Nusselt number correlation provided by a previous study.

Analysing the Nusselt number correlations formulated as a function of vital independent parameters such as pore density, porosity, Richardson number, Grashof number and Reynolds number, following key observations were made:

- Under natural convection dominant regime (Eq. (4.16), for $Ri \geq 39$), effect of pore density at constant porosity is not as influencing as in case of mixed and forced convection dominant regimes in altering heat transfer characteristics of metal foams.
- However, the consideration of the effects of combination of pore density and porosity of metal foams, under mixed convection (Eq. (4.21), for $0.6 \leq Ri \leq 40$) and forced convection (Eq. (4.17), for $Ri \leq 0.6$) scenario is crucial in analysing and distinguishing heat transfer characteristics.

4.4 CLOSURE

In this work the influence and significance of twin structural properties (porosity and pore density) of metal foams in exhibiting various thermal and flow-resistance characteristics are demonstrated with an aim to arrive at different possible thermo-hydraulic characteristics to further comprehensively analyze the behaviour as a means to handle the incurred pressure drop that accompanies the benefit of heat transfer enhancement.

CHAPTER – 5

VARIOUS TRADE OFF SCENARIOS IN THERMO-HYDRODYNAMIC PERFORMANCE OF METAL FOAMS OWING TO THEIR THICKNESS AND STRUCTURAL CONDITIONS

5.1 INTRODUCTION

Long standing issue of increased heat transfer always being accompanied by increased pressure drop using metal foams is something that concerns the implementation of such media in engineering applications, specifically pertaining to thermal management systems. As seen in earlier chapters variation of structural properties can be one of the prime variables that can be used to control the trade-off between the desirable heat transfer and unsought flow resistance. In this work, variation of thickness is introduced simultaneously with the variations of structural properties (porosity and pore density) and various trade-off scenarios between the potentials of metal foams to enhance heat transfer and ability to minimize flow resistance are analyzed.

Heat transfer and pressure drop, both of various magnitudes can be observed corresponding to various heat transfer and flow influencing parameters of considered metal foams. In this regard, orderly varying pore density and porosity along with varied thickness is considered to comprehensively analyze variation in the trade off scenario between flow resistance minimization and heat transfer augmentation behavior of metal foams with the help of numerical simulations and TOPSIS (Technique for Order of Preference by Similarity to Ideal Solution) a multi-criteria decision-making tool to address the considered multi objective problem. Metal foams of four thickness ratios are considered along with varied pore density and porosity combinations. Numerically obtained pressure and temperature field data are critically analyzed for various trade off scenarios exhibited under the above-mentioned variable conditions. Type of metal foam based on its morphological (pore density and porosity) and configurational (thickness) aspect that can participate in a desired trade off scenario between flow resistance and heat transfer is illustrated.

5.2 PROBLEM STATEMENT

The numerical details and the methodology remain same as described in chapter 3 for analyzing the metal foams. Aluminum metal foam of 0.95, 0.9, 0.85 and 0.8 porosity each with pore density of 25, 20, 15, 10 and 5 PPI are analyzed. Air flow of 0.4 m/s is allowed into the channel consisting of heater-plate (Al)-porous assembly. At steady-state condition, temperature field across the aluminum plate is obtained in terms of average wall temperature, at every case considering 20 various types of metal foams (of various structural aspects i.e., pore density and porosity) each at 4 different thickness scenarios, totaling 80 different cases for simulations. The studied 4 thickness conditions (100%, 75%, 50% and 25%) of the metal foams are shown in Figure 5.1.

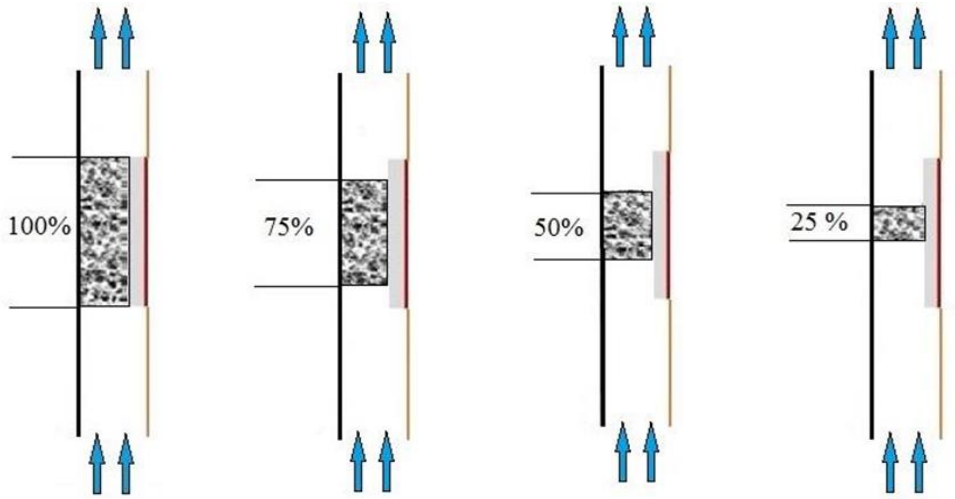

Figure 5.1 Sketch depicting the various thickness configurations considered in the present study (a) 100% thickness; (b) 75% thickness; (c) 50% thickness; (d) 25% thickness.

Using each structural (pore density and porosity combination) and configurational (various thickness) information, average wall temperature of the aluminum plate is computed along with pressure drop incurred across the foam samples. Further, pressure drop (representing flow resistance), wall heat transfer co-efficient (representing heat transfer enhancement) are comprehensively analyzed using TOPSIS a multi-objective multi-criteria decision-making tool to comprehend the trade-off scenario between enhanced heat transfer and increased pressure drop for all the considered scenarios.

5.3 PRESSURE DROP AND HEAT TRANSFER CHARACTERISTICS

Pressure drop variations are shown in Figure 5.2 for varying thickness scenarios, each for foam samples of various pore density and porosity combinations. It can be observed that for any given thickness of the foam sample considered, pressure drop variation increases with increase in pore density (for a given porosity condition) and decreases with increase porosity (for a given pore density conditions). This is due to varied flow obstruction as a result of varied fiber diameter (due to change in porosity for a given pore density) and varied number of porous fibers (due to change in pore density for a given porosity), following the explanations provided in the previous chapter.

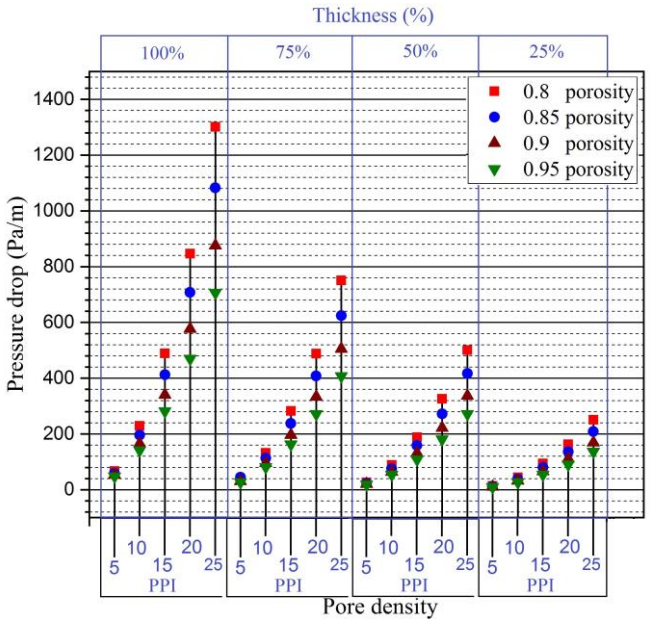

Figure 5.2 Variation of pressure drop for varying thickness scenario at various pore density and porosity conditions.

When thickness of the metal foams are reduced, as an obvious behavior the pressure drop is observed to decrease. Interesting observations can be made from Figure 5.2 such as, though pressure drop continuously decreases or increases for a given pore density and porosity combination with variation in thickness, a certain pressure drop characteristics can be observed to be closely exhibited from foam samples of different foam structural properties (pore density and porosity) under varied thickness scenario. Since, heat transfer characteristics also vary with the mentioned variables, it would be interesting to analyze what combinations of pore density and porosity of a foam sample

under which thickness scenario would participate in a desired trade-off between curtailing pressure drop and enhancing heat transfer.

Heat transfer characteristics of the metal foams of considered pore density and porosity combinations with varying thickness condition is shown in Figure 5.3 in terms of average wall heat transfer coefficient.

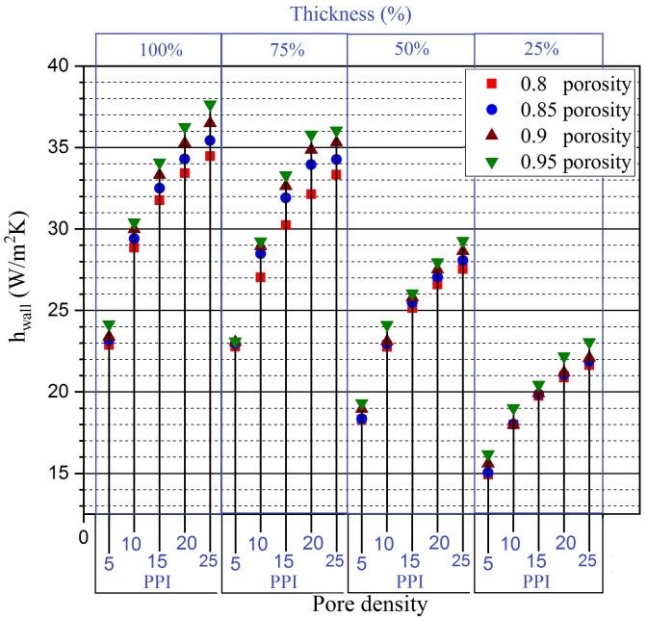

Figure 5.3 Variation of wall heat transfer coefficient for varying thickness scenario at various pore density and porosity conditions

It can be observed that for any given thickness scenario, the average wall heat transfer coefficient increases with increase in pore density for a given porosity condition as a result of increased interfacial surface area participating in increased interfacial heat transfer. Similarly for a given pore density condition at any thickness scenarios considered, wall heat transfer coefficient is observed to slightly increase with increase in porosity. This is primarily due to increased fluid to solid ratio with increase in porosity enabling more fluid participating in heat transfer promoting direct heat transfer along with the supplemented interfacial heat transfer. It can be seen that wall heat transfer coefficient increases greatly with increase in pore density for a given porosity condition compared to increase in the same with increase in porosity for a given pore density condition. Direct heat transfer by the fluid from the heat source (heated wall) and interfacial heat transfer (by the fluid from solid structures of the porous sample) are

the key features of total heat transfer associated with introduction of porous medium in a heat transfer domain. Interfacial specific surface area (a_{sf}) and interfacial heat transfer co-efficient (h_{sf}) being the interfacial parameters, the product ($a_{sf} \times h_{sf}$) of which can be seen appearing in the energy equation (Eq. (1.14) in section 1.5.3.2 of chapter 1), accounts for the interfacial heat transfer. Increase in pore density with constant porosity increases both interfacial specific surface area and interfacial heat transfer co-efficient. Thereby, since porosity is constant (void space accommodating fluid being constant), maintaining direct heat transfer the same, there is further increase in heat transfer due to enhanced interfacial heat transfer. Whereas, increase in porosity at constant pore density, slightly decreases interfacial specific surface area that results in a slight decrease in the interfacial heat transfer while the direct heat transfer still being increased due to more void space accommodating more fluid that participates in enhanced direct heat transfer from the heater plate. Owing to these effects heat transfer characterized by wall heat transfer co-efficient can be observed to greatly increase with pore density for a given porosity condition (due to enhanced total heat transfer as a result of further supplement from interfacial heat transfer to the existing direct heat transfer) compared to slight increase in the same with increase in porosity for a given pore density condition (due to enhanced direct heat transfer with a slight decrease in interfacial heat transfer, that together contributes for only a slight increase in total heat transfer). In addition to this, the increase in heat transfer can be observed with increase in thickness due to the existence of more porous structures promoting more interfacial heat transfer.

Each metal foam of given pore density and porosity combination under considered thickness exhibits a unique heat transfer and pressure drop characteristics. It brings in an interesting question of by what magnitude the pressure drop is compensated to exhibit the corresponding heat transfer behavior. Noting that this trade off scenario varies with the structural (pore density and porosity) and as well as with configurational (thickness) aspects, a comprehensive analysis on understanding the tradeoff mechanism between minimizing pressure drop abilities and maximizing heat transfer characteristics of a metal foam under a given variable condition would be very beneficial in the field of heat transfer involving metal based porous media.

5.4 TRADE-OFF ANALYSIS USING TOPSIS

As a well-known fact, the benefit of increase in heat transfer is always accompanied by undesired increased pressure drop with use of metal foams in heat exchanging applications. It is a long-standing issue which requires attention to arrive at an optimum performance. There are several aspects that determines the exhibited trade off process in heat transfer enhancement and pressure drop minimization phenomenon, among them varying thickness scenario and varying pore density and porosity of metal foams become the best choice of parameters to be involved in analyzing the tradeoff process as they can be easily varied. In the present chapter, varying thickness scenario of four kinds are considered simultaneously with altering pore densities of five kinds (5, 10, 15, 20 and 25 PPI) each with combination of various porosity like 0.8, 0.85, 0.9 and 0.95 porosity. The flow resistance characterized by pressure drop and heat transfer characterized by average wall heat transfer coefficient exhibited by metal foams of above-mentioned variable conditions as shown in Figure 5.2 and Figure 5.3 respectively do not give information on what is the trade-off in flow resistance minimization behavior of metal foams while exhibiting a given heat transfer characteristic. It is here, TOPSIS (technique for order of preference by similarity to ideal solution) a multi objective, multi criteria decision making tool plays a key role in analyzing which metal foams of given variable condition performs best in meeting a desired trade off scenario. In other words, TOPSIS methodology enables one to understand how flow resistance minimization behavior of metal foams are compromised in order to exhibit a given heat transfer behavior subjected to variable conditions such as pore density and porosity of the metal foam and the thickness considered. In this section, the results of TOPSIS analysis on the present problem are presented for various trade-off scenarios (in terms of Criteria I to V) involving variable conditions such as pore density, porosity and thickness of the metal foam that can alter the trade-off between pressure drop and heat transfer. The detailed description of the methodology and formulations involved in TOPSIS technique is illustrated in section 3.7 of chapter 3.

5.4.1 Criteria 1 (h_{max} : P_{min} :: 0 : 1)

Criteria I, that represents the trade-off scenario between pressure drop and heat transfer where complete importance is given to minimization of pressure drop with no attention given to enhancement of heat transfer. Various performances of metal foams under the considered variable conditions in order to meet the specific weighted objective pertaining to criteria 1 are shown in Figure 5.4 considering trade-off between pressure drop with wall heat transfer coefficient.

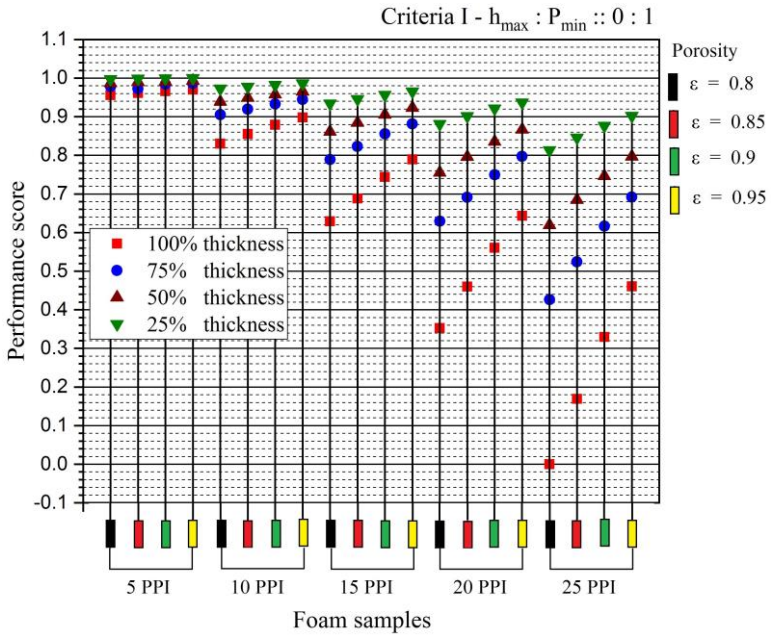

Figure 5.4 Criteria I (h_{max} : P_{min})

Under the circumstance of criteria 1, where all the importance is focused on minimization of pressure drop (by placing complete weight of '1' on minimizing pressure drop objective) and zero importance is given on maximizing heat transfer (by placing weight of '0' on maximizing heat transfer objective), as an obvious interpretation it can be noted that, for a given thickness scenario metal foams of lower pore density (PPI) that offer less obstruction to flow is scored best for a given porosity condition. Similarly, for a given thickness scenario, it can be observed that for a metal foam sample of a considered pore density, the performance of higher porosity foams are better in relative to lesser porosity foams that offer higher flow resistance. Comparing this performance with varying thickness condition, it can be noted that for any foam sample of a given pore density and porosity condition, a better performance

is achieved with decrease in thickness as an obvious result of reduced flow resistance accompanying reduced thickness scenario of the metal foams. It's interesting to note that, the performance of metal foam of a particular pore density and porosity conditions at given thickness scenario can be closer to performance of metal foam of a different pore density and porosity combination under different thickness scenario. This kind of performance charts help one to choose a desired variable condition for instance thickness of metal foams where there are restricted variations in pore density and porosity combinations of the metal foams.

5.4.2 Criteria 2 (h_{max} : P_{min} :: 0:25 : 0.75)

Criteria 2, representing a scenario where slight importance is given to heat transfer maximization capabilities of foams (with 25% distributed weight on maximizing heat transfer objective) and still a larger importance given to minimizing pressure drop objective (with 75% distributed weight on this objective) are shown in Figure 5.5.

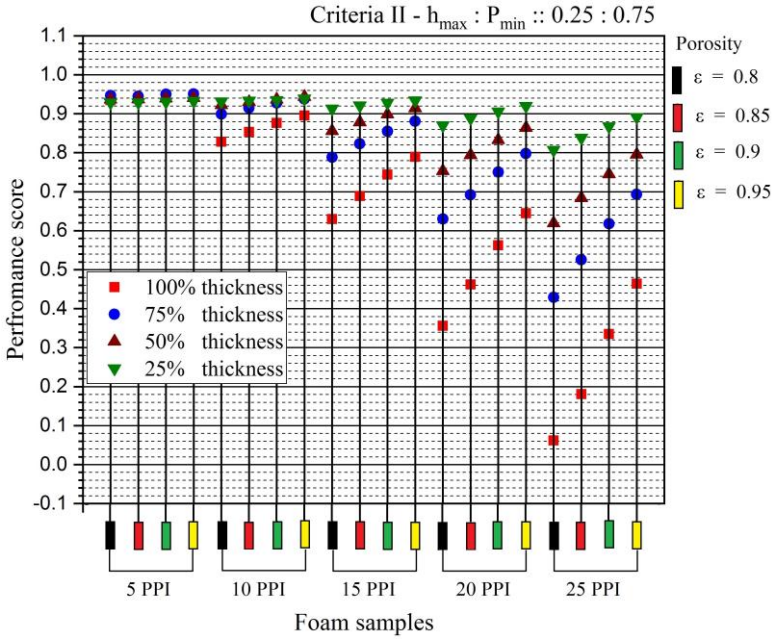

Figure 5.5 Criteria II (h_{max} : P_{min})

It can be observed that 5 PPI foam sample of 25% thickness that performed best in meeting the objectives of criteria 1, performs lowest while subjected to objectives of criteria 2. However, for other pore density scenario apart from 5 PPI, the relative deviation of performance scores of foam samples is observed to get closer to that of criteria 1 particularly with increase in pore density (PPI) condition.

5.4.3 Criteria 3 (h_{max} : P_{min} :: 0:5 : 0:5)

Criteria 3, representing a scenario where equal importance is given to heat transfer maximization capabilities of foams (with 50% distributed weight on maximizing heat transfer objective) and to minimizing pressure drop objective (with 50% distributed weight on this objective) and the results are shown in Figure 5.6.

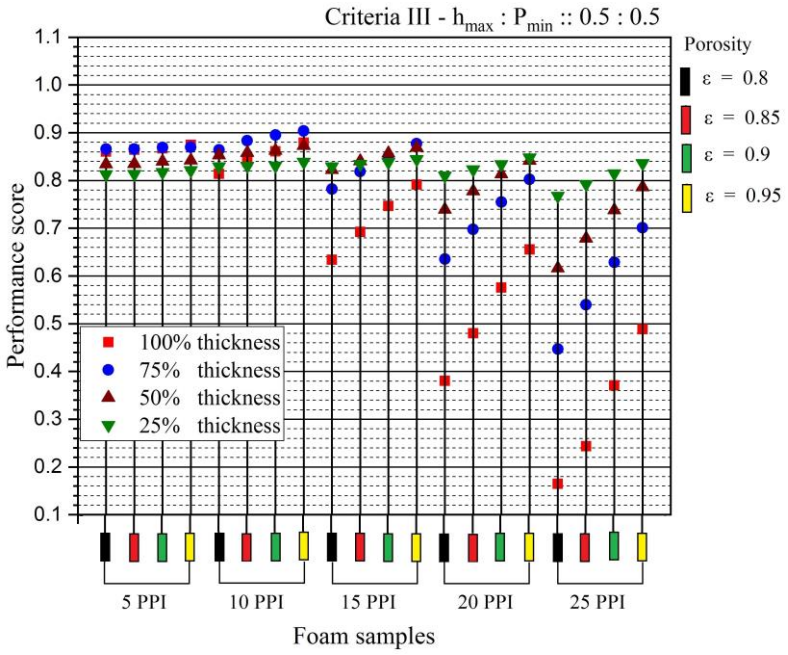

Figure 5.6 Criteria III (h_{max} : P_{min})

It can be observed that foam samples of 10 PPI pore density at 75% thickness condition performs best in meeting the criteria with increase in porosity. 50% thickness foam samples of 15 PPI pore density can be observed to outperform 25% thickness foam samples of 15 PPI at higher porosity condition, unlike the situation in criteria 1 and 2 where, 25% thickness foam samples still performed the better than foam samples of 50%thickness. Tendency of 50%thickness foam samples of 20 PPI pore density to outperform 25% thickness scenario can also be observed at higher porosity condition. At 5 PPI pore density condition, 75% and 100% thickness conditions are observed to perform very close to each other. However, at scenarios of higher pore density like 25 PPI, relative deviation of performance scores of foam samples of considered variable conditions are similar to that, criteria 1 and 2 where a foam sample a given pore density and porosity condition performance best at 25% thickness condition followed by 50, 75 and 100 percent thickness conditions.

5.4.4 Criteria 4 (h_{max} : P_{min} :: 0:75 : 0:25)

Criteria 4, representing a scenario where more importance is given to heat transfer maximization capabilities of foams (with 75%distributed weight on maximizing heat transfer objective) and comparatively lesser importance given to minimizing pressure drop objective (with 25%distributed weight on this objective) are shown in Figure 5.7. Foam samples of 75% and 100%thickness are observed to closely perform (subjected to objectives of this criteria) at all porosity conditions at 5 PPI and 10 PPI conditions, with 100%thickness condition showing inclinations to perform better than 75%thickness condition at highest porosity case. However, this behavior is clearly exhibited with higher pore density conditions such as 15, 20 and 25 PPI where foam samples of 75% thickness can be seen dominating all other thickness scenarios at highest porosity condition. Variation in performance (either increasing or decreasing behavior) can be seen at varying porosity condition due to changes in the trade off scenarios between pressure drop and heat transfer.

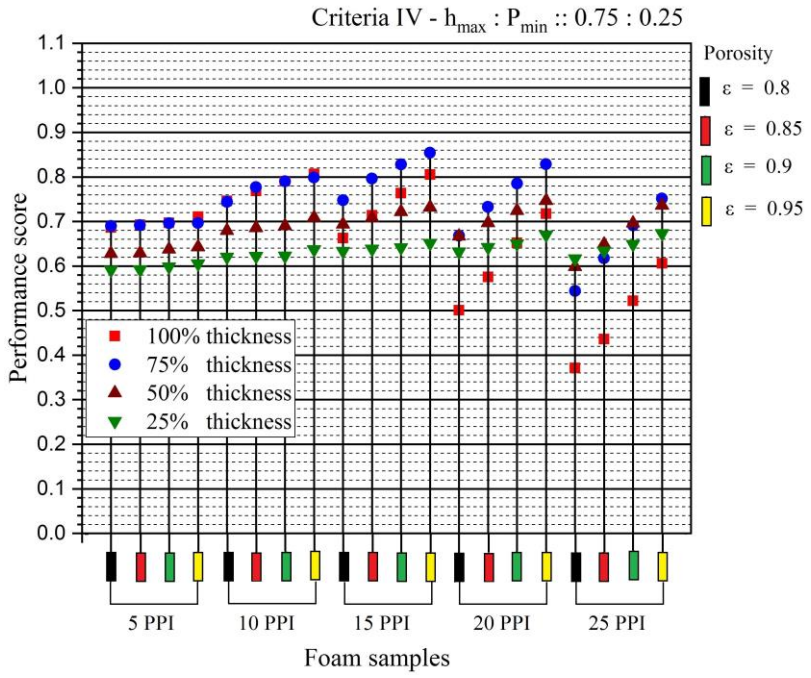

Figure 5.7 Criteria IV (h_{max} : P_{min})

5.4.5 Criteria 5 (h_{max} : P_{min} :: 1 : 0)

Criteria 5, representing a scenario where highest importance is given to heat transfer maximization capabilities of foams (with 100%distributed weight on maximizing heat

transfer objective) and least importance given to minimizing pressure drop objective (with 25%distributed weight on this objective) are shown in Figure 5.8. In other words, criteria 5 ranks the foam samples subjected to different variable conditions such as variable pore density, porosity and thickness conditions based on complete attention given to maximizing heat transfer abilities of the foam samples with no attention given to minimization of pressure drop. Hence subjected to this criterion, those foams samples of a given variable conditions are scored best that exhibits highest heat transfer irrespective of the pressure drop.

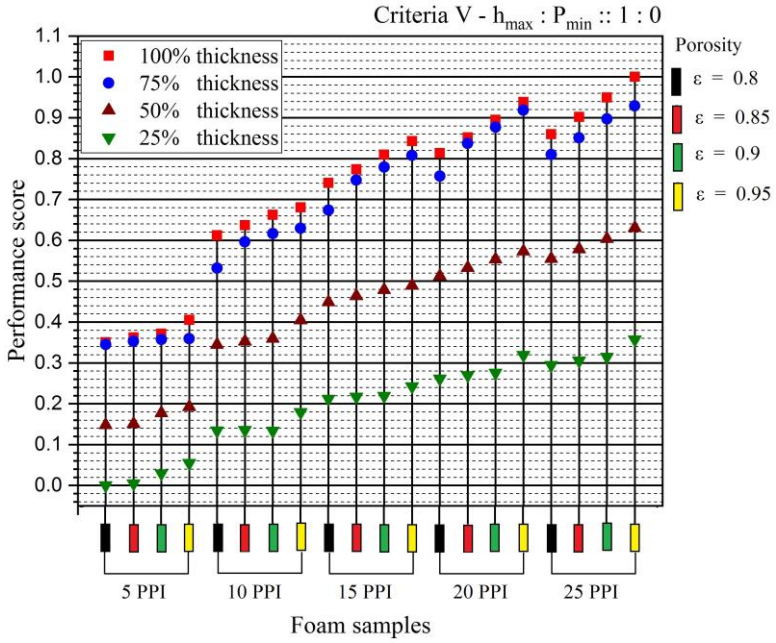

Figure 5.8 Criteria V (h_{max} : P_{min})

As it can be observed from **Figure 5.8**, for any foam sample of given pore density and porosity case 100%thickness foams perform best in meeting this criterion followed by 75, 50 and 25%thickness condition. For a given thickness and pore density condition the performance scores (subjected to objectives of criteria 5) of foam samples are observed to increase with porosity. In each pore density condition 100%filled case with highest porosity can be seen performing best in meeting this criterion. Highest pore density case with highest porosity and 100%thickness exhibits the highest heat transfer which can be seen ranked the best in Figure 5.8. It can be noted that though pressure drop is relatively larger in higher pore density case and complete thickness case 25 PPI foam of completely filled case is ranked best considering its highest heat transfer

enhancement behaviour irrespective of its flow resistance behaviour as decided by criteria 5.

From Figure 5.4 to Figure 5.8 it can be noted that, every foam sample of given variable conditions (pore density, porosity and thickness) shows different magnitude of inclinations towards meeting a specific criterion (subjected to different objectives of various magnitudes of importance). The variation in relative performance of foams of particular variable condition with changes in criteria shows how differently does a foam sample of particular variable condition participates in trade-off between heat transfer and flow resistance. Such analysis not only helps one to decide which variable conditions to consider for a given or desired heat transfer and pressure drop characteristics but also judges on how well a given condition is participating in trade-off between heat transfer and pressure drop which is a crucial point in designing a heat exchanging device especially dealing with metal foam like materials to enhance heat transfer that always comes with a penalty of increased pressure drop in a thermal system.

5.5 SUMMARY

In the present chapter a critical analysis on various trade-off scenarios between heat transfer and pressure drop involving metal foams has been illustrated. For this purpose, metal foams of three prime variable conditions including pore density (5, 10, 15, 20 and 25 PPI), porosity (0.8, 0.85, 0.9 and 0.95 porosity) and thickness (100, 75, 50 and 25 percent) were considered in a vertical channel subjected to constant heat flux condition. Individually analyzing, heat transfer characteristics were observed to increase with pore density, porosity and thickness of the foam sample as expected. Also, pressure drop was observed to decrease with decrease in pore density and thickness condition and with increase in porosity. Both flow resistance and heat transfer characteristics are simultaneously analyzed for foam samples of three orderly varying variable conditions namely pore density, porosity and thickness under different objectives (one is to maximize heat transfer and another to minimize pressure drop) subjected to various magnitudes of importance, to understand various trade-off scenario a foam sample of given variable condition would participate in. Interesting trade-off scenarios between the enhancement of heat transfer and reduction of flow resistance behavior was

demonstrated using TOPSIS a multi-objective multi criteria decision making tool that comprehensively illustrates various potentials of every foam sample of considered variable conditions in meeting a desired trade-off condition.

The criteria of h_{max} : P_{min} is used to represent the trade-off scenario between pressure drop and heat transfer. For the criteria of h_{max} : P_{min} :: 0 : 1, metal foam with 5 PPI, 25% thickness yields the best score. For the criteria of h_{max} : P_{min} :: 0.5: 0.5, the best score belonged to the metal foam with 10 PPI, 75% thickness with porosity of 0.95. The metal foam with 25 PPI, 100% thickness with porosity of 0.95 received the best score for the criteria of h_{max} : P_{min} :: 1.0 : 0.0.

The selection of the best pore density, thickness and porosity was observed to be depending on the criteria representing the trade-off between the pressure drop and heat transfer. It is found that a score given by TOPSIS method can deduce the best configurational and structural parameters for a specified application, demanding a specific cost and benefit trade-off scenario.

5.6 CLOSURE

An effort to efficiently comprehend the nature and magnitude of the enhanced heat transfer benefit of metal foam porous media in relation to the corresponding cost incurred in terms flow resistance is undertaken in the present study. Various possible heat transfer and flow resistance characteristics of such medium is demonstrated considering variable conditions such as its structural (porosity and pore density) and thickness conditions. For every various combination of these properties, how the trade-off between the heat transfer enhancement property and flow resistance minimization properties of such medium varies is comprehensively analyzed.

CHAPTER – 6

CORRELATIONS AND NUMERICAL MODELLING OF STACKED WOVEN WIRE-MESH POROUS MEDIA FOR HEAT EXCHANGE APPLICATIONS

6.1 INTRODUCTION

Stacked woven wire-mesh porous media can be seen aiding the process of flow and thermal management in several engineering applications. However, the exploration of their potentials, characteristics, possible controllable features leading to optimized performance seem to be lacking in the open literature. So far, metal foams have gained enormous attention due to their heat transfer augmenting capabilities. In the literature, correlations describing relations among their morphological characters have successfully been established and well discussed which has enabled the process of numerical techniques using REV (representative eliminatory volume) scale modeling, leading to efficient utilization of such media. However, collective expressions that categorize stacked wire mesh based on their morphology and thermo-hydraulic expressions required for numerical modeling are less explored in literature. Cross relations among the morphological characters of stacked wire-mesh based on mesh-size, wire diameter and stacking type, are very much essential for describing such medium and aids the process of determining the key input parameters required for numerical modeling. Correlation for specific surface area, a vital parameter that plays major role in interstitial heat transfer can also be seen not available in the open literature. With these correlations arrived, properties of stacked wire-mesh samples of orderly varied mesh-size and porosity can be obtained for various stacking scenario, mesh-size and corresponding thermo-hydraulic parameters appearing in the governing equations can be evaluated. And thus, the potentials of such stacked woven wire-mesh porous media in controlling the flow and heat transfer phenomena can be elaborately analyzed using numerical modeling technique.

As it is quite evident that the discussion related to expressions required for modeling of stacked wire-mesh type of porous medium is limited in the open literature, but plays a

major role in analyzing the flow and heat transfer characteristics obtained from the numerical studies carried out considering such type of porous medium. In the present chapter, expressions that describe morphological characteristics of stacked woven wire-mesh type of porous medium is arrived, that can categorize various samples of such type of porous medium with varied characteristics such as porosity, specific surface area as a result of variation in parameters like fiber diameter of the woven wires, pore-density/mesh-size and type of stacking. Further with the use of the obtained expressions, the categorized stacked wire-mesh porous samples of orderly varying porosity and mesh size are investigated for their performance in enhancing heat transfer in a vertical channel subjected to constant heat flux and laminar air flow. The flowchart of the present work methodology is shown in Figure 6.1.

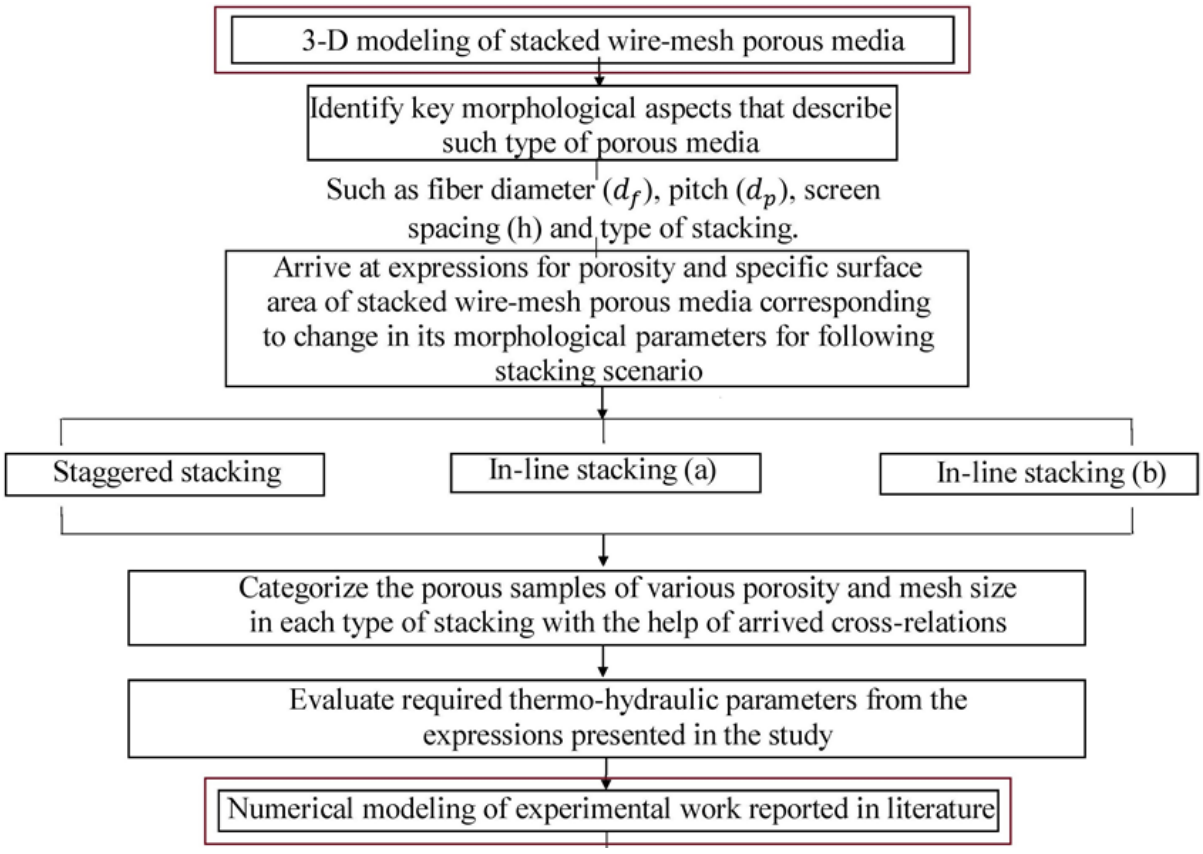

Figure 6.1 Chart describing the flow of the present work

6.2 PROBLEM STATEMENT

With the knowledge of, significance of morphological parameters of porous media in numerical modeling of flow and heat transfer, cross relations for evaluating

morphological parameters such as porosity, specific surface area of stacked brass wire-mesh porous media are arrived for various stacking types, with the help of only easily available information such as fiber diameter (d_f) and pitch (d_p) of the woven mesh screen. Generalized expressions for screen spacing (h) for closely packed scenario under various stacking scenario are obtained and identified. With the help of the arrived expressions, such stacked wire-mesh samples are categorized based on orderly varying porosity and pore- density/mesh-size combination and respective heat transfer and flow influencing parameters are evaluated thereby allowing to numerically model the categorized porous samples using REV (representative eliminatory volume) scale technique for analyzing their thermal performance.

6.3 GEOMETRICAL MODELLING AND ARRIVING AT EXPRESSIONS FOR STACKED WOVEN WIRE-MESH POROUS SAMPLES

A cubic size of ΔX×ΔY×ΔZ is adopted within which the whole fluid saturated woven wire-mesh samples are geometrically modelled. The straight cylindrical wires are drawn in 'Y' direction and the curved woven wires are woven in 'X' direction along the length of the straight cylindrical wires. Woven wire mesh screens thus obtained are arranged in 'Z' direction to obtain block of stacked woven wire mesh screens forming a fluid (empty spaces) saturated wire-mesh porous medium. Various views of obtained geometry of the considering wire-mesh blocks are shown in Figure 6.2 (a) to (d).

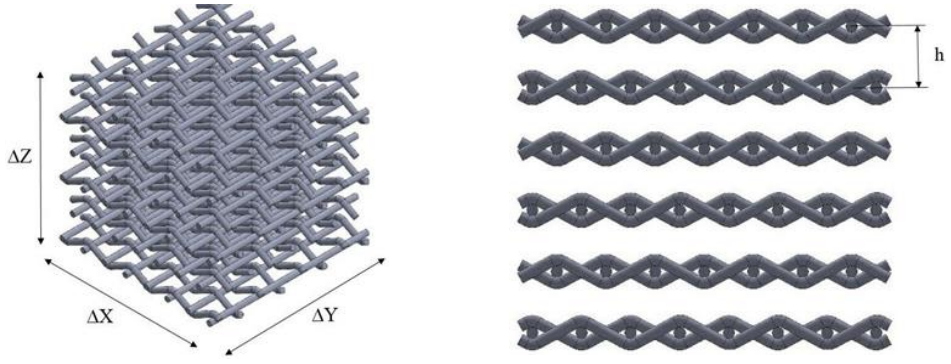

(a) (b)

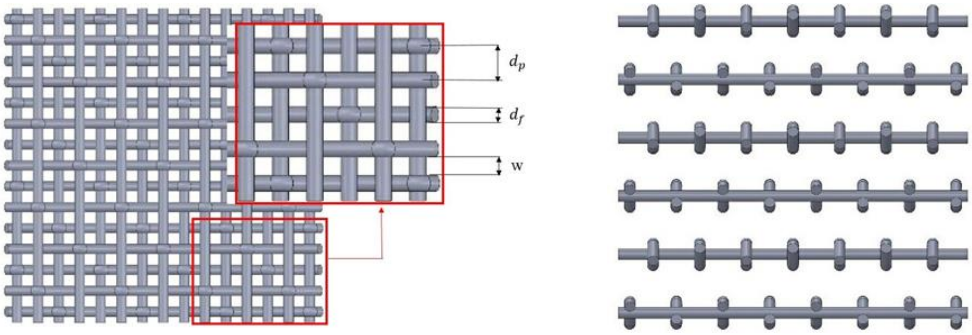

(c) (d)

Figure 6.2 Corresponding to woven wire-mesh geometry with spacing between screens (a) Isometric view. (b) Top view. (c) Front view and (d) Side view.

Front view of wire mesh layers of staggered, inline type-a and inline type-b stacking under closely packed scenario are shown in Figure 6.3, Figure 6.4 and Figure 6.5 respectively.

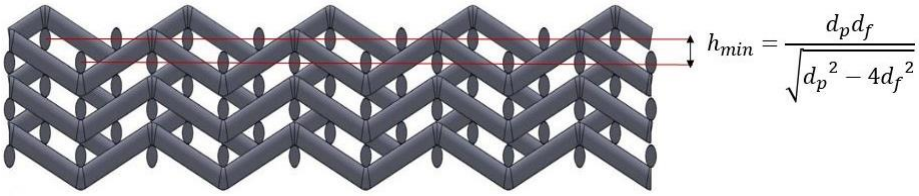

Figure 6.3 Front view of staggered stacking for closely packed scenario (with h_{min} spacing).

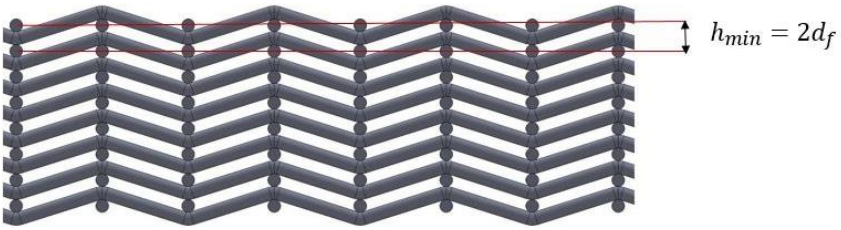

Figure 6.4 Front view of Inline stacking type-a for closely packed scenario (with h_{min} spacing).

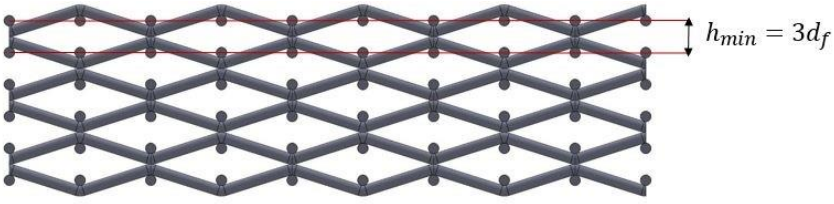

Figure 6.5 Front view of Inline stacking type-b for closely packed scenario (with h_{min} spacing).

6.3.1 Determination of interstitial area density or specific area

By definition (Kaviany 1995) interstitial area density or specific area (a_{sf}) is determined as follows.

$$a_{sf} = \frac{\text{Total surface area of wire} - \text{mesh}}{\text{volume of the whole block (entire fluid saturated wire} - \text{mesh block)}} \tag{6.1}$$

Where, the dimension of the cube comprising of fluid saturated woven wire-mesh porous media is represented as, $\Delta X \times \Delta Y \times \Delta Z$.

Referring to Figure 6.2, number of woven wire-mesh screens (n) can be expressed as shown in Eq. (6.2), where 'h' is the distance between two consecutive mesh layers measured from centre to centre of straight running.

$$n = \frac{\Delta Z}{h} \tag{6.2}$$

It can be observed from Figure 6.2 that, each layer of the wire-mesh block is formed by weaving cylindrical wires onto those cylindrical wires passing straight in perpendicular direction. Therefore, total surface area of the wires forming each layer of the wire-mesh block can be put in the following form.

Total surface area of each mesh layer (a_1) is the sum of product of a) Area of straight running cylindrical wire (a_s) and total number of straight running cylindrical wires (N_s) and b) Area of the weaving cylindrical wire (a_w) and total number of weaving cylindrical wires (N_w) and that can be expressed as,

$$a_1 = (a_s \times N_s) + (a_w \times N_w) \tag{6.3}$$

Observing Eqs. (6.2) and (6.3) total area of the solid cylindrical wires forming the whole mesh block (A_{sm}) can be expressed as,

$$A_{sm} = ((a_s \times N_s) + (a_w \times N_w)) \times \frac{\Delta Z}{h} \tag{6.4}$$

Now, the parameters appearing in Eq. (6.4) can individually be expressed as follows,

$$N_s = \frac{\Delta X}{d_p} \tag{6.5}$$

$$N_w = \frac{\Delta Y}{d_p} \tag{6.6}$$

$$a_s = \pi d_f \Delta Y + \frac{\pi}{2}(d_f)^2 \tag{6.7}$$

$$a_w = \pi d_f L + \frac{\pi}{2}(d_f)^2 \tag{6.8}$$

Parameter 'L' appearing in Eq. (6.8) is the length of the weaving wire, where its value can be expressed from observing Figure 6.6 (a) and (b) as,

$$L = OD(\text{as shown in}) \times \text{number of pores (as there exists a curve } 'OD' \text{ in every pore)} \tag{6.9}$$

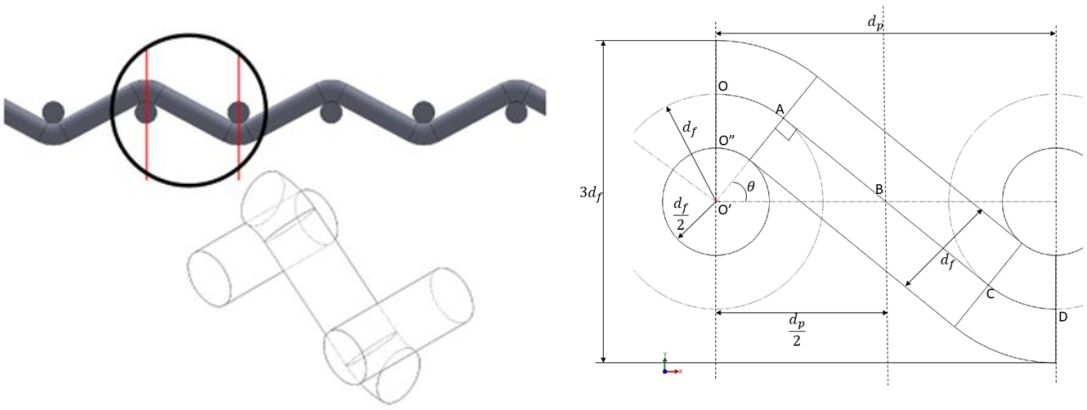

(a) (b)

Figure 6.6 (a) Sketch of single cylindrical wire woven over straight cylindrical wires. (b) Description of parameters involving in expressing length of each woven cylindrical wire.

Expression for number of pores can be approximated as,

$$N_p = N_s = \frac{\Delta X}{d_p} \tag{6.10}$$

In Eq. (6.9) in order to find expression for length 'L', expression for 'OD' is derived and multiplied with number of pores. For that, observing Figure 6.6(b) angle $AO'B$ can be expressed as,

$$\mathrm{Cos}\theta = \frac{O'A}{O'B} = \frac{2d_f}{d_p} \tag{6.11}$$

$$\theta = \cos^{-1}\left(\frac{2d_f}{d_p}\right) \tag{6.12}$$

Therefore, angle $AO'O = \frac{\pi}{2} - \theta$ (6.13)

Length of arc $OA = d_f\left(\frac{\pi}{2} - \theta\right)$ (6.14)

Considering $\Delta AO'B$, (6.15)

$$(AB)^2 = (O'B)^2 - (AO')^2$$

Therefore, (6.16)

$$AB = \sqrt{\left(\frac{{d_p}^2}{4} - {d_f}^2\right)}$$

However, length OD = OA + AB + BC + CD, but OA = CD which yields,

$$OD = 2(OA + AB) \tag{6.17}$$

Therefore, the above equation for length 'OD' can be rewritten, from expressions for 'OA' and 'AB' as given in Eqs. (6.14) and (6.16) as,

$$OD = 2\left(d_f\left(\frac{\pi}{2} - \theta\right) + \sqrt{\frac{{d_p}^2}{4} - {d_f}^2}\right) \tag{6.18}$$

Inserting expression for $'\theta'$ as given in Eq. (6.12), we get,

$$OD = \pi d_f - 2d_f \cos^{-1}\left(\frac{2d_f}{d_p}\right) + 2\sqrt{\frac{{d_p}^2}{4} - {d_f}^2} \tag{6.19}$$

From Eq. (6.10) and (6.19) lengths of each woven wire can be obtained as,

$$L = \frac{\Delta X}{d_p}\left(\pi d_f - 2d_f \cos^{-1}\left(\frac{2d_f}{d_p}\right) + 2\sqrt{\left(\frac{{d_p}^2}{4} - {d_f}^2\right)}\right) \tag{6.20}$$

Therefore, the obtained expression for 'L' can be used in Eq. (6.8). Now expression for total area of solid cylindrical wires both straight passing as well as weaving ones as expressed in Eq. (6.4) can be rewritten by referring to Eqs. (6.7), (6.5), (6.8), (6.6) and (6.2) as,

$$A_{sm} = \left[\left(\pi d_f \Delta Y + \frac{\pi}{2}{d_f}^2\right)\frac{\Delta X}{d_p} + \left(\pi d_f\left(\frac{\Delta X}{d_p}\left(\pi d_f - 2d_f \cos^{-1}\left(\frac{2d_f}{d_p}\right) + 2\sqrt{\left(\frac{{d_p}^2}{4} - {d_f}^2\right)}\right)\right) + \frac{\pi}{2}{d_f}^2\right)\frac{\Delta Y}{d_p}\right]\frac{\Delta Z}{h} \tag{6.21}$$

Interstitial area density or specific surface area is expressed as,

$$a_{sf} = \frac{A_{sm}}{\Delta X \Delta Y \Delta Z} \tag{6.22}$$

Therefore, from Eq. (6.21), expression for 'a_{sf}' (for woven-mesh block of spacing 'h' can be deduced by simplification as,

$$a_{sf} = \frac{A_{sm}}{\Delta X \Delta Y \Delta Z} \tag{6.23}$$

$$= \frac{\pi d_f}{h d_p}\left[1 + \frac{d_f}{d_p}\left\{\pi - 2\mathrm{Cos}^{-1}\left(\frac{2d_f}{d_p}\right)\right\} + \sqrt{1 - \left(\frac{2d_f}{d_p}\right)^2} + \frac{d_f}{2}\left(\frac{1}{\Delta X} + \frac{1}{\Delta Y}\right)\right]$$

Since, term $\frac{d_f}{2}\left(\frac{1}{\Delta X} + \frac{1}{\Delta Y}\right)$ yields very negligible value, the above expressions can be simplified by neglecting this term as,

$$\alpha_{sf} = \frac{\pi d_f}{h d_p}\left[1 + \frac{d_f}{d_p}\left\{\pi - 2\mathrm{Cos}^{-1}\left(\frac{2d_f}{d_p}\right)\right\} + \sqrt{1 - \left(\frac{2d_f}{d_p}\right)^2}\right] \tag{6.24}$$

By taking $\frac{d_f}{d_p} = r$, the above equation can be rewritten as,

$$\alpha_{sf} = \frac{\pi r}{h}\left[1 + r\pi - 2r\mathrm{Cos}^{-1}(2r) + \sqrt{1 - 4r^2}\right] \tag{6.25}$$

Stacking of the wire-mesh layers can be made in three different ways that include staggered stacking as shown in Figure 6.3, inline type-a as shown in Figure 6.4 and inline type-b as shown in Figure 6.5. For closely packed scenario, the value of 'h_{min}' varies with type of stacking. For staggered type it is difficult to be interpreted by mere observation and the same is expressed mathematically in the following way. The upper layer of the woven mesh screen rests on the lower layer as shown in Figure 6.7. It can be observed in Figure 6.7 that length of 'OC' is the minimum spacing 'h_{min}' for closely packed wire-mesh block scenario for staggered type of stacking. Expression for 'h_{min}' with reference to the Figure 6.7 can be obtained as,

Let $OC = AC' = h_{min}$, we know that from ΔAOB

$$\cos\emptyset = \frac{2d_f}{d_p} \tag{6.26}$$

Also, from ΔOBC,

$$\sin\emptyset = \frac{d_f}{h_{min}} \tag{6.27}$$

From trigonometric relation $\cos^2\emptyset + \sin^2\emptyset = 1$, the above equations can be written as,

$$\frac{4{d_f}^2}{{d_p}^2} + \frac{{d_f}^2}{{h_{min}}^2} = 1 \tag{6.28}$$

$$h_{min} = \frac{d_p d_f}{\sqrt{{d_p}^2 - 4{d_f}^2}} \tag{6.29}$$

Hence, for closely packed woven wire-mesh scenario for staggered stacking type, expression for 'h_{min}' as given in Eq. (6.29) can be used in Eq. (6.23) for obtaining corresponding value of specific surface area. Detailed sketch of inline type-a and type-b stacking scenario is shown in Figure 6.8 and Figure 6.9 following which, expressions 'h_{min}' $= 2d_f$ and 'h_{min}' $= 3d_f$ can be used in Eq. (6.23) for obtaining specific surface area of wire-mesh porous medium of inline type-a and inline type-b stacking, respectively.

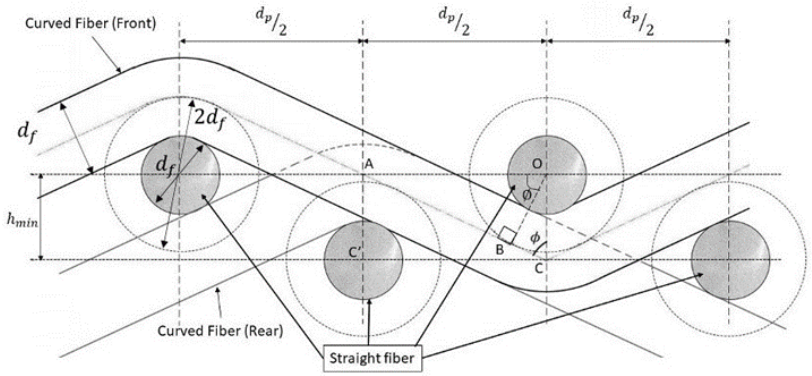

Figure 6.7 Description of parameters for closely packed wire-mesh layers in staggered type of stacking.

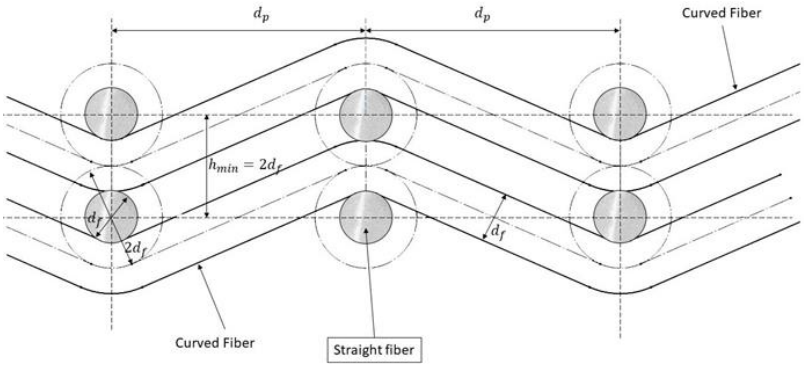

Figure 6.8 Description of parameters for closely packed wire-mesh layers in stacking of inline type- a.

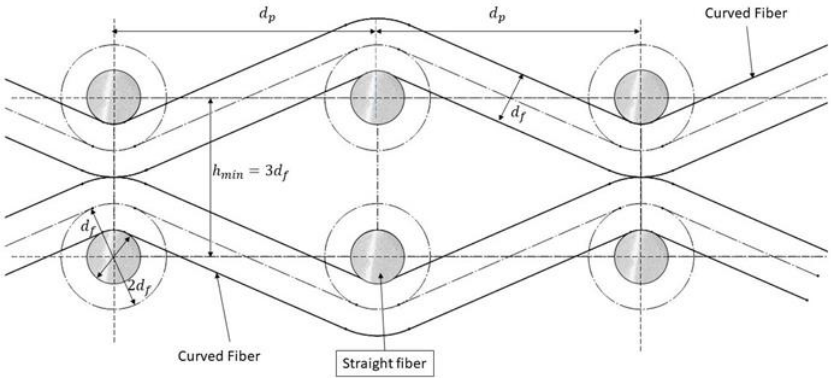

Figure 6.9 Description of parameters for closely packed wire-mesh layers in stacking of inline type-b.

6.3.2 Cross-relations between porosity, fiber diameter and pore width

Cross-relationships between morphological characteristic of wire-mesh layers such as fiber diameter and pore width and characteristics of stacked wire-mesh porous structures such as porosity would serve a great purpose by making it easier to avail information of unknown parameters that are difficult to evaluate (for instance, porosity and specific surface area that depend on several other parameters such as stacking manner, fiber diameter and pitch) with information on easily distinguishable parameters. Procedure for arriving at such cross-relations is mentioned below.

Volume of the solid woven mesh layer can be written in analogous to Eq. (6.13) as,

$$v_1 = (v_s \times N_s) + (v_w \times N_w) \tag{6.30}$$

The total volume of the solid cylindrical wires (both woven as well as straight running) forming the mesh block can therefore be written as,

$$V_{sm} = n((v_s \times N_s) + (v_w \times N_w)) \tag{6.31}$$

Volume of a single straight running cylindrical wire can be expressed as,

$$v_s = \frac{\pi {d_f}^2 \Delta Y}{4} \tag{6.32}$$

Similarly, volume of the weaving cylindrical wire can be expressed as,

$$v_w = \frac{\pi {d_f}^2 L}{4} \tag{6.33}$$

Porosity is defined as (Kaviany 1995),

$$\text{Porosity} = \frac{\text{Total volume of the void space (fluid region)}}{\text{Total volume of the whole block}} \tag{6.34}$$

Which in this case can be written as,

$$\varepsilon = \frac{V - V_{sm}}{V} \tag{6.35}$$

$$1 - \varepsilon = \frac{V_{sm}}{V} \tag{6.36}$$

Where, 'V' is total volume of the whole fluid saturated porous mesh block expressed as $\Delta X \Delta Y \Delta Z$.

From, Eqs. (6.31), (6.32), (6.33), (6.20) and (6.2), V_{sm}/V can be expressed as,

$$\frac{V_{sm}}{V} = \frac{\pi {d_f}^2}{4 h d_p}\left[1 + \frac{1}{d_p}\left(\pi d_f - 2 d_f \text{Cos}^{-1}\left(\frac{2 d_f}{d_p}\right) + \sqrt{{d_p}^2 - 4{d_f}^2}\right)\right] \tag{6.37}$$

Comparing Eqs. (6.36) and (6.37), expression for porosity for woven wire-mesh block with spacing 'h' between the mesh layers can be written as,

$$\varepsilon = 1 - \frac{\pi {d_f}^2}{4 h d_p}\left[1 + \frac{1}{d_p}\left(\pi d_f - 2 d_f \text{Cos}^{-1}\left(\frac{2 d_f}{d_p}\right) + \sqrt{{d_p}^2 - 4{d_f}^2}\right)\right] \tag{6.38}$$

For closely packed woven wire-mesh block of staggered type, expression for porosity can be obtained by incorporating expression for 'h_{min}' given in Eq. (6.29) into Eq. (6.38) as,

$$\varepsilon_{staggered} = 1 - \frac{\pi d_f \sqrt{{d_p}^2 - 4{d_f}^2}}{4{d_p}^2}\left[1 + \frac{1}{d_p}\left(\pi d_f - 2d_f \mathrm{Cos}^{-1}\left(\frac{2d_f}{d_p}\right) + \sqrt{{d_p}^2 - 4{d_f}^2}\right)\right] \quad (6.39)$$

Taking,

$$\frac{d_f}{d_p} = r \quad (6.40)$$

Eq. (6.39) can be rewritten as,

$$\varepsilon_{staggered} = 1 - \frac{r\pi}{4}\sqrt{1-4r^2}\left[1 + r\pi - 2r\mathrm{Cos}^{-1}(2r) + \sqrt{1-4r^2}\right] \quad (6.41)$$

Valid for $0 \leq r \leq 0.5$

For closely packed woven wire-mesh block of inline type-a and inline type-b stacking scenario, expression for porosity can be obtained by incorporating expression for 'h_{min}' equal to $2d_f$ in Eq. (6.38), which for inline stacking of type-a becomes,

$$\varepsilon_{Inline-type-a} = 1 - \frac{\pi {d_f}^2}{4(2d_f)d_p}\left[1 + \frac{1}{d_p}\left(\pi d_f - 2d_f \mathrm{Cos}^{-1}\left(\frac{2d_f}{d_p}\right) + \sqrt{{d_p}^2 - 4{d_f}^2}\right)\right] \quad (6.42)$$

$$\varepsilon_{Inline-type-a} = 1 - \frac{\pi d_f}{8d_p}\left[1 + \left(\pi\frac{d_f}{d_p} - 2\frac{d_f}{d_p}\mathrm{Cos}^{-1}\left(\frac{2d_f}{d_p}\right) + \sqrt{1 - \left(\frac{2d_f}{d_p}\right)^2}\right)\right] \quad (6.43)$$

$$\varepsilon_{Inline-type-a} = 1 - \frac{r\pi}{8}\left[1 + r\pi - 2r\mathrm{Cos}^{-1}(2r) + \sqrt{1-4r^2}\right] \quad (6.44)$$

Similarly, for stacking of inline type-b incorporating expression for 'h_{min}' equal to $3d_f$, generalized expression for porosity becomes,

$$\varepsilon_{\text{Inline-type-b}} = 1 - \frac{\pi {d_f}^2}{4(3d_f)d_p}\left[1 + \frac{1}{d_p}\left(\pi d_f - 2d_f \text{Cos}^{-1}\left(\frac{2d_f}{d_p}\right) + \sqrt{{d_p}^2 - 4{d_f}^2}\right)\right] \quad (6.45)$$

$$\varepsilon_{\text{Inline-type-b}} = 1 - \frac{\pi d_f}{12 d_p}\left[1 + \left(\pi \frac{d_f}{d_p} - 2\frac{d_f}{d_p}\text{Cos}^{-1}\left(\frac{2d_f}{d_p}\right) + \sqrt{1 - \left(\frac{2d_f}{d_p}\right)^2}\right)\right] \quad (6.46)$$

$$\varepsilon_{\text{Inline-type-b}} = 1 - \frac{r\pi}{12}\left[1 + r\pi - 2r\text{Cos}^{-1}(2r) + \sqrt{1 - 4r^2}\right] \quad (6.47)$$

For various values of 'k' in the range of $0 \leq r \leq 0.5$, fitting a polynomial curve with R^2 value 0.99866, 0.99963 and 0.99933 for staggered, inline type-a and inline type-b stacking scenario, by considering 501 data points obtained from the above equation provides a compact equation expressing porosity of woven wire-mesh for the mentioned stacking types, as a function of only two morphological properties (fiber diameter and pore-density / mesh-size) of the wire-mesh, can be obtained as,

$$\varepsilon_{\text{staggered}} = 1.01051 - 1.87112(r) + 1.60829(r^2) \quad (6.48)$$

$$\varepsilon_{\text{Inline-type-a}} = 0.99358 - 0.63809(r) + 0.68232(r^2) \quad (6.49)$$

$$\varepsilon_{\text{staggered}} = 0.99572 - 0.42539(r) + 0.45488(r^2) \quad (6.50)$$

6.3.3 Interpretation of results from the expressions arrived

Expressions arrived in the present study that enables to obtain vital morphological properties which play a key role in thermo-hydraulic performance of stacked woven wire-mesh porous media is interpreted in this section. The present study provides cross relations between important parameters such as pore density/mesh size of the wire-mesh screen (mesh per inch / PPI) used in stacking, fiber diameter (d_f) of the wires used to weave the mesh screen, porosity and specific surface area of the stacked wire-mesh blocks corresponding to three various kinds of stacking such as staggered, inline type-a and inline type-b. It can be noted that, from the expressions provided in the present study, porosity and specific surface area that plays a prominent role in momentum and energy equations can be evaluated with the knowledge of only fiber diameter (d_f) and pitch (d_p) of wire-mesh screens used for various stacking conditions. Thus, porous media of various characteristics that can be obtained by changing the fiber diameter and pitch of the woven screens for various stacking conditions can easily be studied using

porous media formulation in variety of applications in order to arrive at optimum thermo-hydraulic behaviour of such type of porous media.

Variation of porosity of the stacked wire-mesh porous blocks with respect to change in fiber diameter for various type of stacking and pore-density / mesh size is shown in Figure 6.10. for better visual observation, variation of porosity and fiber diameter of only 15PPI and 5PPI mesh-size samples are randomly chosen, however the respective changes for other pore densities are also observed to follow similar trend. It can be observed that, for any type of stacking of wire-mesh screens of given mesh size (PPI / mesh per inch), porosity decreases with increase in fiber diameter as expected.

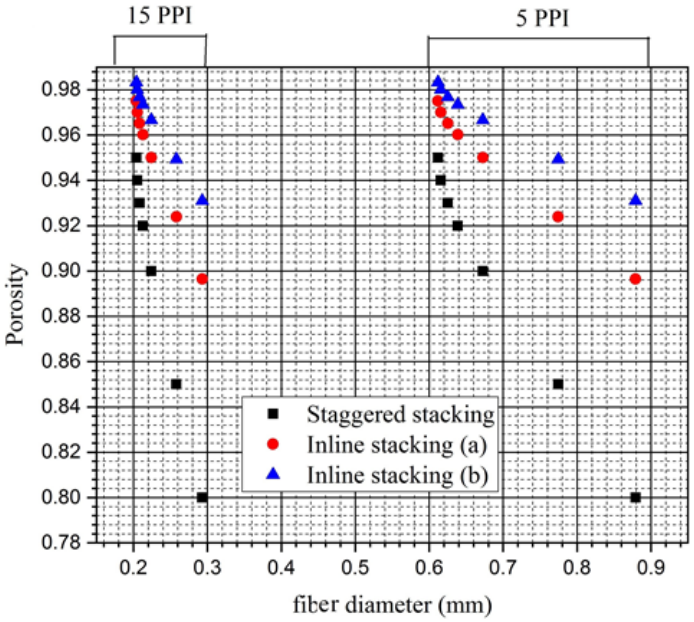

Figure 6.10 Variation of porosity with respect to change in fiber diameter for various stacking of wire-mesh screens of given pore density or mesh size (pores per inch / mesh per inch).

Magnitude of variation in porosity with change in fiber diameter can be seen relatively high for staggered stacking followed by inline stacking type-a and type-b. For a given fiber diameter, stacked block of high porosity can be achieved with inline stacking type-a followed by inline stacking type-b and staggered stacking. Also, it can be observed that with increase in fiber diameter, a fixed porosity can be achieved by decreasing the mesh size (MPI) or pore density (PPI). The present study enables numerical study of various stacked wire-mesh porous samples subjected to change in its morphological

parameters and stacking condition by providing information on hydro-dynamic parameters of corresponding stacked wire-mesh porous samples.

Variation of specific surface area of stacked wire-mesh porous media for various stacking conditions is shown in Figure 6.11, the variations are discussed by depicting randomly chosen 0.95 porosity foam sample, however the variations show similar trend for any other porosity case.

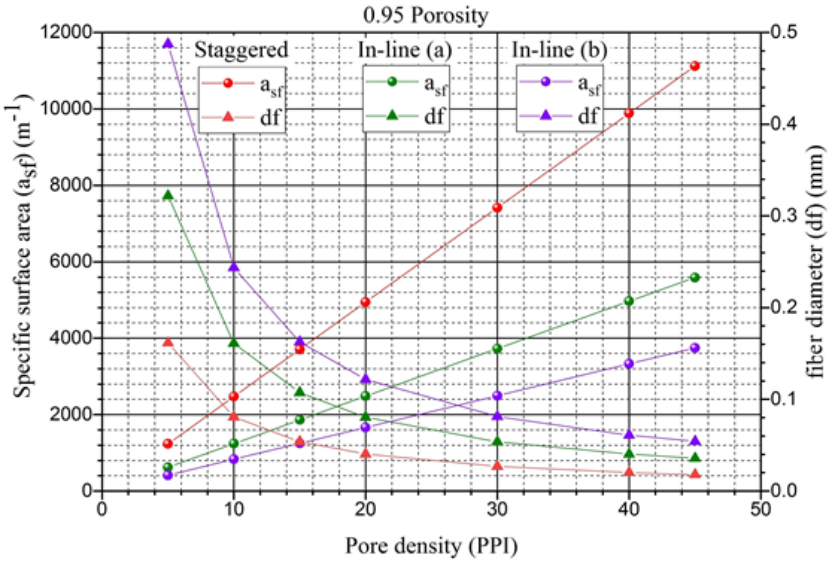

Figure 6.11 Variation of specific surface area of stacked wire-mesh porous media comprising of wire-mesh screens of various mesh size or pore density (pores per inch / mesh per inch).

It can be observed that, for a given porosity, specific surface area increases with increase in mesh size or pore density of the stacked screens for all type of stacking, however it is dominated by staggered type of stacking followed by inline type-a and type-b kinds of stacking. Also, it has to be noted that, a fixed porosity can be achieved for the considered different kinds of stacking with compromise in fiber diameter of weaved wires. Staggered type of stacking provides the required porosity for a given mesh size (PPI / MPI) at lesser fiber diameter compared to inline stacking of type-b and type-a scenario for same porosity at given mesh size or pore density condition.

6.3.4 Numerical modelling of wire mesh porous media

In modelling any type of porous media with LTNE approach, information on interstitial heat transfer coefficient h_{sf} is crucial in solving the energy equation. An effort to

identify suitable correlation for interstitial heat transfer coefficient can be witnessed in a study by (Kotresha and Gnanasekaran 2019), the study was focused on determining interstitial heat transfer coefficient based on correlations that were available in literature for packed bed scenario (Wakao et al. 1979), cross-flow through cylinders (Zukauskas 1987b) and for situation with metal foam. The study showed that the thermal phenomenon assessed (wall heat transfer co-efficient of vertical channel) was relatively in good argument with experimental data when interstitial heat transfer coefficient as provided by (Calmidi and Mahajan 2000c) was used in numerical modelling. Suitability of the correlation, was upheld on the basis of a better relative deviation of the thermal phenomenon expressed based on results obtained when interstitial heat transfer coefficient was evaluated with the respective correlations considered which were not for stacked wire mesh cases. However, in a recent study, (Garg et al. 2019) successfully modelled regenerator with wire-mesh porous modelling method by using interstitial heat transfer coefficient obtained from relation provided by (Geodeon 1999). In the present study, same relation provided by (Xiao et al. 2017) as given in Eq. (6.51) is used to evaluate interstitial heat transfer coefficient and thermal phenomenon expressed through numerical modelling using this relation is compared with that of experimental data in order to emphasize the suitability of this correlation. Figure 6.12 shows the comparison of thermal phenomenon characterized by wall heat transfer co-efficient of the vertical channel of present numerical work from that of experimental work of (Kurian et al. 2016c). Good agreement in the thermal phenomenon can be witnessed here as a result of incorporation of interstitial heat transfer co-efficient evaluated from relation provided by (Geodeon 1999) to solve the energy equation. Thus, for further analysis, evaluation of interstitial heat transfer co-efficient is carried out based on relation provided by (Geodeon 1999) as emphasized by (Garg et al. 2019).

Inertial and viscous resistance co-coefficients are another set of important parameters that are vital in modeling wire-mesh porous media using Darcy-Forchheimer model. For steady state case, (Xiao et al. 2017) provided the expressions for calculating these parameters by referring to friction factor expressions provided by (Tanaka et al. 1990) and modified-Ergun equation provided by (Gedeon and Wood 1996). The obtained relations were compared with pressure drop as described by Darcy-Forchheimer law

and expressions for viscous and inertial resistance coefficients were provided as given in Eqs. (6.52) and (6.53) respectively. It can be observed that, these flow parameters are functions of both porosity as well as fiber diameter and rightly predicts flow resistance through the considered wire-mesh type of porous medium. Hence, these expressions are used for evaluating viscous and inertial resistance coefficients required for modelling the flow phenomenon through the considered wire-mesh porous media.

$$h_{sf} = \frac{\lambda_f (1 + 0.99(Re_{dh} Pr)^{0.66}) \varepsilon^{1.79}}{d_h} \tag{6.51}$$

$$\frac{1}{K} = \frac{134}{2\varepsilon {d_h}^2} \tag{6.52}$$

$$C = \frac{5.44}{\varepsilon^2 d_h {Re_{dh}}^{0.188}} \tag{6.53}$$

The simulated results from the modelled numerical domain is compared with that of experimental data of (Kurian et al. 2016c) for validation of the followed modelling methodology. From Figure 6.12 a good agreement between average wall heat transfer coefficient and average wall temperature obtained through present numerical simulation and experimental results reported in literature can be observed.

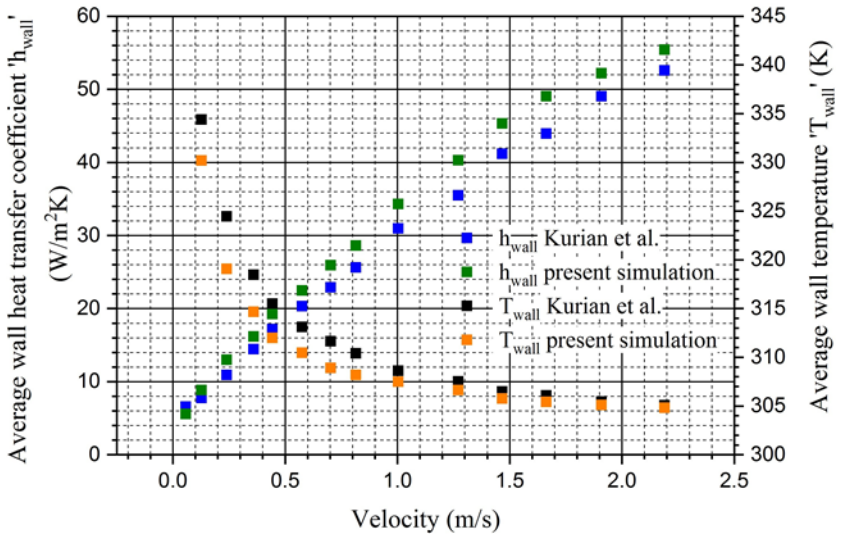

Figure 6.12 Comparison of wall heat transfer coefficient obtained from present numerical work from that of experimental work of (Kurian et al. 2016c).

An average difference of 4.2 W/m^{2}K with maximum and minimum difference of 5.13 W/m^{2}K and 0.973 W/m^{2}K, respectively is observed between wall heat transfer coefficients. In terms of deviation between experimentally measured temperature and numerically simulated temperature data, an average percentage deviation of as less as 0.79 percent is observed with highest and lowest deviation of 1.65 percent and 0.09 percent respectively. This demonstrates the correctness and suitability of the followed methodology in order to mimic heat transfer in considered type of porous medium. In terms of flow phenomenon, variation of experimentally measured and numerically obtained pressure drop with velocity is shown in Figure 6.13. A good agreement between present numerically obtained data and experimentally reported data is observed with 6 percent and 8 percent average percentage deviation for 0.71 and 0.81 porosity wire-mesh stack. Thus, the followed methodology for numerically mimicking the flow and heat transfer through stacked wire mesh porous media can be seen to be appropriate for further analysis.

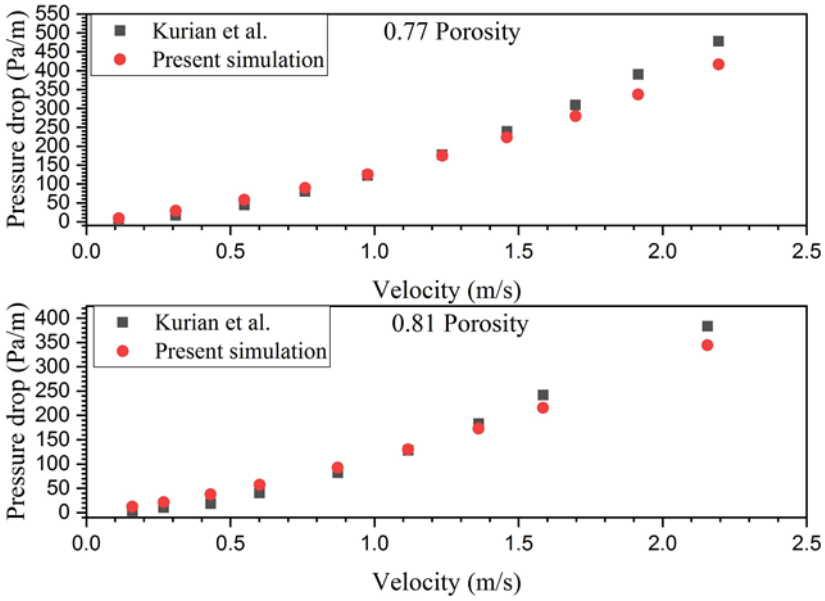

Figure 6.13 Comparison of pressure drop of present simulations with that of experimental work reported in literature.

6.4 SUMMARY

In the present work, a set of cross-relations that can describe / classify a given stacked wire-mesh porous medium is arrived based on the mesh-size, fiber (wire) diameter and type of stacking involved. Expressions presented from this study enables to evaluate

heat transfer and flow influencing morphological properties such as porosity and specific surface area that are unique to wire-mesh porous type of given mesh-size/pore-density, fiber diameter and stacking conditions. Such thermo-hydraulic properties of stacked woven wire-mesh samples of orderly varying mesh-size/pore- density and porosity are categorized corresponding to each type of various stacking scenario namely staggered, inline type-a and type-b. The mentioned key parameters that highly influence thermo-hydraulic performance of the categorized porous medium are evaluated using the expressions provided in the present study and can be incorporated in momentum equation (Darcy-Forchheimer model) and energy equation (LTNE model) for evaluation of thermal and hydraulic performances of such class of porous media. Through this study it is demonstrated that, required changes in porosity and specific surface area that highly influence flow and heat transfer through porous media can be achieved at most ease in stacked wire-mesh type of porous media compared to other type of porous media like metal foams. The expressions arrived in the present study is intended to be useful in numerical modeling of flow and heat transfer through such class of porous medium of various morphological characteristics such as porosity and mesh size that can be carefully employed in variety of applications. It can be observed that, unlike metal foams, since the required changes in the properties of porous medium can be easily achieved with stacked wire-mesh structures, it can present a wide opportunity for obtaining a variety of trade off scenarios between the heat transfer and the incurred pressure drop which is quite crucial in dealing with such phenomenon where a benefit is always accompanied by a cost and the same is elaborated in the further work.

6.5 CLOSURE

In the present work, advantages of stacked wire-mesh porous structures in terms of their potentials of presenting a wide variety of trade-off scenarios between enhanced heat transfer and incurred flow resistance is demonstrated with the help of much easily variable morphological and stacking features that play a crucial role in thermo-hydraulic characteristics. Expressions that relate key morphological parameters of such medium are provided that can be used to numerically model such type of porous media for comprehensively analyzing their thermo-hydraulic behavior.

CHAPTER – 7

WIRE-MESH POROUS MEDIA UNDER VARIED THICKNESS CONDITIONS

Subjecting the stacked woven wire mesh porous media under various thickness scenarios along with their structural variations corresponding to various stacking types, a variety of trade off conditions between enhanced heat transfer and encountered flow resistance can be expected that further contributes to the wide range of options for consideration of specific porous medium in order to operate at a desired cost and benefit scenario. In this regard as explained in the previous chapter (chapter 6), with the help of arrived expressions, stack of woven wire-mesh samples of orderly varying porosity (0.8, 0.85, 0.9 and 0.95) for each stack of woven wire-mesh screens of 5, 10, 15, 20, and 25PPI pore-density / mesh-size are obtained. For the categorized stacks of woven wire mesh screens, specific area (a_{sf}), porosity are evaluated based on expressions arrived in the present work described in the previous chapter for considered stacking scenarios. Vertical channel numerical domain as described in Figure 7.1 is modelled.

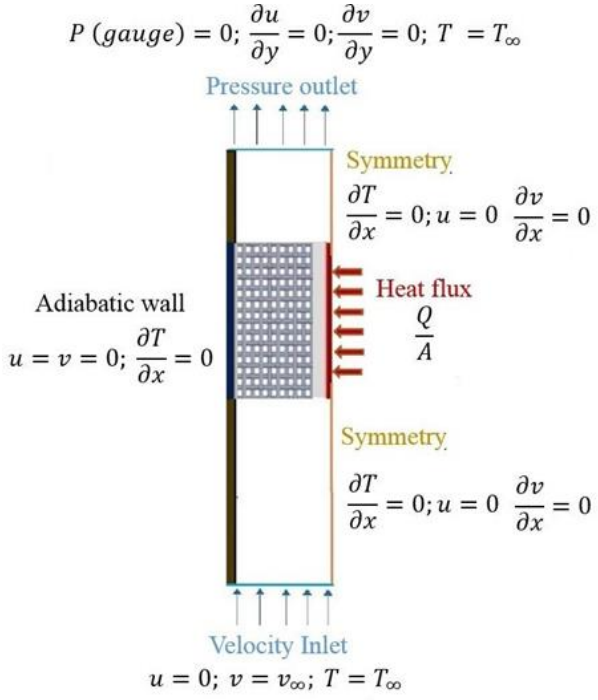

Figure 7.1 Illustration of computational domain with boundary condition.

7.1 THERMO-HYDRAULIC ANALYSIS

Flow resistance, characterized by pressure drop phenomenon through the considered wire-mesh type of porous medium corresponding to mesh size and porosity of the samples under various stacking types and thickness scenarios is shown in Figure 7.2 to Figure 7.4.

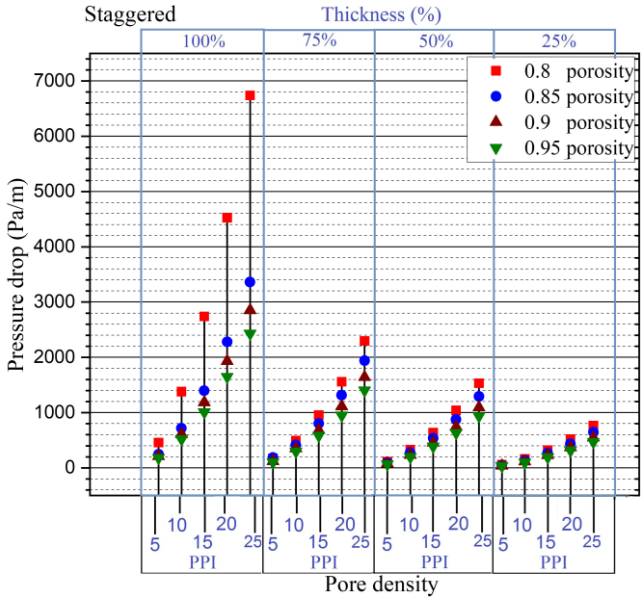

Figure 7.2 Variation of pressure drop for staggered stacking type woven wire mesh porous structure for various porosity and pore density under different thickness scenarios.

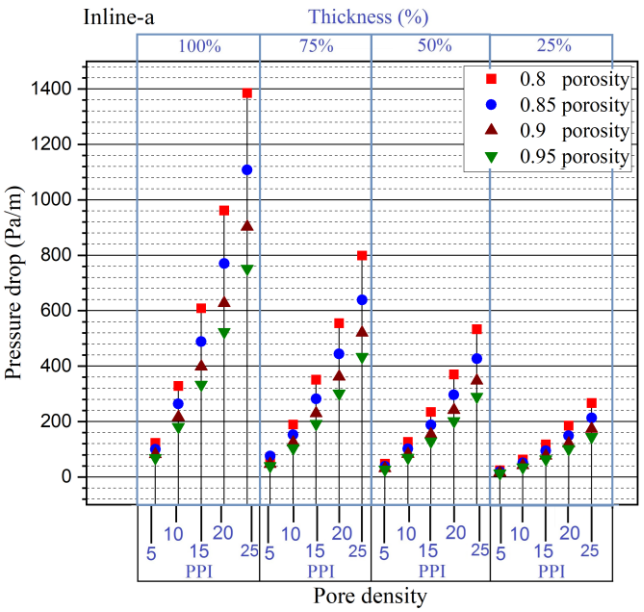

Figure 7.3 Variation of pressure drop for woven wire mesh porous structure of inline type-a stacking for various porosity and pore density under different thickness scenarios.

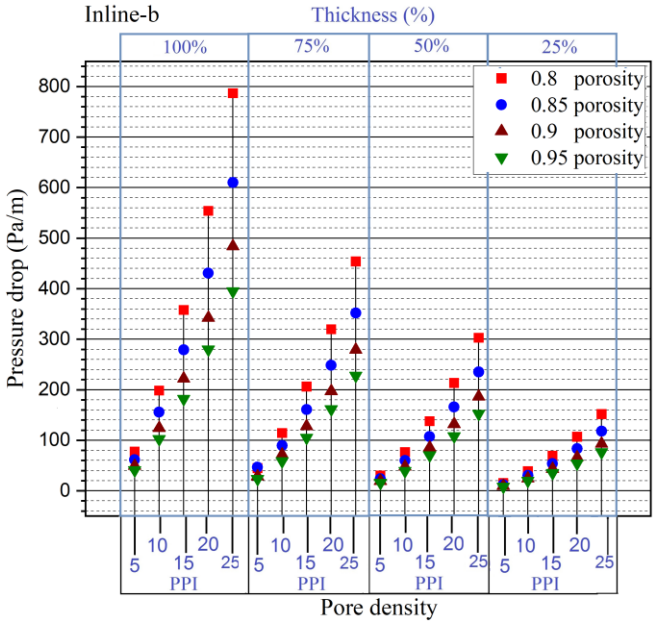

Figure 7.4 Variation of pressure drop for woven wire mesh porous structure of inline type-b stacking for various porosity and pore density under different thickness scenarios.

It can be observed that, for a given stacking scenario, pressure drop decreases with increase in porosity for a given mesh size (pore density), due to increased permeability to the fluid through the wire mesh structures with increase in porosity. However, for a given porosity with increase in mesh size, pressure drop can be observed to be increasing due to increased obstruction to the flow with increase in mesh-size / pore-density. For a given thickness scenario it can be observed that, the flow resistance represented by the pressure drop value is evidently found the highest for staggered stacking type followed by stacking of inline type-a and type-b. This is due to the nature of flow passage that is allowed in the three different stacking scenarios. An easier passage to the fluid flow in stacking type of inline type-b is observed to offer least resistance to the flow whereas the much-restricted passage exhibited through staggered stacking is seen offering high resistance to the flow. However, stacking of inline type-b can be seen expressing the flow resistance in between that of the other two stacking

types. Also, pressure drop can be observed to be increasing with increase in thickness of the wire mesh sample of any structural and stacking conditions.

As explained in the previous chapter (chapter 6), with the help of arrived expressions, stack of woven wire-mesh samples of orderly varying porosity (0.8, 0.85, 0.9 and 0.95) for each stack of woven wire-mesh screens of 5, 10, 15, 20, and 25PPI pore-density/mesh-size are obtained. It can be noted that for a given pore density of wire-mesh screens, stacks of various porosity can be achieved by changing the fiber diameter of the wires that forms the mesh screens. For the categorized stacks of woven wire mesh screens, specific area (a_{sf}), porosity are evaluated based on expressions arrived in the present work, described in the previous chapter for considered stacking scenarios. Vertical channel numerical domain as described in Figure 7.1 is modelled with these categorized stacked wire-mesh porous samples.

Thermal performance of the categorized porous samples (based on changes in thickness, mesh-size/pore-density and porosity) is shown in Figure 7.5 to Figure 7.7 in terms of wall heat transfer co-efficient for all stacking scenarios, structural variations and thickness conditions.

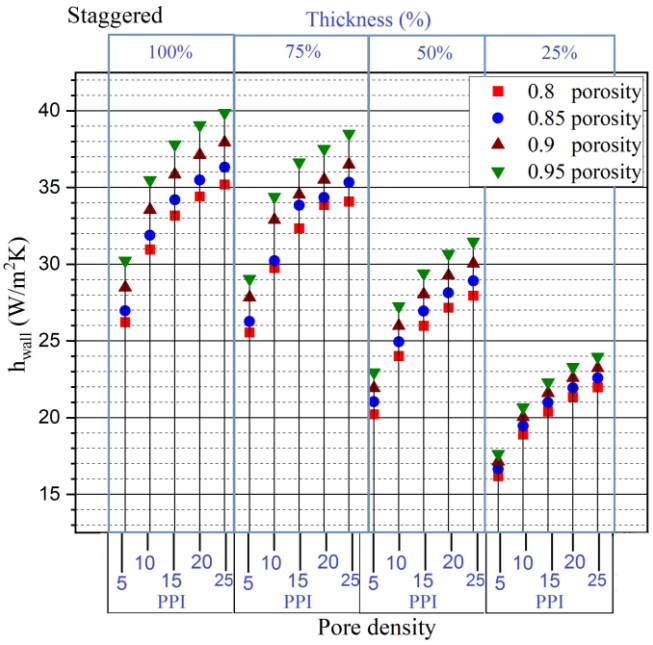

Figure 7.5 Variation of wall heat transfer coefficient for staggered stacking type of woven wire mesh porous structure for various porosity and pore density under different thickness scenarios.

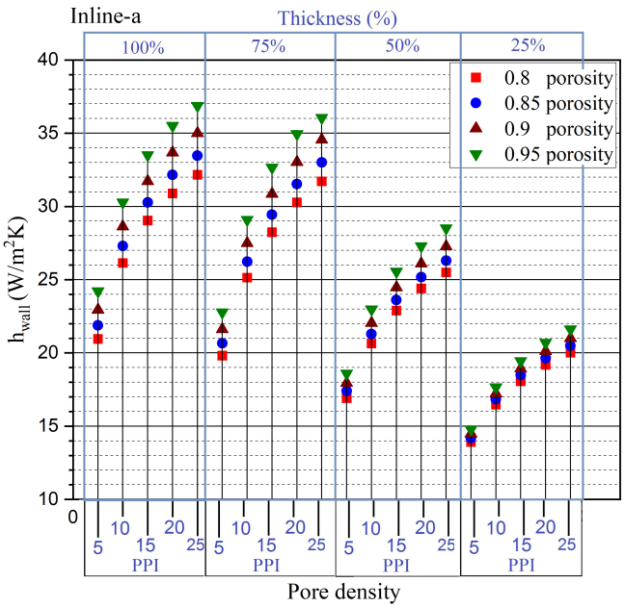

Figure 7.6 Variation of wall heat transfer coefficient for woven wire mesh porous structure of inline type-a stacking for various porosity and pore density under different thickness scenarios.

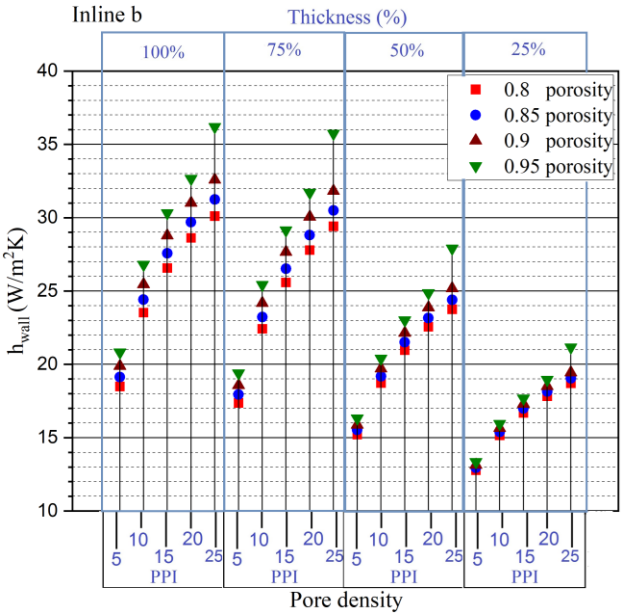

Figure 7.7 Variation of wall heat transfer coefficient for woven wire mesh porous structure of inline type-b stacking for various porosity and pore density under different thickness scenarios.

It can be observed that, wall heat transfer co-efficient increases with increase in both pore density as well as porosity. However, for a stack of given porosity, heat transfer

greatly increases with pore density compared to the increase of same parameter with increase in porosity for a stack of given pore density. This variation is similar to that as observed with metal foams (discussed in section 5.3 of chapter 5). In LTNE modelling, the total heat transfer is accounted as heat transfer due to fluid's direct interaction with the heat source (this increases with porosity) and interstitial heat transfer this increases with increase in interfacial parameters interfacial specific surface area (a_{sf}), and interfacial heat transfer co-efficient (h_{sf})). As a result of which for a given pore density, wall heat transfer co-efficient increases with porosity due to enhanced availability of fluid to carry the subjected heat due to direct heat transfer. Enhanced heat transfer is also witnessed with increase in pore-density for wire mesh stack of given porosity, as a result of increased interstitial heat transfer. The variation of wall heat transfer co-efficient is observed to be in similar trend, corresponding to changes in porosity and mesh size for all type of stacking. However, for same thickness, porosity and mesh size conditions, relative deviation of wall heat transfer of wire-mesh porous medium formed by various stacking types is observed to show significant variations. This is mainly due to increased specific surface area of staggered type for a given porosity enabling higher heat transfer, followed by inline type-a and inline type-b that relatively have lesser specific surface area for a given mesh-size/pore-density and porosity condition. As a result of which interstitial heat transfer is increased for staggered type compared to wire-mesh porous samples formed as a result of inline stacking of type-a and type-b conditions. Considering thickness, for any given structural properties and stacking type, the heat transfer is found to be increasing with increase in the thickness of the wire mesh porous samples due to increased volume of the porous material that promotes further enhancement of heat transfer.

In the present study it is observed that, with variation in structural, thickness and stacking scenarios, corresponding variation in flow and heat transfer phenomenon are largely varied. This gives an interesting idea on the extents of the range of flow resistances and heat transfer enhancements that could be presented by a porous structure formed by stacking the woven wire meshes by simply varying the easily controllable features of wire mesh such as porosity, pore density and the stacking manner. It is quite evident from this study that heat transfer enhancement, with change in thickness,

porosity and mesh size for various stacking types of wire-mesh porous medium is accompanied by individually / distinctly varying flow resistance phenomenon, hence optimum selection of the such class of porous medium with respect to mentioned variable conditions has to be the prime aspect for achieving the desired thermo-hydraulic performance in any heat exchange applications, involving such stacked wire-mesh porous medium. In this regard various trade-off scenarios between heat transfer and flow resistance are discussed corresponding to the mentioned variable parameters.

7.1.1 Trade-off analysis between flow resistance and heat transfer

Analysing the various trade-off scenarios between the potentials of stacked wire mesh porous structures in maximising heat transfer and minimizing flow resistance, following characteristics have been observed. Since criteria 1 and 5 are quite straight forward (as described in section 3.7 of chapter 3 and as illustrated in sections 5.4.1 and 5.4.5 of chapter 5 analysing metal foams), in this work, remaining criteria (criterion 2 to criterion 4) are elaborately discussed.

7.1.1.1 Criteria 2:

Criteria two as shown in Figure 7.8 to Figure 7.10, analyses on the possible situations of the requirement where potentials of stacked wire mesh porous structures on maximizing heat transfer enhancement is sought however by just 25% of concern compared to a much higher concern (75%) still on the potential of minimizing flow resistance. Among all other criteria considered in the present study we can observe that this criterion is much closer to the interests as set by criteria one, and accordingly quite similar performance characteristics can be seen exhibited by the considered scenarios of stacked porous structures. Following which we can observe that this criterion can be met exceedingly well with lowest thickness conditions at all pore density conditions excluding at the lowest 5 PPI pore density situations for all type of stackings. At 5 PPI pore density conditions it can be seen that, 75% thickness scenario performs the best followed by 50, 25 and 100 percent thickness scenarios taken in the mentioned order. However, since the difference in the performance is not much significant at 5 PPI pore density situation, one can opt for higher thickness scenarios to gain a little advantage of heat transfer as the cost of flow resistance is not much significant while operating at

this criterion. However, at larger pore density conditions, thickness play a crucial role and choosing the lowest thickness meets the required criteria followed with largely reduced performance characteristics by thickness conditions taken in increasing order.

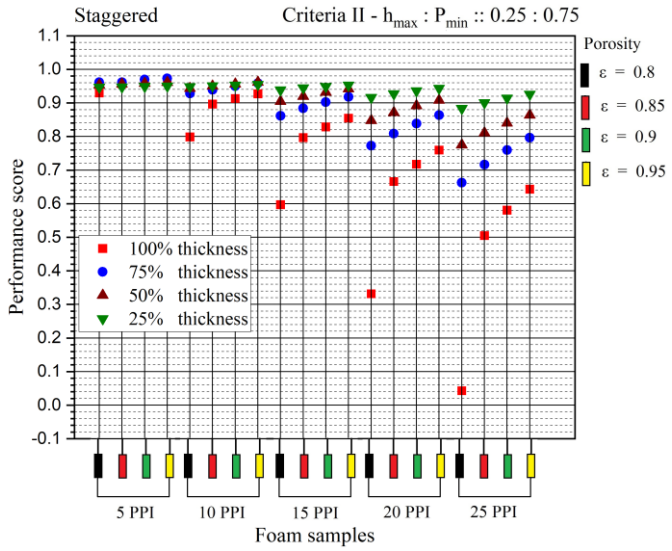

Figure 7.8 Performance characteristics of staggered stacking type corresponding to second criterion.

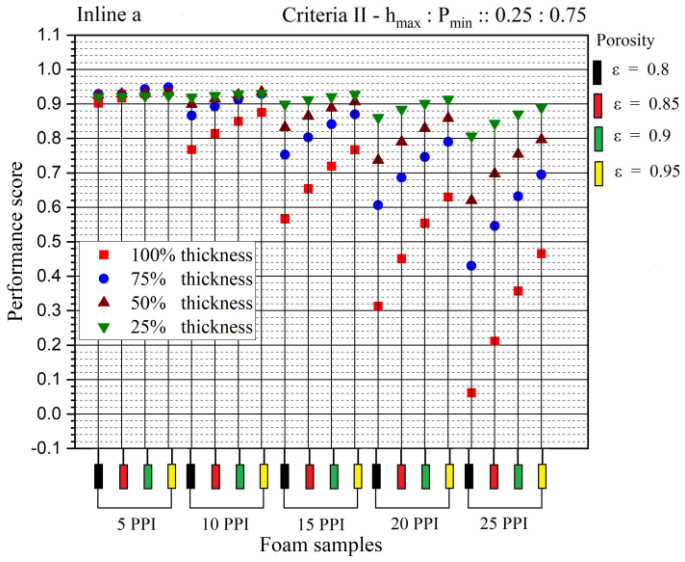

Figure 7.9 Performance characteristics of inline stacking of type-a, corresponding to second criterion.

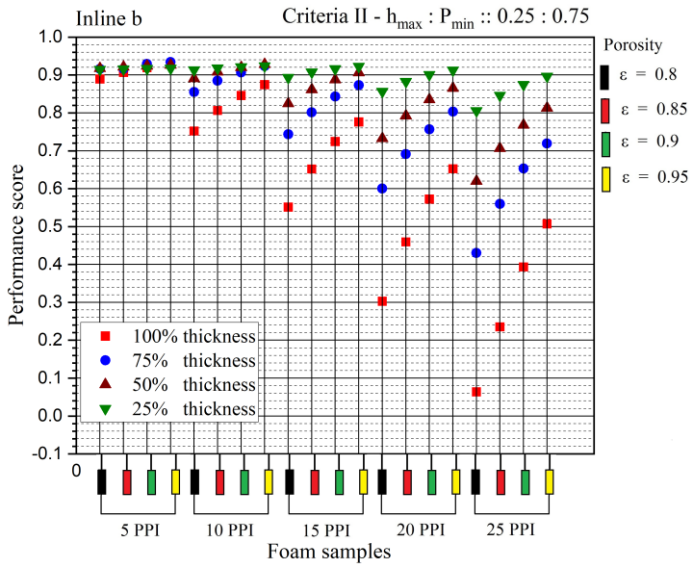

Figure 7.10 Performance characteristics of inline stacking of type-b, corresponding to second criterion.

7.1.1.2 Criteria 3:

Criteria three, focuses on arriving at situations where potential of every considered scenario on maximization of heat transfer and minimization of flow resistance is equally sought. By subjecting the trade-off analysis under this criterion one can arrive at the existing or possible scenarios where equal importance is given on the achievable benefit at an equal importance given at avoiding the cost involved. Unlike the earlier mentioned or analysed situations which were quite easy to comprehend, here in this situation one can observe how the required criterion can be met by the considered scenarios differently with their different combinations as can be observed from Figure 7.11 to Figure 7.13. Following which, it is observed that, maximum scores of performances of the considered scenarios were seen to be exhibited from 10 PPI pore density case at 75% thickness. It is interesting to observe that under low pore density scenarios 75% thickness and 100% thickness scenarios performed closely to each other meeting this criterion better than the other pore density conditions. However, the situation with higher pore density situations is observed not same as with the lower pore density conditions. At higher pore density conditions such as 20 PPI and 25 PPI, the highest performance, meeting this criterion was seen exhibited from the lowest thickness scenario of 25% followed by increasing order of the thickness conditions. This is due to considerations of the altered flow and heat transfer characteristics

associated with increase in thickness as well as porous conditions not ignoring the magnitude of the variations with every other scenario.

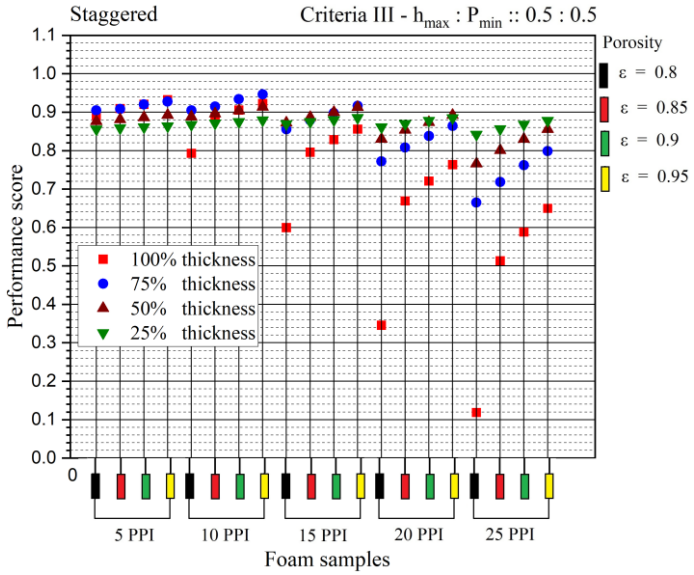

Figure 7.11 Performance characteristics of staggered stacking type corresponding to third criterion.

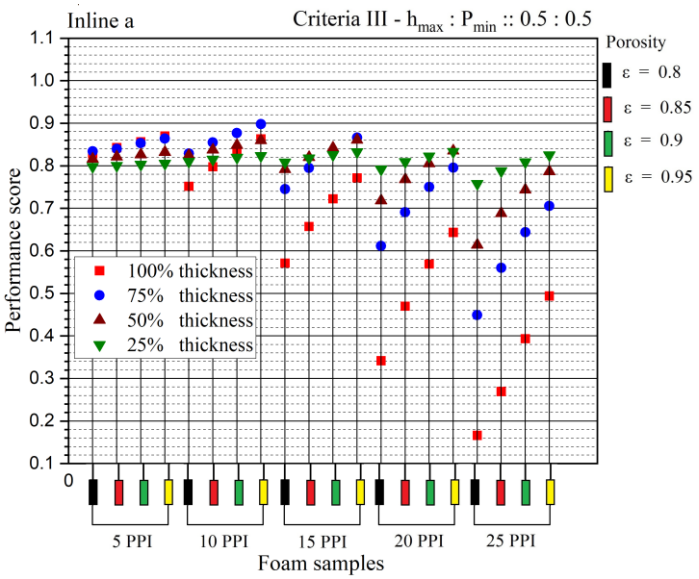

Figure 7.12 Performance characteristics of wire mesh stacking of inline type-a, corresponding to third criterion.

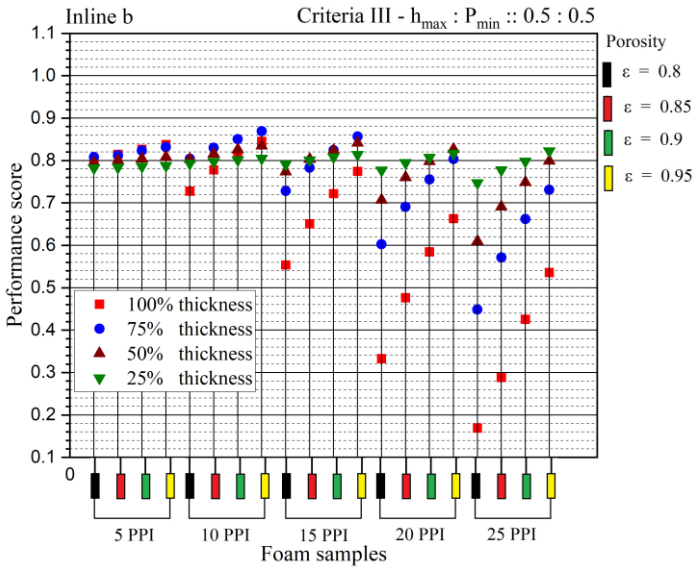

Figure 7.13 Performance characteristics of wire mesh stacking of inline type-b, corresponding to third criterion.

Also, one can observe that considering the lowest pore density conditions, it is always advantageous as all the thickness conditions under this porous condition perform close and considerably high in meeting this criterion. In such scenarios where an application is intended to work with an equal gain in the advantage of heat transfer enhancement at the same time an equal emphasis on reducing the cost (flow resistance) associated with it, it is wise to consider the lower pore density conditions and with a lower thickness scenario which would only cost a little margin of performance in ultimately achieving the required criterion.

7.1.1.3 Criteria 4:

Criteria four, assesses the ability of the considered scenarios for maximizing heat transfer prioritizing 75% compared to the ability of minimizing flow resistance prioritizing at only 25%. This scenario majorly focusses on the heat transfer enhancement potentials of stacked wire mesh porous structures with just an appreciable level of flow resistance reducing capabilities as shown from Figure 7.14 to Figure 7.16.

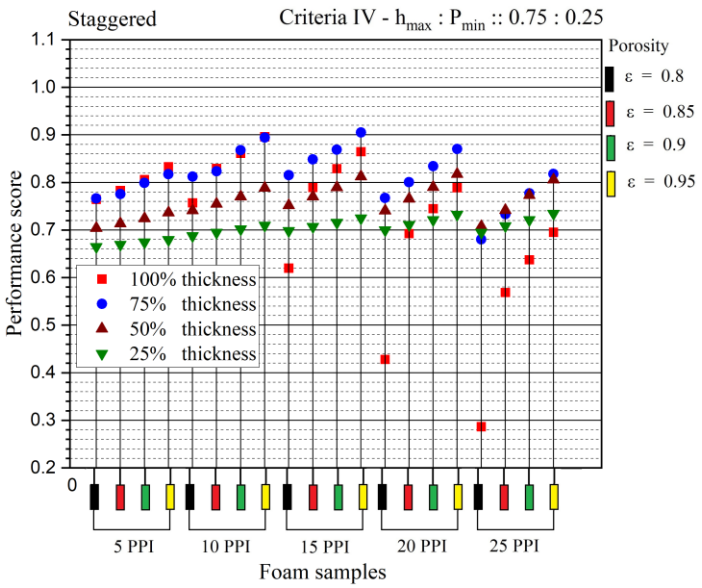

Figure 7.14 Performance characteristics of staggered stacking type corresponding to fourth criterion.

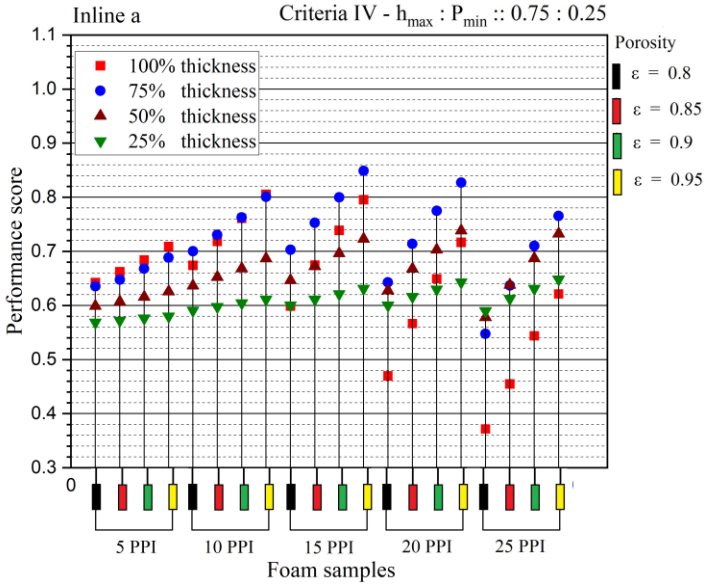

Figure 7.15 Performance characteristics of wire mesh stacking of inline type-a, corresponding to fourth criterion.

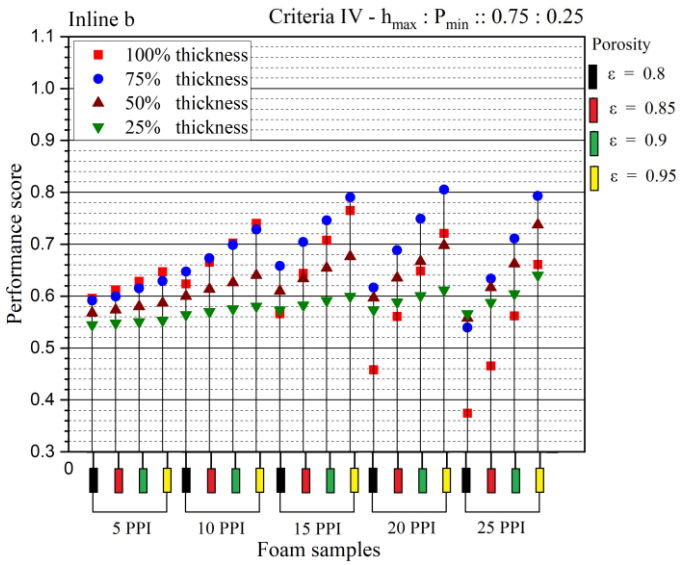

Figure 7.16 Performance characteristics of wire mesh stacking of inline type-b, corresponding to fourth criterion.

In terms of thickness, this criterion can be seen met excellently well with the 75% thickness scenarios almost at all pore density situations under all stacking types. At lower pore density cases (5 and 10 PPI), it can be seen that both 75% and 100% thickness performs closely and thereby opting for 75% thickness condition would give a gain on reduced flow resistance with just a marginal compromise in heat transfer enhancement which would otherwise have resulted with 100% thickness scenario. Excluding this behaviour observed for 5 and 10 PPI cases, at all pore density conditions the deviation in performances of stacked wire mesh porous media can be seen significantly varying with thickness conditions and should be considered accordingly. The highest performance score was observed for 75% thickness scenario of 15 PPI porous condition in the case of staggered and inline-a type stackings, whereas it was observed for 75% thickness condition of 20 PPI pore density case for an inline-b type of stacking.

7.2 SUMMARY

In the present chapter a critical analysis on various trade-off scenarios between heat transfer and pressure drop involving stacked wire mesh porous media has been illustrated. For this purpose, wire mesh porous structures of three prime variable conditions including pore density (5, 10, 15, 20 and 25 PPI), porosity (0.8, 0.85, 0.9

and 0.95 porosity) and thickness (100, 75, 50 and 25 percent) were considered. Individually analyzing, heat transfer characteristics were observed to increase with pore density, porosity and thickness of the porous sample similar that observed with metal foams. Also, pressure drop was observed to decrease with decrease in pore density and thickness condition and with increase in porosity. Both flow resistance and heat transfer characteristics are simultaneously analyzed for wire mesh samples of the mentioned variable conditions under different objectives (one is to maximize heat transfer and another to minimize pressure drop) subjected to various magnitudes of importance, to understand various trade-off scenario a wire mesh sample of given variable condition would participate in. Interesting trade-off scenarios between the enhancement of heat transfer and reduction of flow resistance behavior was demonstrated using TOPSIS the multi-objective multi criteria decision making tool that comprehensively illustrates various potentials of every wire mesh sample of considered variable conditions in meeting a desired thermos-hydraulic trade-off condition.

It is thus illustrated in the present study that the stacked wire mesh porous structures which not only are advantageous in terms of the cost involved in their manufacturing and set up but also are potential candidates aiding the control of the heat transfer and flow resistance involved with the application of metal based porous media. They provide large and easily achievable alternatives to control the trade-off between the heat transfer and flow resistance through much easily tuneable properties such as porous conditions, stacking types and thickness. Analysing their behaviours under the objective of various trade off scenarios between their potentials of maximizing heat transfer and minimizing flow resistance, unique performance characteristics have been illustrated by the porous structures of various features. Some critical observations include:

- Aiming at second criterion, at lower pore density conditions (5 PPI), one can opt for higher thickness scenarios to gain a little advantage of heat transfer as the cost of flow resistance is not much significant. However, at larger pore density conditions, thickness play a crucial role and choosing the lowest thickness meets the required criteria followed with largely reduced performance characteristics by higher thickness conditions.

- Under the analysis subjected to third criteria, considering the lowest pore density conditions, it is found to be always advantageous as all the thickness conditions under this porous condition perform close and considerably high in meeting this criterion. In such scenarios where an application is intended to work with an equal gain in the advantage of heat transfer enhancement at the same time an equal emphasis on reducing the cost (flow resistance) associated with it, it is wise to consider the lower pore density conditions and with a lower thickness scenario which would only cost a little margin of performance in ultimately achieving the required criterion.
- For criteria four, it is found that, excluding 5 and 10 PPI cases, at all pore density conditions the deviation in performances of stacked wire mesh porous media can be seen significantly varying with thickness conditions and should be considered accordingly. The highest performance score was observed for 75% thickness scenario of 15 PPI porous condition in the case of staggered and inline-a type stackings, whereas it was observed for 75% thickness condition of 20 PPI pore density case for an inline-b type of stacking.

7.3 CLOSURE

In the present work, stacked wire mesh porous structure's thermal and hydraulic characteristics are demonstrated corresponding to the changes in its structural, thickness and staking conditions. It is observed that, a variety of thermal and flow resistance characteristics can be exhibited by these porous structures that can efficiently be utilized in applications upon a comprehensive understanding on the trade-off scenario between the enhanced heat transfer which is simultaneously accompanied by the pressure drop. A comprehensive performance analysis using TOPSIS method showed that the optimal choice of selection of a thickness configuration, stacking manner and structural parameters dependence on the demand of an application for a specific trade-off scenario between the desired heat transfer enhancement and its affordability to bear the cost resulting out of the incurred flow resistance.

CHAPTER – 8

CONCLUSIONS

The present thesis is aimed at numerically analysing the thermo-hydraulic performances of metal based porous media such as metal foams and stacked wire mesh porous structures, focusing on investigating their various potentials of maximizing heat transfer and minimizing flow resistance characteristics. Starting with the introduction to porous media and their applications in **Chapter 1,** a detailed discussion on the numerical modelling aspects associated with them is provided followed by governing laws and equations to mimic the flow and heat transfer through such media. It is then followed by a collective literature review on works related to thermo-hydraulic investigations of metal foams, stacked wire mesh porous structures in **Chapter 2** where it is found that, the twin structural properties (porosity and pore density), thickness configurations and their combined effect is not comprehensively studied, undertaking which could present a better way to understand and deal with the penalty of incurred flow resistance that is always accompanied by the increased heat transfer using such media. Following which, motivation and scope for the present research work is stated with specified objectives of the present study.

Chapter 3 describes the detailed methodology that is followed in the present study in order to numerically analyse the metal based porous media. Starting with the description of the experimental work and domain considered for the current numerical modelling, discretization and boundary conditions are described with numerical details, grid independence study and validation of the numerical results emphasizing on the aptness of the numerical procedure for further analysis of the metal based porous media adhering to the objectives of the present research work.

Chapter 4 highlights on the significance of considerations of both the twin structural properties (porosity and pore density) to comprehend the thermal and flow resistance characteristics of metal foam porous media. Through this study it is found that, interfacial characteristics such as interfacial specific surface area and interfacial heat transfer co-efficient greatly alters the heat transfer and flow resistance phenomenon.

Both of these interfacial parameters are shown to be dependent on the combination of these twin structural properties. The influence of various combinations of these structural properties are further emphasized specific to various convection regimes with the help of Nusselt number correlations. Through this, it is found that, under natural convection regime (for $Ri \geq 39$) the effect of pore density at constant porosity was not as influencing as in case of mixed and forced convection regimes in altering the heat transfer characteristics of metal foams. The consideration of the effects of combination of pore density and porosity of metal foams, under mixed convection for ($0.6 \leq Ri \leq 40$) and forced convection (for $Ri \leq 0.6$) scenario is found to be very much evident in altering heat transfer characteristics, thus proving to be the key controllable features of metal based porous media that can exhibit various desired heat transfer and flow resistance phenomenon.

Chapter 5 comprises of the study that is aimed at comprehensively analysing the various trade-off scenarios between the potentials of metal foams in enhancing heat transfer and curtailing flow resistance phenomenon. Metal foams of various combinations of their structural properties (0.8, 0.85, 0.9 and 0.95 porosity with various pore density conditions such as 5, 10, 15, 20 and 25 PPI) and thickness conditions (100, 75, 50 and 25) percent are analysed. Individually analysing, heat transfer characteristics were observed to increase with pore density, porosity and thickness of the foam samples. In terms of pressure drop, it was observed to be decreasing with decrease in pore density and thickness conditions, whereas it is found to be increasing with decrease in porosity. Observing heat transfer and flow phenomenon it is found that with every unique combination of these mentioned variable conditions different heat transfer and flow resistance characteristics can be observed, which then is comprehensively analysed using TOPSIS a multi objective multi attribute decision making tool. Using this methodology the trade-off performances of metal foams are analysed under five different criteria. Criteria 1 ($h_{max} : P_{min} :: 0 : 1$), representing a scenario that seeks and rank the possible conditions where maximizing heat transfer potentials are given zero percent importance while 100 percent importance is given at seeking or ranking those variable conditions that minimizes the pressure drop. Various other criteria are such as Criteria 2 ($h_{max} : P_{min} :: 0.25 : 0.75$), Criteria 3 ($h_{max} : P_{min} :: 0.5 : 0.5$), Criteria 4 ($h_{max}$:

P_{min} :: 0.75 : 0.25) and Criteria 5 (h_{max} : P_{min} :: 1 : 0) are considered subjecting various weights of importance on the potentials of metal foams for their potentials of enhancing heat transfer and cutting down flow resistance. Through this analysis it is found that, metal foam with 5 PPI, 25% thickness with 0.95 porosity performs the best pertaining to criteria 1. Criteria 2 was observed to be best met by 5 PPI and 0.95 porosity but under 75% thickness condition. Similarly best performance was observed for the metal foam with 10 PPI, 75% thickness with porosity of 0.95 while meeting criteria 3 and for criteria 4 the best performance was found to be exhibited from metal foams of 15 PPI, 0.95 porosity and 75% thickness conditions. Performance owing to criteria 5 was observed to be best met by 25 PPI conditions with 0.95 porosity at 100% thickness scenario. The relative performances of metal foams of other variable conditions are clearly depicted, that provides a wide variety of optimal choices that meets various requirement of specific trade-off scenarios between the benefit of heat transfer enhancement and the cost that can be affordable to bare the resulting flow resistance.

Chapter 6 focused on providing numerical modelling requirements of stacked wire mesh porous media to explore their advantages in controlling flow and thermal phenomenon. Essential expressions that correlate easily controllable flow and heat transfer influencing features such as fiber diameter, wire-mesh size, specific surface area, porosity of wire mesh porous structures are provided for three different possible stacking manner such as staggered stacking (highest compactness), stacking of inline-b type (least compactness) and stacking of inline-a type (intermediate compactness). Upon identification of suitable heat transfer influencing parameters required for numerical modelling of such media, further scope for obtaining various heat transfer and flow-resistance characteristics is emphasized.

Chapter 7 further aimed at comprehensively analysing various trade-off scenarios that can be extracted out of the stacked wire mesh porous structures under various structural variations (0.8, 0.85, 0.9, and 0.95 porosity each with various pore density of 5, 10, 15, 20, and 25 PPI), thickness conditions (100, 75, 50, and 25 percent) and stacking manner (staggered, inline-a, inline-b). Based on individual analysis, it was found that the thickness, porosity, and pore density of these porous sample all increased the heat transfer characteristics similar to that as observed with meta foams. Similarly, it was

showed that when porosity increases, decrease in flow resistance is observed whereas with increase in pore density and thickness conditions elevation in flow resistance is observed. For wire mesh samples with three orderly varying conditions, pore density, porosity, and thickness, both flow resistance and heat transfer characteristics are simultaneously analysed under two distinct objectives (maximizing heat transfer potential and minimizing pressure drop potential), each with varying degrees of significance resulting in various criteria. Performance analysis under second criterion ($h_{max} : P_{min} :: 0.25 : 0.75$) showed that, in situations with lower pore density (5 PPI) that performed best in meeting this criteria, one may still choose higher thickness conditions in order to somewhat benefit from heat transfer, while the cost of flow resistance is found to be not very high compared to other thickness scenarios. Thickness is found to be significant in greater pore density conditions. At higher pore density conditions selecting the lowest thickness is found to better meet the subjected requirement of criteria 2, with higher thickness conditions leading to much inferior performance characteristics. Analysis, under criteria 3 ($h_{max} : P_{min} :: 0.5 : 0.5$) showed that, maximum scores of performances of the considered scenarios were seen to be exhibited from 10 PPI pore density case at 75% thickness. Under low pore density scenarios 75% thickness and 100% thickness scenarios performed closely to each other meeting this criterion better than the other pore density conditions. However, at higher pore density conditions such as 20 PPI and 25 PPI, the highest performance, meeting this criterion was seen exhibited from the lowest thickness scenario of 25% followed by increasing order of the thickness conditions. Further, criteria 4 is observed to be met excellently well with the 75% thickness scenarios almost at all pore density situations under all stacking types. At lower pore density cases (5 and 10 PPI), it was observed that both 75% and 100% thickness performed closely. Excluding this behaviour observed for 5 and 10 PPI cases, at all pore density conditions the deviation in performances of stacked wire mesh porous media is found significantly varying with thickness conditions. The highest performance score was observed for 75% thickness scenario of 15 PPI porous condition in the case of staggered and inline-a type stackings, whereas it was observed for 75% thickness condition of 20 PPI pore density case for an inline-b type of stacking.

8.1 SCOPE OF FUTURE WORK

The present work mainly aimed at handling the phenomenon of incurred pressure drop accompanying the enhanced heat transfer that is generally associated with metal based porous media. In this regard variable conditions such as porosity, pore density, thickness and stacking manner were considered and resulting altered heat transfer and flow resistance characteristics were comprehensively analysed to investigate the trade-off between these vital thermo-hydraulic phenomena. However, following considerations can further be implemented in order to obtain various other heat transfer and flow characteristics that can provide alternate optimal choices for various applications demanding various trade-off scenarios.

- Introduction of different fluid may exhibit different magnitude of heat transfer and flow-resistance that can result in an altered trade-off scenario between the mentioned thermo-hydraulic phenomenon.
- Investigating the porous material property for altered heat transfer characteristics may also provide better trade-off scenarios.
- Evaluation of other porous materials such as lattice structures may further provide better alternatives to counter the effect of flow resistance.
- Analysis of similar trade-off scenarios between heat transfer enhancement and actual cost involved with the corresponding pumping power may be a quick decision-making criterion in terms of industrial affordability.

REFERENCES

Albanakis, C., Missirlis, D., Michailidis, N., Yakinthos, K., Goulas, A., Omar, H., Tsipas, D., and Granier, B. (2009). "Experimental analysis of the pressure drop and heat transfer through metal foams used as volumetric receivers under concentrated solar radiation." *Exp Therm Fluid Sci*, 33(2), 246–252.

Arbak, A., Dukhan, N., Bağcı, Ö., and Özdemir, M. (2017). "Influence of pore density on thermal development in open-cell metal foam." *Exp Therm Fluid Sci*, 86, 180–188.

Armour, J. C. (1968). "Fluid Through Woven Screens." *AIChE J.*, 14(3), 415–420.

Baragh, S., Shokouhmand, H., Soheil, S., and Ajarostaghi, M. (2018). "International Journal of Thermal Sciences An experimental investigation on forced convection heat transfer of single- phase fl ow in a channel with di ff erent arrangements of porous media." *International Journal of Thermal Sciences*, 134(August), 370–379.

Barbieri, M., Ilio, G. Di, Patanè, F., and Bella, G. (2017). "Experimental investigation on buoyancy-induced convection in aluminum metal foams." *International Journal of Refrigeration*, 76, 385–393.

Bejan, A., and Kraus, A. D. (2003). *Heat transfer handbook*. J. Wiley.

Bhattacharya, A., Calmidi, V. V., and Mahajan, R. L. (2002). "Thermophysical properties of high porosity metal foams." *Int J Heat Mass Transf*, 45(5), 1017–1031.

Bianco, N., Iasiello, M., Mauro, G. M., and Pagano, L. (2021). "Multi-objective optimization of finned metal foam heat sinks: Tradeoff between heat transfer and pressure drop." *Appl Therm Eng*, 182(July 2020), 116058.

Boroujerdi, A. A., and Esmaeili, M. (2015). "Characterization of the frictional losses and heat transfer of oscillatory viscous flow through wire-mesh regenerators." *Alexandria Engineering Journal*, 54(4), 787–794.

Bussière, W., Rochette, D., Clain, S., André, P., and Renard, J. B. (2017). "Pressure drop measurements for woven metal mesh screens used in electrical safety switchgears." *Int J Heat Fluid Flow*, 65, 60–72.

Caket, A. G., Wang, C., Nugroho, M. A., Celik, H., and Mobedi, M. (2022). "Recent studies on 3D lattice metal frame technique for enhancement of heat transfer: Discovering trends and reasons." *Renewable and Sustainable Energy Reviews*, Elsevier Ltd.

Calmidi, V. V., and Mahajan, R. L. (2000a). "Forced convection in high porosity metal foams." *J Heat Transfer*, 122(3), 557–565.

Calmidi, V. V., and Mahajan, R. L. (2000b). "Forced convection in high porosity metal foams." *J Heat Transfer*, 122(3), 557–565.

Calmidi, V. V., and Mahajan, R. L. (2000c). “Forced convection in high porosity metal foams.” *J Heat Transfer*, 122(3), 557–565.

Calmidi, V. V., and Mahajan, R. L. (2002). “Forced Convection in High Porosity Metal Foams.” *J Heat Transfer*, 122(3), 557.

Cattaneo, L., Comunian, A., Filippis, G. de, Giudici, M., and Vassena, C. (2016). “Modeling groundwater flow in heterogeneous porous media with YAGMod.” *Computation*, 4(1).

Chen, L., He, A., Zhao, J., Kang, Q., Li, Z. Y., Carmeliet, J., Shikazono, N., and Tao, W. Q. (2022). “Pore-scale modeling of complex transport phenomena in porous media.” *Prog Energy Combust Sci*, Elsevier Ltd.

Churchill, S. W., and Usagi, R. (1972). “A general expression for the correlation of rates of transfer and other phenomena.” *AIChE Journal*, 18(6), 1121–1128.

Costa, S. C., Barrutia, H., Esnaola, J. A., and Tutar, M. (2013). “Numerical study of the pressure drop phenomena in wound woven wire matrix of a Stirling regenerator.” *Energy Convers Manag*, 67, 57–65.

Costa, S. C., Barrutia, H., Esnaola, J. A., and Tutar, M. (2014). “Numerical study of the heat transfer in wound woven wire matrix of a Stirling regenerator.” *Energy Convers Manag*, 79, 255–264.

Das, M. K., Mukherjee, P. P., and Muralidhar, K. (n.d.). *Mechanical Engineering Series Modeling Transport Phenomena in Porous Media with Applications*.

Detmann, B. (2021). “Modeling chemical reactions in porous media: a review.” *Continuum Mechanics and Thermodynamics*, Springer Science and Business Media Deutschland GmbH.

Gandomkar, A., and Gray, K. E. (2018). “International Journal of Heat and Mass Transfer Local thermal non-equilibrium in porous media with heat conduction.” *Int J Heat Mass Transf*, 124, 1212–1216.

Garg, S. K., Premachandran, B., and Singh, M. (2019). “Numerical study of the regenerator for a miniature Stirling cryocooler using the local thermal equilibrium (LTE) and the local thermal nonequilibrium (LTNE) models.” *Thermal Science and Engineering Progress*, 11(March), 150–161.

Garg, S. K., Premachandran, B., Singh, M., Sachdev, S., and Sadana, M. (2020). “Effect of Porosity of the regenerator on the performance of a miniature Stirling cryocooler.” *Thermal Science and Engineering Progress*, 15.

Garrity, P. T., and Klausner, J. F. (2010). “Performance of Aluminum and Carbon Foams for Air Side Heat Transfer Augmentation.” 132(December), 1–9.

Gedeon, D., and Wood, J. G. (1996). *Oscillating-Flow Regenerator Test Rig : Hardware and Theory With Derived Correlations for Screens and Felts*.

Geodeon, D. (1999). *Baseline Stirling modeling*. Athens (OH): Gedeon Associates.

Hendiani, S., and Walther, G. (2023). "TOPSISort-L: An extended likelihood-based interval-valued intuitionistic fuzzy TOPSIS-sort method and its application to multi-criteria group decision-making." *Expert Syst Appl*, 233.

Hoseini, S. S., Seyedkanani, A., Najafi, G., Sasmito, A. P., and Akbarzadeh, A. (2023). "Multiscale architected porous materials for renewable energy conversion and storage." *Energy Storage Mater*, Elsevier B.V.

Hsieh, W. H., Wu, J. Y., Shih, W. H., and Chiu, W. C. (2004). "Experimental investigation of heat-transfer characteristics of aluminum-foam heat sinks." *Int J Heat Mass Transf*, 47(23), 5149–5157.

Hwang, G. J., Wu, C. C., and Chao, C. H. (1995). *Investigation of Non-Darcian Forced Convection in an Asymmetrically Heated Sintered Porous Channel*.

Hwang, J. J., Hwang, G. J., Yeh, R. H., and Chao, C. H. (2002). "Measurement of interstitial convective heat transfer and frictional drag for flow across metal foams." *J Heat Transfer*, 124(1), 120–129.

Iasiello, M., Bianco, N., Chiu, W. K. S., and Naso, V. (2020). "Anisotropic convective heat transfer in open-cell metal foams: Assessment and correlations." *Int J Heat Mass Transf*, 154, 119682.

Iasiello, M., Cunsolo, S., Bianco, N., Chiu, W. K. S., and Naso, V. (2017). "Developing thermal flow in open-cell foams." *International Journal of Thermal Sciences*, 111, 129–137.

Ichimiya, K., and Asme, M. (1999). *A New Method for Evaluation of Heat Transfer Between Solid Material and Fluid in a Porous Medium*.

Iwaniszyn, M., Sindera, K., Gancarczyk, A., Korpy, M., Roman, J. J., Ko, A., and Jod, J. (2021). "Experimental and CFD investigation of heat transfer and flow resistance in woven wire gauzes." *Chemical Engineering and Processing - Process Intensification*, 163(March).

Jadhav, P. H., Gnanasekaran, N., Perumal, D. A., and Mobedi, M. (2021). "Performance evaluation of partially filled high porosity metal foam configurations in a pipe." *Appl Therm Eng*, 194(May), 117081.

Jiafei, Z., Mingrui, S. U. N., Lunxiang, Z., Chengzhi, H. U., Dawei, T., and Lei, Y. (2021). "Forced Convection Heat Transfer in Porous Structure : Effect of Morphology on Pressure Drop and Heat Transfer Coefficient." *Journal of Thermal Science*, 30(2), 363–393.

Kamath, P. M., Balaji, C., and Venkateshan, S. P. (2011). "Experimental investigation of flow assisted mixed convection in high porosity foams in vertical channels." *Int J Heat Mass Transf*, 54(25–26), 5231–5241.

Kamath, P. M., Balaji, C., and Venkateshan, S. P. (2013). “Convection heat transfer from aluminium and copper foams in a vertical channel - An experimental study.” *International Journal of Thermal Sciences*, 64, 1–10.

Kang, K. J. (2015). “Wire-woven cellular metals: The present and future.” *Prog Mater Sci*, 69, 213–307.

Kaviany, M. (1995). *Principles of Heat Transfer in Porous Media*. New York: Springer-Verlag.

Kim, D. Y., and Kim, K. C. (2019a). “International Journal of Heat and Mass Transfer An experimental study on the thermal and hydraulic characteristics of open-cell nickel and copper foams for compact heat exchangers.” *Int J Heat Mass Transf*, 130, 162–174.

Kim, D. Y., and Kim, K. C. (2019b). “An experimental study on the thermal and hydraulic characteristics of open-cell nickel and copper foams for compact heat exchangers.” *Int J Heat Mass Transf*, 130, 162–174.

Kim, S. Y., Paek, J. W., and Kang, B. H. (2000). “Flow and heat transfer correlations for porous fin in a plate-fin heat exchanger.” *J Heat Transfer*, 122(3), 572–578.

Kotresha, B., and Gnanasekaran, N. (2019). “Determination of interfacial heat transfer coefficient for the flow assisted mixed convection through brass wire mesh.” *International Journal of Thermal Sciences*, 138(April 2018), 98–108.

Kumar, S., Premachandran, B., and Singh, M. (2019). “Numerical study of the regenerator for a miniature Stirling cryocooler using the local thermal equilibrium (LTE) and the local thermal nonequilibrium (LTNE) models.” *Thermal Science and Engineering Progress*, 11(December 2018), 150–161.

Kurian, R., Balaji, C., and Venkateshan, S. P. (2016a). “Experimental investigation of near compact wire mesh heat exchangers.” *Appl Therm Eng*, 108, 1158–1167.

Kurian, R., Balaji, C., and Venkateshan, S. P. (2016b). “Experimental investigation of convective heat transfer in a vertical channel with brass wire mesh blocks.” *International Journal of Thermal Sciences*, 99, 170–179.

Kurian, R., Balaji, C., and Venkateshan, S. P. (2016c). “Experimental investigation of convective heat transfer in a vertical channel with brass wire mesh blocks.” *International Journal of Thermal Sciences*, 99, 170–179.

Kurian, R., Balaji, C., and Venkateshan, S. P. (2017). “An experimental study on hydrodynamic and thermal performance of stainless steel wire mesh blocks in a vertical channel.” *Exp Therm Fluid Sci*, 86, 248–256.

Lai, Z., Hu, H., and Ding, G. (2019). “Influence of pore density on heat transfer and pressure drop characteristics of wet air in hydrophilic metal foams.” *Appl Therm Eng*, 159(June), 113897.

Leong, K. C., and Jin, L. W. (2005). “An experimental study of heat transfer in oscillating flow through a channel filled with an aluminum foam.” *Int J Heat Mass Transf*, 48(2), 243–253.

Li, Y., Gong, L., Xu, M., and Joshi, Y. (2020). “Hydraulic and thermal performances of metal foam and pin fin hybrid heat sink.” *Appl Therm Eng*, 166, 114665.

Li, Y., Wang, S., and Zhao, Y. (2018). “Experimental study on heat transfer enhancement of gas tube partially filled with metal foam.” *Exp Therm Fluid Sci*, 97, 408–416.

Lin, W., Sundén, B., and Yuan, J. (2013). “A performance analysis of porous graphite foam heat exchangers in vehicles.” *Appl Therm Eng*, 50(1), 1201–1210.

Lin, W., Xie, G., Yuan, J., and Sundén, B. (2016). “Comparison and Analysis of Heat Transfer in Aluminum Foam Using Local Thermal Equilibrium or Nonequilibrium Model Comparison and Analysis of Heat Transfer in Aluminum Foam Using Local Thermal Equilibrium or Nonequilibrium Model.” 7632.

Liu, H., Ahmad, S., Shi, Y., and Zhao, J. (2021). “A parametric study of a hybrid battery thermal management system that couples PCM/copper foam composite with helical liquid channel cooling.” *Energy*, 231, 120869.

Liu, J. F., Wu, W. T., Chiu, W. C., and Hsieh, W. H. (2006). “Measurement and correlation of friction characteristic of flow through foam matrixes q.” 30, 329–336.

Lu, W., Zhang, T., and Yang, M. (2016). “Analytical solution of forced convective heat transfer in parallel-plate channel partially filled with metallic foams.” *Int J Heat Mass Transf*, 100, 718–727.

Ma, Z., and Ranjith, P. G. (2019). “Review of application of molecular dynamics simulations in geological sequestration of carbon dioxide.” *Fuel*, Elsevier Ltd.

Mancin, S., Zilio, C., Cavallini, A., and Rossetto, L. (2010). “International Journal of Heat and Mass Transfer Heat transfer during air flow in aluminum foams.” *Int J Heat Mass Transf*, 53(21–22), 4976–4984.

Mancin, S., Zilio, C., Diani, A., and Rossetto, L. (2012a). “Experimental air heat transfer and pressure drop through copper foams.” *Exp Therm Fluid Sci*, 36, 224–232.

Mancin, S., Zilio, C., Diani, A., and Rossetto, L. (2013a). “Internati onal Journ al of Heat and Mass Transfe r Air forced convection through metal foams : Experimental results and modeling.” *Int J Heat Mass Transf*, 62, 112–123.

Mancin, S., Zilio, C., Diani, A., and Rossetto, L. (2013b). “Air forced convection through metal foams: Experimental results and modeling.” *Int J Heat Mass Transf*, 62(1), 112–123.

Mancin, S., Zilio, C., Rossetto, L., and Cavallini, A. (2012b). “Foam height effects on heat transfer performance of 20 ppi aluminum foams.” *Appl Therm Eng*, 49, 55–60.

Mishra, N. K., Muthukumar, P., and Panigrahy, S. (2018). “A Review on Clean Combustion Within Porous Media.” *Energy, Environment, and Sustainability*, Springer Nature, 209–224.

Nakate, P., Kotresha, B., and Gnanasekaran, N. (2019). “Inexpensive computations using computational fluid dynamics combined with asymptotics applied to laminar mixed convection in a vertical channel.” *J Heat Transfer*, 141(12), 1–7.

Nield, D. A., and Bejan, A. (2017). *Convection in porous media*. *Convection in Porous Media*, Springer International Publishing.

Nithyanandam, K., and Mahajan, R. L. (2018). “International Journal of Heat and Mass Transfer Evaluation of metal foam based thermoelectric generators for automobile waste heat recovery.” *Int J Heat Mass Transf*, 122, 877–883.

Noh, J. S., Lee, K. B., and Lee, C. G. (2006). “Pressure loss and forced convective heat transfer in an annulus filled with aluminum foam.” *International Communications in Heat and Mass Transfer*, 33(4), 434–444.

Okoroafor, E. R., Saltzer, S. D., and Kovscek, A. R. (2022). “Toward underground hydrogen storage in porous media: Reservoir engineering insights.” *Int J Hydrogen Energy*, 47(79), 33781–33802.

Phanikumar, M. S., and Mahajan, R. L. (2002). “Non-Darcy natural convection in high porosity metal foams.” *Int J Heat Mass Transf*, 45(18), 3781–3793.

Prashant Singh, Karthik Nithyanandam, Mingyang Zhang, R. L. M. (2020). “The effect of metal foam thickness on jet array impingement heat transfer in high-porosity aluminum foams.” *J. Heat Transfer*, 142(5), 052301.

Qi, C., Huang, K., Liu, J., Wang, G., and Yan, Y. (n.d.). *4 Thermal Management and Heat Transfer Enhancement Using Porous Materials*.

Qian, M., Li, J., Xiang, Z., Dong, Z., Xiao, J., and Hu, X. (2023). “Study on heat dissipation performance of a lattice porous structures under jet impingement cooling.” *Case Studies in Thermal Engineering*, 49.

Ribeiro, G. B., and Barbosa, J. R. (2013). “Comparison of metal foam and louvered fi ns as air-side heat transfer enhancement media for miniaturized condensers.” *Appl Therm Eng*, 51(1–2), 334–337.

Saedodin, S., Zamzamian, S. A. H., Nimvari, M. E., Wongwises, S., and Jouybari, H. J. (2017). “Performance evaluation of a flat-plate solar collector filled with porous metal foam: Experimental and numerical analysis.” *Energy Convers Manag*, 153(August), 278–287.

Sayed, M. A., ELdein Hussin, A. M. T. A., Mahmoud, N. A., and Aboelsoud, W. (2020). “Performance evaluation of wire mesh heat exchangers.” *Appl Therm Eng*, 169.

Sener, M., and Yataganbaba, A. (2016). “Forchheimer forced convection in a rectangular channel partially filled with aluminum foam.” 75, 162–172.

Shikh Anuar, F., Ashtiani Abdi, I., Odabaee, M., and Hooman, K. (2018). “Experimental study of fluid flow behaviour and pressure drop in channels partially filled with metal foams.” *Exp Therm Fluid Sci*, 99(May), 117–128.

Shu, X., Wu, Y., Zhang, X., and Yu, F. (2023). “Experiments and models for contaminant transport in unsaturated and saturated porous media – A review.” *Chemical Engineering Research and Design*, Institution of Chemical Engineers.

Siavashi, M., Talesh Bahrami, H. R., and Aminian, E. (2018). “Optimization of heat transfer enhancement and pumping power of a heat exchanger tube using nanofluid with gradient and multi-layered porous foams.” *Appl Therm Eng*, 138, 465–474.

Sun, M., Hu, C., Zha, L., Xie, Z., Yang, L., Tang, D., Song, Y., and Zhao, J. (2020). “Pore-scale simulation of forced convection heat transfer under turbulent conditions in open-cell metal foam.” *Chemical Engineering Journal*, 389(February), 124427.

Sypeck, D. J. (2001). “Multifunctional microtruss laminates: Textile synthesis and properties.” *Journal of material research*, 16(3).

Tanaka, M., Yamashita, I., and Chisaka, F. (1990). “Flow and heat transfer characteristics of the stirling engine regenerator in an oscillating flow.” *JSME international journal*, 33, 283–289.

Tian, J., Lu, T. J., Hodson, H. P., Queheillalt, D. T., and Wadley, H. N. G. (2007). “Cross flow heat exchange of textile cellular metal core sandwich panels.” *Int J Heat Mass Transf*, 50, 2521–2536.

Torabi, M., Karimi, N., and Zhang, K. (2015). “Heat transfer and second law analyses of forced convection in a channel partially fi lled by porous media and featuring internal heat sources.” *Energy*, 93, 106–127.

Tzeng, S. C. (2007). “Spatial thermal regulation of aluminum foam heat sink using a sintered porous conductive pipe.” *Int J Heat Mass Transf*, 50(1–2), 117–126.

Tzeng, S. C., and Jeng, T. M. (2006). “Convective heat transfer in porous channels with 90-deg turned flow.” *Int J Heat Mass Transf*, 49(7–8), 1452–1461.

Udenni Gunathilake, T. M. S., Ching, Y. C., Ching, K. Y., Chuah, C. H., and Abdullah, L. C. (2017). “Biomedical and microbiological applications of bio-based porous materials: A review.” *Polymers (Basel)*, MDPI AG.

Venugopal, G., Balaji, C., and Venkateshan, S. P. (2010a). “Experimental study of mixed convection heat transfer in a vertical duct filled with metallic porous structures.” *International Journal of Thermal Sciences*, 49(2), 340–348.

Venugopal, G., Balaji, C., and Venkateshan, S. P. (2010b). “Experimental study of mixed convection heat transfer in a vertical duct filled with metallic porous structures.” *International Journal of Thermal Sciences*, 49(2), 340–348.

Vijay, D., Goetze, P., Wulf, R., and Gross, U. (2015). “Forced convection through open cell foams based on homogenization approach: Transient analysis.” *International Journal of Thermal Sciences*, 98, 395–408.

Wakao, N., Kaguei, S., and Funazkri, T. (1979). “Effect of fluid dispersion coefficients on particle-to-fluid heat transfer coefficients in packed beds: correlation of nusselt numbers.” *Chem Eng Sci*, 34, 325–336.

Wang, Y., Yang, G., Huang, Y., Huang, Y., Zhuan, R., and Wu, J. (2021). “Analytical model of flow-through-screen pressure drop for metal wire screens considering the effects of pore structures.” *Chem Eng Sci*, 229, 116037.

Wu, Z., Caliot, C., Flamant, G., and Wang, Z. (2011). “Numerical simulation of convective heat transfer between air flow and ceramic foams to optimise volumetric solar air receiver performances.” *Int J Heat Mass Transf*, 54(7–8), 1527–1537.

Xia, X., Chen, X., Sun, C., Li, Z., and Liu, B. (2017). “International Journal of Heat and Mass Transfer Experiment on the convective heat transfer from airflow to skeleton in open-cell porous foams.” *Int J Heat Mass Transf*, 106, 83–90.

Xiao, G., Peng, H., Fan, H., Sultan, U., and Ni, M. (2017). “Characteristics of steady and oscillating flows through regenerator.” *Int J Heat Mass Transf*, 108, 309–321.

Xu, J., Tian, J., Lu, T. J., and Hodson, H. P. (2007). “On the thermal performance of wire-screen meshes as heat exchanger material.” *Int J Heat Mass Transf*, 50(5–6), 1141–1154.

Xu, Z. G., and Gong, Q. (2018). “International Journal of Thermal Sciences Numerical investigation on forced convection of tubes partially fi lled with composite metal foams under local thermal non-equilibrium condition.” 133(July), 1–12.

Zhao, C. Y., Lu, T. J., and Hodson, H. P. (2005). “Natural convection in metal foams with open cells.” *Int J Heat Mass Transf*, 48(12), 2452–2463.

Zhao, Z., Peles, Y., and Jensen, M. K. (2013). “Properties of plain weave metallic wire mesh screens.” *Int J Heat Mass Transf*, 57(2), 690–697.

Zukauskas, A. (1987a). “Convective heat transfer in cross flow.” *Handbook of Single-Phase Convective Heat Transfer*.

Zukauskas, A. (1987b). *Convective heat transfer in cross flow. Handbook of single-phase convective heat transfer*. Hoboken, NJ, USA: John Wiley &sons.

Zuo, H., Wu, M., Zeng, K., Zhou, Y., Kong, J., Qiu, Y., Lin, M., and Flamant, G. (2021). “Numerical investigation and optimal design of partially filled sectorial metal foam configuration in horizontal latent heat storage unit.” *Energy*, 237, 121640.

LIST OF PUBLICATIONS

INTERNATIONAL JOURNALS

1. Trilok, G. and Gnanasekaran, N., (January 2021). “Numerical study on maximizing heat transfer and minimizing flow resistance behaviour of metal foams owing to their structural properties”. *International Journal of Thermal Sciences*, 159, p.106617.

International Journal of Thermal Sciences (SCIE)
Impact factor: 5.69
ISSN: 1290-0729
DOI: https://doi.org/10.1016/j.ijthermalsci.2020.106617

2. Trilok, G., K. Kiran Kumar, N. Gnanasekaran, and Moghtada Mobedi. "Numerical assessment of thermal characteristics of metal foams of orderly varied pore density and porosity under different convection regimes." *International Journal of Thermal Sciences* 172 (2022): 107288.

International Journal of Thermal Sciences (SCIE)
Impact factor: 5.69
ISSN: 1290-0729
DOI: https://doi.org/10.1016/j.ijthermalsci.2021.107288

3. Trilok, G., Srinivas, K. E. S., Harikrishnan, D., Gnanasekaran, N., & Mobedi, M. (2022). Correlations and Numerical Modeling of Stacked Woven Wire-Mesh Porous Media for Heat Exchange Applications. *Energies*, 15(7), 1-25.

Energies (SCIE)
Impact factor: 3.51
ISSN: 1996-1073
DOI: https://doi.org/10.3390/en15072371

4. Trilok, G., Gnanasekaran, N., & Mobedi, M. (2021). Various Trade-Off Scenarios in Thermo-Hydrodynamic Performance of Metal Foams Due to Variations in Their Thickness and Structural Conditions. *Energies*, 14(24), 8343.

Energies (SCIE)
Impact factor: 3.51
ISSN: 1996-1073
DOI: https://doi.org/10.3390/en14248343

5. Trilok, G., Gnanasekaran, N. and Mobedi, M. (2024), Reconciliation of wire woven mesh porous media in controlling the desired heat transfer and pressure drop. *International Journal of Numerical Methods for Heat & Fluid Flow*. https://doi.org/10.1108/HFF-01-2024-0014.

Energies (SCIE)
Impact factor: 5.18
ISSN: 0961-5539
DOI: https://doi.org/10.1108/HFF-01-2024-0014.

INTERNATIONAL CONFERENCES

1. **Trilok, G**., and N. Gnanasekaran. "Comparison of Numerical Models of Flow and Heat Transfer Through Porous Medium in a Vertical Channel." In IOP Conference Series: Earth and Environmental Science, vol. 850, no. 1, p. 012023. IOP Publishing, 2021. (Published)

2. **Trilok, G**., and N. Gnanasekaran. “Numerical Modelling of Metal Based Porous Media: A Focus on REV Scale Modelling” 2nd International Conference on Sustainable Technologies and Advances in Automobile, Aerospace and Robotics, STAAAR-23, VIT, December, 2023, Bhopal.

BIO DATA

NAME: TRILOK G

DATE OF BIRTH 14/01/1995

Mobile No. +91 8123539478

Email: trilokg.tristar@gmail.com

ADDRESS:

Samethanahalli (village and post), Hoskote -Talluk, Bangalore Rural -District, 560067

QUALIFICATION:

Degree / Level	**Area / Specialization**	**Board / Institute**	**Year**	**Percentage / CGPA**
ME	Thermal science and engineering	(UVCE), Bangalore	2016-2018	91.16 %
BE	Mechanical Engineering	(UVCE), Bangalore	2012-2016	72.67 %
PUC / Intermediate	PCMB	Karnataka State board	2010-2012	84.84 %
SSLC / Xth	-NA-	Karnataka State board	2000-2010	88.88 %

ACHIEVEMENTS

- University 5th Rank in master programme (ME).
- Qualified GATE ME (Mechanical) and XE (Engineering Sciences).

AREAS OF INTERESTS

- CFD
- HEAT TRANSFER
- FLUID FLOW
- OPTIMIZATION